UNIVERSITY OF CAPE TOWN

Department of Astronomy
and Institute of Theoretical Physics and Astrophysics

Southern Voids: Structure and Cosmological Implications

Yuri Luis Escutia Andersson

Dissertation submitted in partial fulfilment of the
requirements for the degree of

Master of Science in Astronomy

April 1997

Abstract

A review of standard cosmology theory and observational results is presented. The main tool for investigating large-scale structure in this thesis is a visually compiled void catalogue. Void selection effects that cause the detected distribution of voids to differ from the true distribution are discussed and suggestions are made for how to correct for these effects in the catalogue. The geometrical distribution of voids is then studied by dividing the void catalogue into two parts — wall voids and non-wall voids. The wall voids are smaller with typical radii of around 150 km s^{-1} whereas non-wall voids have a mean radius of approximately 1150 km s^{-1} . The non-wall, and therefore, the larger voids are distributed isotropically and their correlation function is found to correspond roughly to that of Abell clusters, thus suggesting a link between the two structures. A relation between the velocity dispersions of clusters and the void radii is found using a spherical collapse model for structure formation. The ratio of these two quantities is used to put constraints on the cosmic density parameter Ω and observational data indicate that the universe is open.

Contents

Preface

Hubble's 1929 discovery that galaxies recede away from us and the ensuing interpretation in a general relativistic context of an expanding universe was the confirmation of an evolving, non-static universe. The existence of the Cosmic Microwave Background Radiation which was serendipitously discovered in 1965 has its most compelling explanation in the framework of the Big Bang model which has therefore since become the standard paradigm for cosmology.

An important parameter in the standard model is the background density of the universe ρ. It is usual to define the dimensionless density parameter in terms of a critical density so that $\Omega = \rho/\rho_{\mathrm{crit}}$. If the density parameter is larger than unity, gravity will work against the expansion until the universe turns around, contracts and eventually collapses. If, on the other hand, $\Omega \geq 1$ then the universe will expand forever. Observations have not yet been able to put sufficient constraints on the value of Ω and the determination of what kind of universe we inhabit is one of the outstanding questions that needs to be resolved in cosmology.

The relative ease with which modern observational techniques allow for the acquisition of redshifts of galaxies has enabled an approximate 3-dimensional mapping of the galaxy distribution in the local universe. Maps of this kind clearly show that the distribution of luminous matter is not at all random but in fact structured. Galaxies aggregate in clusters and they align in sheet-like structures leaving large regions devoid of matter. A comprehensive understanding of the universe must include an explanation for the existence of this cellular pattern of galaxies. By studying the formation and evolution of these structures in detail one does not only learn a great deal about the structures themselves but also about the nature of the cosmological background and its parameters.

This thesis will mainly be concerned with the study of the large, empty and roughly spherical regions known as voids. The main source of information is a visually compiled catalogue of Southern Voids which will be used not only to deduce some properties of the void distribution but also to give some information about the background models.

The thesis is organised as follows. Chapter 1 discusses the standard model, and presents pivotal observational results. Some quantitative tools for investigating and analysing structure are reviewed and the standard gravitational instability scenario is exposed. Chapter 2 is devoted to a discussion concerning the data in the void catalogue. Using this information in Chapter 3, the geometrical distribution of voids is investigated. The voids are linked to clusters by a simple structure formation scenario and using the void catalogue combined with cluster data a constraint on the value of Ω is inferred in Chapter 4. Finally, a brief summary of the main results is given in Chapter 5.

Chapter 1

Introduction

1.1 Standard Cosmology

Modern cosmology has as one of its founding pillars the so-called *Cosmological Principle* which states that the universe on large scales is *homogeneous* and *isotropic* implying that it looks roughly the same from any vantage point and that no position is preferential. The current formulation of the principle can be attributed to Milne (1935) but traces its philosophical roots back to the gradual shift away from an anthropocentric world view that started with the discoveries of Copernicus, Galilei and Kepler. It is of course not satisfactory to have a science built on a philosophical principle alone and therefore it must be subjected to confrontation with observations. On smaller scales the universe, replete with structure in the form of stars and galaxies, is clearly not homogeneous but on larger scales it seems that the Cosmological Principle is valid. Some of the observational evidence is discussed in Section 1.2.

The dominant force on cosmic scales is gravity, so General Relativity consequently provides a natural theoretical framework in which an understanding of the universe can be developed. The assumptions of homogeneity and isotropy as prescribed by the Cosmological Principle give rise to the Friedmann-Robertson-Walker (FRW) line element

$$ds^2 = (cdt)^2 - a^2(t)\left(\frac{dr^2}{1-kr^2} + r^2(d\theta^2 + \sin^2\theta d\phi^2)\right) \tag{1.1}$$

where r, θ and ϕ are the usual spherical (comoving) coordinates, t is proper time, $a(t)$ is the *cosmic scale factor* or *expansion parameter* which describes the dynamics of the

universe and k is the *curvature parameter* which takes on values 0 for a flat universe, +1 for a closed universe and -1 for an open universe. The scale factor cannot be directly observed so it is useful to define the *redshift* z of a luminous source such as a galaxy by

$$z = \frac{\lambda_o - \lambda_e}{\lambda_e} \tag{1.2}$$

where λ_o is the observed wavelength of a signal from the source at present time t_0 and λ_e is the wavelength as measured in a laboratory rest frame of the corresponding emitted signal at some earlier time t_e. It can be shown that the relation between the expansion parameter and the redshift is

$$1 + z = \frac{a_0}{a} \tag{1.3}$$

where a_0 is the scale factor at present time.

The matter content of the universe, expressed in terms of the energy-momentum tensor, is coupled to the geometry of space-time by the Einstein field equations, $G_{ij} \equiv R_{ij} - \frac{1}{2}g_{ij}R - \Lambda g_{ij} = \frac{8\pi G}{c^4}T_{ij}$ where R_{ij} and R are the Ricci tensor and the Ricci scalar respectively, g_{ij} is the metric, Λ is the cosmological constant and T_{ij} is the energy momentum tensor. In most cases it is appropriate to assume that the contents of the universe can be described as a perfect fluid with pressure p and energy density ρc^2. The Einstein equations with a zero cosmological constant then reduce to

$$\left(\frac{\dot{a}}{a}\right)^2 = \frac{8\pi G}{3}\rho - \frac{k}{a^2}\ , \quad \frac{\ddot{a}}{a} = -\frac{4\pi G}{3}(\rho + 3\frac{p}{c^2})\ , \quad \dot{\rho} = -3\frac{\dot{a}}{a}(\rho + \frac{p}{c^2})\ . \tag{1.4}$$

It is usual to set $H = \dot{a}/a$ where H is called the *Hubble constant.* Since a is a function of time obviously, so is H; the term constant simply refers to the fact that it has the same value for all points in space at any given time. The curvature parameter is obtained from the first equation as

$$k = a^2\frac{8\pi G}{3}(\rho - \rho_{\rm crit})\ . \tag{1.5}$$

where the critical density $\rho_{\rm crit} = \frac{3H^2}{8\pi G}$. One can further define the dimensionless density parameter

$$\Omega \equiv \frac{\rho}{\rho_{\rm crit}} = \frac{8\pi G\rho}{3H^2}\ . \tag{1.6}$$

In terms of Ω, the geometry of the universe can be determined so that it is flat if $\Omega = 1$, open if $\Omega < 1$, and closed if $\Omega > 1$.

In order to solve the differential equations (1.4) one needs an equation of state $p = p(\rho)$ which relates the pressure to the energy density. The solutions to the equations (1.4) with a simple equation of state of the form $p = w\rho c^2$ where $0 \leq w \leq 1$ are called the Friedmann models and they generally describe a universe that starts in a singularity where a vanishes and which then expands up until present time and which, depending on the density parameter, may or may not continue to expand forever. One important special case for cosmology is when the universe is matter or dust-filled and has the equation of state $p = 0$. The other important case is when the universe is filled with radiation or equivalently with relativistic particles; the equation of state is then $p = \frac{1}{3}\rho c^2$. The result of solving the Friedmann equations for these two cases can be summarised in

Component	Scale factor	Energy density	Temperature
Matter	$a(t) \propto t^{2/3}$	$\rho_m \propto a^{-3} \propto (1+z)^3 \propto t^{-2}$	$T_m \propto (1+z)^{3(\gamma-1)}$
Radiation	$a(t) \propto t^{1/2}$	$\rho_r \propto T^4 \propto (1+z)^4 \propto t^{-2}$	$T_r \propto 1+z$

(1.7)

assuming adiabatic expansion of the gas and where $\gamma = 5/3$ for a monatomic gas. The time evolution of the scale factor obviously depends on Ω and the simple power laws given in (1.7) are only valid for an Einstein–de Sitter universe ($\Omega = 1$).

The Friedmann models, although successful in many ways, are marred by a number of problems such as *e.g.* the so-called horizon and flatness problems. Inflationary models first presented by Guth in 1981 and later improved by Linde and independently by Albrecht & Steinhardt in 1982 were proposed as a way to address some of the problems associated with the Friedmann models. Though not strictly speaking being part of the Standard model, inflation has found much support and has been raised almost to the level of paradigm.

The main idea upon which most inflationary models are based is that there was an epoch in the early stages of the evolution of the universe where the dominating component of the energy density was provided by the vacuum state of a scalar field. Under certain conditions the equation of state for the scalar field is effectively $p = -\rho c^2$ yielding a time evolution of the scale factor as $a(t) \propto \exp(Ht)$ during a period of time which is typically on the order of 10^{-34} sec. Linde refined and developed the ideas of inflation to include chaotic and later stochastic arguments (see Linde 1990 for review) but these

new models retain the same basic characteristic of producing very fast growth of the scale factor during a short period of time.

Coming out of inflation the universe is filled with a number of relativistic particle species such as quarks, leptons, their respective antiparticles, photons and gauge bosons. At this stage the equation of state $p = \frac{1}{3}\rho c^2$ applies. As the temperature drops to around 10^{12} K (200-300 MeV) quark-antiquark pairs join together to form hadrons, *i.e.* pions and nucleons. Shortly thereafter at energies of about 130 MeV the charged pions annihilate and the π^0 decay into photons. This marks the beginning of an epoch called the lepton era where initially all the constituent particles were in thermal equilibrium.

There are two factors that determine whether particles participate in thermal equilibrium — the reaction rate and the expansion rate of the universe. If the reaction rate is slow compared to the expansion rate then the typical distance between particles grows so fast that the probability of a reaction occurring is small. In terms of the corresponding times τ for the expansion and collision, the condition for a particle to take part in the equilibrium can be expressed as

$$\tau_H = H^{-1} > \tau_{\text{coll}} = \frac{1}{\langle n\sigma v \rangle} \tag{1.8}$$

where n is the number density of particles, σ is the relevant cross-section and v is the velocity of the particles. When this condition is no longer satisfied the particles in question *decouple* or *freeze out* from all interactions and begin a free expansion. For neutrinos this happens at a temperature of approximately 3×10^{10}K. What follows is a period of nucleosynthesis where nuclei of the light elements H, He and Li along with some of the isotopes of these elements are produced. The standard theory of nucleosynthesis predicts the abundances of the light elements in terms of a baryon-to-photon ratio η. Observations of the abundances from *e.g.* planetary and stellar atmospheres requires η to lie in a narrow interval and knowing the photon energy density, this translates into constraints on the amount of baryonic matter that can exist in the universe. Measurements place the contribution of baryonic matter to the density parameter in the range $0.01 < \Omega_B < 0.09$. Most Inflationary models predict $\Omega = 1$ and this together with other reasons that will be explained later has led to the postulated existence of dark matter that would make up the missing mass needed to close the universe.

When the temperature goes below $m_e c^2/k_B \simeq 5 \times 10^9$K, electron–positron pairs annihilate. The light elements are still ionised and mainly due to Thompson scattering of photons by electrons, matter and radiation are still tightly coupled and in thermal equilibrium. As the universe keeps expanding the matter energy density which scales roughly as z^3 will become equal to the radiation energy density which scales as z^4. The epoch at which this happens is referred to as the time of equivalence $t_{\rm eq}$ and marks the transition from a radiation dominated universe to a matter dominated universe. When the electrons slow down sufficiently they undergo a *recombination* process whereby they are captured into atomic orbits by the protons to form neutral atoms. As the free electrons disappear and as photons do not interact with neutral atoms the radiation *decouples* from matter and photons continue in straight lines from the point of last scattering with a mean free path exceeding the Hubble length $\sim cH^{-1}$. This is not an instantaneous process though, and the last scattering surface extends about $\Delta z = 400$ around a mean of $\simeq 1100$. After decoupling, the two components evolve independently of each other and any primordial fluctuations in the matter distribution that survive the radiative era can grow and eventually giver rise to cosmic structures.

At the time just before recombination the radiation is held in thermal equilibrium so that its intensity is described by the black body spectrum. When the creation and absorption of photons has become negligible, the number of photons is preserved requiring the Planck's function $(\exp(hc/k_B T\lambda) - 1)^{-1}$ to be constant. Recalling that λ scales as $a(t)$ we conclude that

$$T = T_i \frac{a(t_i)}{a(t)} = T_i(1 + z_i)^{-1} \ . \tag{1.9}$$

Recombination occurs at a temperature of approximately 4000 K and with $z_i \simeq 1100$ we get a rough estimate of the black body temperature that should be detected. First discovered by Penzias & Wilson (1965), the Cosmic Microwave Background Radiation (CMBR) provides one of the most significant pieces of evidence in favour of the Hot Big Bang model. The COBE satellite having the advantage of avoiding atmospheric absorption has established the nearly perfect black body shape of the CMBR and has pinned down the temperature to $T = 2.726 \pm 0.010$ (Smoot *et al.* 1992). A great deal of interest has been paid to the anisotropies in the CMBR since, as will be discussed in Section 1.4, fluctuations in the radiation reflect fluctuations in the matter distribution. For the same reasons as the CMBR exists one expects a spectrum for neutrinos with a

predicted temperature of 1.9K.

The standard FRW model is successful in explaining the general features of the evolution of the universe although the parameters in it are not fully known. In the model, matter is described in terms of a smooth fluid and it does not attempt to describe the structure that we see around us. Before proceeding to discuss theories of structure formation in Sections 1.3–1.5 a brief review of existing observational evidence will be presented in the following Section.

1.2 Observations

The first systematic survey of the galaxy distribution was carried out by Shapley and Ames (1932) where the positions of a little over a thousand galaxies were recorded. Zwicky *et al.* (1961-68) continued this line of work using the Palomar Sky Survey and catalogued 5000 galaxies with apparent magnitudes < 15. A major improvement in the field of cosmography was made by Shane & Wirtanen (1967) who compiled the Lick catalogue containing about a million manually selected galaxies with $m < 19$. More recently, the backbreaking job of identifying galaxies by eye has been taken over by automatic plate measuring machines and has resulted in catalogues such as *e.g.* the APM catalogue (Maddox *et al.* 1990) which is comprised of about two million galaxies.

The Lick map in figure (1.1) gives a strong visual impression of a galaxy distribution which is lumpy, filamentary and where there are large regions of low density. The surveys, however only depict the distribution of galaxies as a two–dimensional projection on the celestial sphere and contain no information about the full spatial distribution. Obtaining accurate distances to extragalactic objects is one of the most difficult tasks in observational astronomy. Distance indicators are obtained by using empirical relations between two intrinsic properties of a galaxy — one of which is distance dependent and another which is distance independent. Usually the distance indicators can be divided into two groups according what property is being used for estimating the distance. Objects that have an intrinsic luminosity which is a function of some other distance independent quantity are called *standard candles* and objects that have a length (or often an angle) as a distance dependent property is called a *standard ruler.*

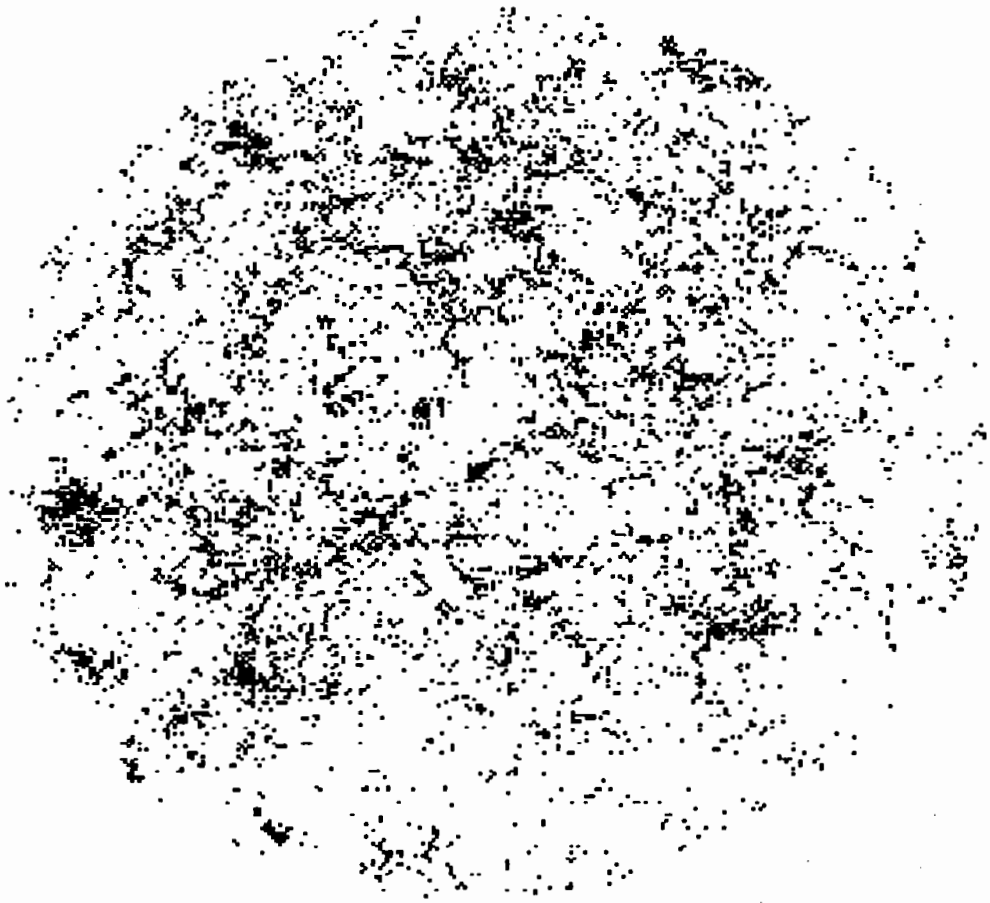

Figure 1.1: High density regions in the Lick Map from Coles & Pilonis (1991)

The distance to nearby galaxies can be determined using *Classical Cepheids* which are bright variable stars that have a well-known period–luminosity relationship but reliable estimates can only be made out to a few Mpc. The *Tully-Fisher* relation models the intrinsic luminosity of spiral galaxies as a function of their rotational velocities so that $L \propto v_{\rm rot}^{\alpha}$ and is one of the most widely used distance indicators. A similar indicator, the $D_n - \sigma$ relation, exists for elliptical galaxies and uses the relation $D_n \propto \sigma^{\gamma}$ where D_n is the diameter interior to which the average surface brightness attains some fiducial value and σ is the *rms* value of the line-of-sight stellar velocities. Both the Tully-Fisher and the $D_n - \sigma$ relations yield distances with an error of about 20 % which can be further improved by statistical analysis of several galaxies in the same cluster. Other methods for measuring distances include using the brightest galaxy in a cluster (Postman *et al.* 1995) as a standard candle

1.2.1 Redshift and the Hubble Law

Acquiring direct distance estimates is rather laborious and time-consuming and does not always give very accurate results. What is more easily obtained are the spectra of galaxies. A galaxy following the general expansion of the universe will be receding away from us and therefore have its spectrum Doppler shifted towards the red end. Thus by identifying emission and absorption lines in the spectrum of a galaxy it is possible to calculate the redshift defined by equation (1.2). With modern observational techniques Doppler velocities can be obtained with a typical accuracy of 30 km s^{-1} for optical measurements and for 21 cm techniques it is even possible to reduce the uncertainty to 5-10 km s^{-1} .

In order to find the relation between distance and redshift one can Taylor expand the cosmic scale factor for times close to t_0, recall some properties of the FRW line element and use the definition of the redshift. The proper distance can then be written as

$$d_{proper} = \frac{c}{a_0 H_0}\left[z - \frac{1}{2}(1+q_0)z^2 + \ldots\right] \tag{1.10}$$

where H_0 is the *Hubble constant* and q_0 is the so-called deceleration parameter defined by the cosmic scale factor and its first and second derivatives as $q_0 = -\,\ddot{a}(t_0)a_0/\,\dot{a}(t_0)^2$. The well-known full relativistic relation between the Doppler velocity and the redshift

is

$$1+z=\left(\frac{1+v/c}{1-v/c}\right)^{1/2} \quad . \tag{1.11}$$

Combining equations (1.10) and (1.11) and keeping only the first, linear terms of the Taylor series in either relation one arrives at the *Hubble law* which states that

$$v = H_0 d \tag{1.12}$$

where now the proper distance is denoted d for simplicity. Incidentally, the Hubble law can be derived from Newtonian theory as well under the additional assumption that the universe is expanding.

It was Hubble who in 1929 observed a linear relation between the distance and redshift for galaxies and was the first to interpret the observations as being a result of an expanding universe. The linear relation of the Hubble law has been verified out to a redshift of about 0.5 by a large number of studies using different distance indicators such as *e.g.* Tully-Fisher (Peebles 1988; Mould *et al.* 1991), field galaxies (Shanks 1991) and radio galaxies (McCarthy 1992). One of the most serious challenges in modern astronomy is to find the correct value for H_0. The original value as quoted by Hubble was 500 km s^{-1} Mpc^{-1} but more recent observations suggest that its value lies somewhere in the interval $50 \leq H_0 \leq 85$ km s^{-1} Mpc^{-1} (Peebles 1994). It is usual to express H_0 as $100h$ km s^{-1} Mpc^{-1} where h is a dimensionless factor that parametrises our ignorance of the true value. In order to avoid problems with the uncertainty in the determination of the Hubble constant it is sometimes more convenient to quote distances in terms of redshift units of km s^{-1} .

1.2.2 Surveys

Systematic surveys of redshifts were pioneered in the late 1970s and early 1980s by Gregory & Thompson, Kirshner *et al.* and Huchra *et al.* ; for a review and references see Strauss & Willick (1995). The Harvard-Smithsonian Center for Astrophysics (CfA) (de Lapparent *et al.* 1986, Geller & Huchra 1989) conducted an extensive survey based on several thousands of galaxies from the Zwicky catalogue and produced the famous CfA 'slice of the universe' galaxy maps shown in figure (1.2). The *IRAS* satellite was launched in 1983 carrying with it instruments for detecting infra-red radiation from galaxies. Since radiation in this wavelength band is not impeded by galactic extinction

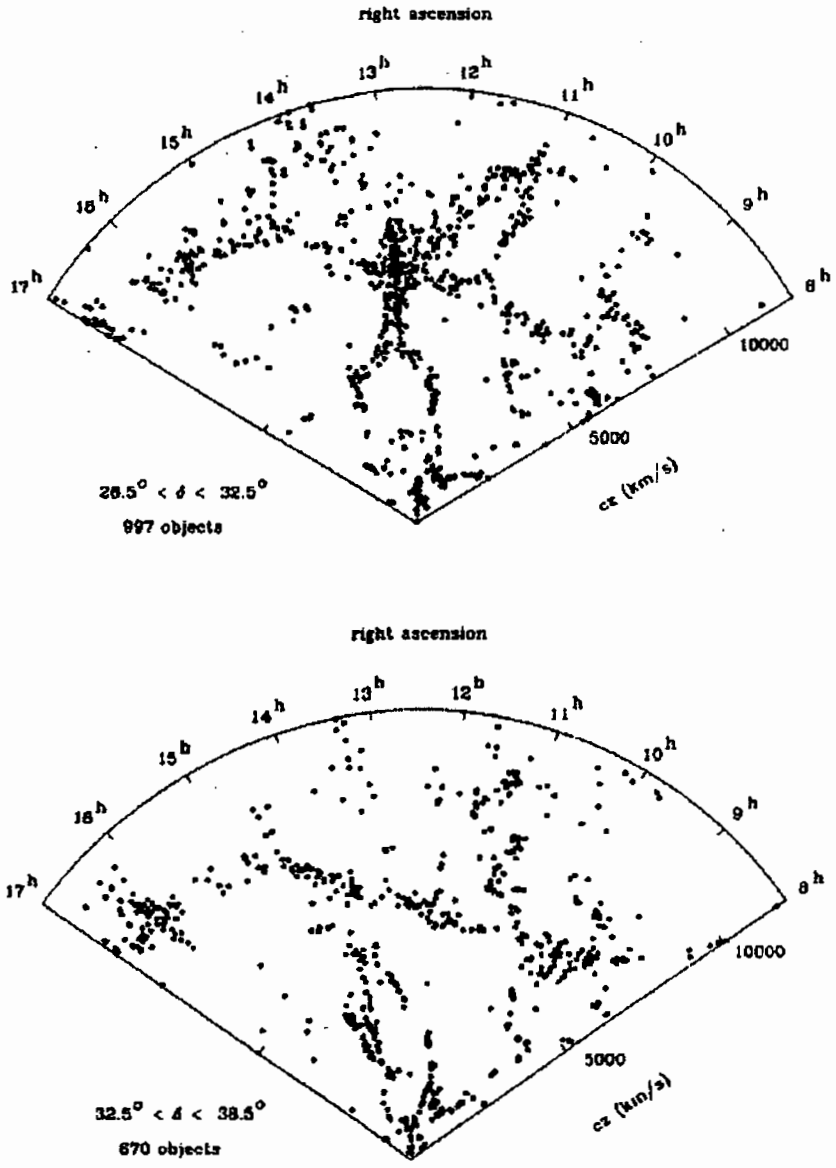

Figure 1.2: CfA slice of the universe, reproduced from Peebles (1994) where references to the original publications of the plots are given.

it allowed *IRAS* to have a full-sky covering and observations gave rise to a number of surveys (Strauss *et al.* 1992, Fisher *et al.* 1995). A deeper but sparser selection of *IRAS* galaxies resulted in the QDOT (Queen Mary, Durham, Oxford, Toronto) survey (see *e.g.* Efsthatiou *et al.* 1990). The Southern Hemisphere has been covered by the Southern Sky Redshift Survey (SSRS) conducted in the optical band (da Costa 1988; 1991). The largest survey to date is the Las Campanas Redshift Survey (LCRS) which has nearly 25,000 redshifts (see *e.g.* Lin 1996) and the deepest existing survey extend out to $2000h^{-1}$ (Broadhurst *et al.* 1990). New surveys that are under way include the Anglo-Australian 2 degree Field (2dF) survey aimed at mapping large scale structures on scales larger than 3000 km s^{-1} (see *e.g.* Taylor, 1995). Using multifibre technology, the Sloan Digital Sky Survey (Gunn & Weinberg 1995) will extend the number of redshifts available from a few tens of thousands today to a million by the end of the decade.

When using redshift surveys for an analysis one must be aware of the possibility that any conclusions drawn from it may be dependent on the manner in which the galaxies have been selected for the survey. If galaxies are excluded on the basis of some predetermined criteria the survey will suffer from *selection effects*. A commonly used criteria is to exclude galaxies fainter than a certain magnitude or to exclude those smaller that a certain diameter. A catalogue which has a well-defined selection criteria and that include all galaxies that satisfy these criteria is said to be *complete*. Controlled samples are not without problems however. *Malmquist bias* (Sandage 1987) arises in magnitude-limited samples as the average (absolute) luminosity of nearby galaxies is lower than the average luminosity of more distant galaxies apparently causing there to be fewer faint galaxies at higher redshifts.

1.2.3 Redshift Distortion

For large redshifts the higher order terms in the relativistic distance-redshift relation (1.10) become important so that the simple linear equation (1.12) no longer holds. For distance scales where corresponding redshifts are comfortably smaller than unity, which is the case for surveys used in this text, relativistic corrections are negligible and the simple Hubble law can be applied. In practice, however, even at modest redshifts the galaxy maps do not exactly correspond to the real positions of the galaxies. The reason for this being that the observed velocity contains other components of motion

which give rise to peculiar velocities that are superimposed on the velocity due to the universal expansion. Therefore in general

$$cz = H_0 d + v_{pec} \tag{1.13}$$

where $v_{\rm pec}$ is the line-of-sight component of the peculiar velocity. Deriving distances to galaxies purely from their observed radial velocities introduces a *redshift distortion* in the mapping from redshift space to real space. However, it can be presumed that outside rich clusters the peculiar velocities of the galaxies do not greatly distort the real space distribution since one sees neither the elongations along the line-of-sight to be expected from random motions nor the effect of collapse which would make the galaxy concentration tend to appear flattened along the line-of-sight (see *e.g.* Peebles 1994).

The peculiar velocities are not only an inconvenience for the study of large-scale structure since the large-scale dynamics of galaxies is coupled to the distribution of matter. Using independent distance indicators one can build up a catalogue of peculiar motions from which large-scale streaming motions have been detected. Our *Local Group* of galaxies made up of The Milky Way along with its satellite galaxies — the two Magellanic Clouds, the Andromeda M31 galaxy and some 20 other galaxies is moving towards the Virgo cluster with a velocity of about 250 km s^{-1} . The Virgocentric infall gives an indication of the amount of non-luminous (dark) matter that exists in the universe and is useful for investigating how luminous matter traces mass. A sophisticated method of using the velocity information known as POTENT was developed mainly by Dekel & Bertschinger (for a review see Dekel 1994). One can show, using the theory of gravitational instability (see Section 1.4) that the peculiar velocity field is proportional to the gravitational acceleration field. The POTENT analysis could therefore give a direct estimate of the density parameter Ω which does not rely only on observations of luminous matter.

1.2.4 Structure in Galaxy Maps

As more surveys are being conducted probing the universe at ever increasingly large scales it is becoming more and more clear that the structure seen in the distribution of galaxies is real. A picture emerges of a 'frothy' and cellular universe with lumps, filaments, walls and large empty regions. Among the first propose this picture was Jôeveer & Einasto (1978) and was later discussed by a number of other workers such as Gregory & Thompson (1978), Fairall (1985) and de Lapparent *et al.* (1986).

Clusters

Perhaps the most prominent feature of the galaxy distribution are the regions where galaxies tend to congregate in large numbers. These *clusters* usually have an excess of early galaxy types toward the cluster centres which indicates that they are localised concentrations in space (Gunn & Gott 1972) and therefore that the cluster members would have a common cosmological redshift. The clusters are dynamically bound systems so that the cluster members consequently have a spread in their line-of-sight peculiar velocities which, when superimposed on the velocity due to the general expansion of the universe, show up as elongated features in redshift space. These elongated features are sometimes referred to as 'Fingers-of-God' as they seem to be pointing in our direction.

Using the Palomar Sky Survey, Abell (1958) catalogued the largest clusters and assigned richness classes to them by counting the number of galaxies within a radius of $r_a = 1.5h^{-1}$ Mpc around the cluster centre. The Abell catalogue and its successor (Abell 1965) which is constantly updated is one of the most important observational sources for the study of large scale structure. The Virgo cluster — our nearest cluster neighbour is located at a distance of about 1200 km s^{-1} . Further away at 7000 km s^{-1} lies the most prominent cluster in the sky — the Coma cluster.

In the next level up in the hierarchy of structures Einasto *et al.* (1980), Huchra *et al.* (1983), Oort (1983) and Tully (1986) claim that clusters themselves group in superclusters. One example of a supercluster is the Virgo Supercluster to which our Local Group belongs; another is the so-called Shapely Concentration.

Filaments and Walls

Cob–web like patterns of filaments seem to be a ubiquitous feature of galaxy maps. Pioneering discussions of the tendency for galaxies to trace linear structures were carried out by Jôeveer, Einasto & Tago (1978) and Gregory *et al.* (1981). The non-radial filamentary structure which cannot be the result of a 'finger-of-God' effect was in particular considered by Chincarini (1983) and Einasto *et al.* (1983). Barrow & Bhavsar (1987) cautioned that the appearance of the filaments can vary quite significantly when the grey scale linking the printed intensity and the cell count number is altered and

therefore stressed the importance of developing objective methods of analysis.

De Vaucouleurs (1953) was the first to speculate about the existence of sheetlike structures that would run like walls through the universe when he identified galaxies lying on a plane that he claimed was part of the Local Supercluster. This local plane defines a structure that extends to $cz \lesssim 3000$ km s^{-1} in optical galaxies (Lahav 1987) and most radio sources out to distances of $cz \lesssim 5000$ km s^{-1} are also concentrated in the same plane (Shaver 1991). De Lapparent, Geller & Huchra (1986) argued that the filaments seen in galaxy maps are not independent structures but are actually cross-sections through sheets of galaxies. Fairall *et al.* (1990) claim that the structure seems to be made up of interlacing filaments and walls and that superclusters seem to occur where such structures intersect.

Voids

Between clusters, filaments and sheets there are regions that are roughly devoid of galaxies — called *voids*. Voids are difficult to detect in 2-dimensional projections of the galaxy distribution but even before any significant information had been obtained from redshift surveys Chincarini (1978) and later Einasto *et al.* (1980) speculated in the existence of voids in the 3-dimensional distribution. Kirshner *et al.* (1981) discovered a large void in the constellation of Boötes in the Northern Hemisphere. In a further study having more exhaustive data Kirshner *et al.* (1987) confirmed their 1981 claim, establishing the existence of the Boötes void as well as estimating its radius to ~ 62 Mpc. In the Southern Hemisphere Winkler (1983), Fairall (1984) and Fairall & Jones (1988) identified voids visually from the Southern Redshift Catalogue. Difficulties with subjectivity arise when voids are detected visually — it is not even clear how one should define a void. Some attempts at automating the detection of voids have been made by Pellegrini *et al.* (1989), Kauffmann & Fairall (1991) , Kauffmann & Melott (1992) and more recently by Ryden (1995) and Lindner *et al.* (1995).

1.2.5 Cosmological Principle

It may seem, with so much evidence for the existence of structure in the universe, that this would be in conflict with the Cosmological Principle of isotropy and homogeneity. Strauss *et al.* (1992) studied the distribution of IRAS galaxies on the scale of $cz \sim$

$10,000$ km s^{-1} and saw no noticeable gradient in the density of galaxies across the sky. The Milky Way is largely transparent to radiation at X-ray energies so that the flux in any direction is directly proportional to the integrated column density. Jahoda *et al.* (1992) found that the flux averaged over 1 steradian of the sky only fluctuated with less than one part in 10^3. Another study — this time in the radio wavelength band was done by Gregory & Condon (1991). The results indicate that the radio sources are galaxies and quasars located at distances comparable to the Hubble length cH_0^{-1} and that at this great depth the fine structure is lost implying that the universe is approximately homogeneous on such scales.

Of course the most convincing evidence for the isotropy of the universe is given by the CMBR which shows a high degree of isotropy. The CMBR is not however exactly the same for all positions on the sky due to a number of different effects. The largest effect is caused by the motion of our galaxy and when this dipole is subtracted the temperature of the CMBR has a variation $\delta T/T$ around the mean of $T_0 = 2.736 \pm 0.010$. The most important intrinsic effect on the anisotropy is the *Sachs-Wolfe* effect (Sachs & Wolfe 1967) which is a result of fluctuations of the metric in the last scattering surface. This effect can be interpreted in a Newtonian context as being due to perturbations in the gravitational potential which in turn are generated by density fluctuations. COBE data suggests that the *rms* temperature anisotropy is on the order of 10^{-5}.

1.3 Density Perturbations

Having established the observational evidence for the existence of structure and thus mass fluctuations, the formalism needed for the treatment of density perturbations is introduced here.

The matter distribution in the universe could at any given time t be described by a continuous mass density function $\rho(\mathbf{x}, t)$ where $\mathbf{x}$ is the position vector of any point with respect to some arbitrary origin. It is usual to define a density contrast $\delta(\mathbf{x}, t)$ as

$$\delta(\mathbf{x}, t) = \frac{\rho(\mathbf{x}, t) - \langle\rho\rangle(t)}{\langle\rho\rangle(t)} \tag{1.14}$$

where $\langle\rho\rangle$ denotes the average density in some volume $\mathcal{V}$. A structure formation scenario is in principle a prescription for how to evaluate the density function at any time

t and its validity could, at least hypothetically, be tested by confronting the predictions of the theory with observational facts.

However, it would be overly optimistic to hope for the calculations to yield the density contrast at any specific location $\mathbf{x}$ since that even if all the mechanisms of structure formation were well-known, this would require exact knowledge of the initial conditions at some earlier time t_i. Therefore there is a need to develop ways of describing the mass distribution in terms of its statistical properties. Even though the present universe is not strictly homogeneous in the sense that the density gradient on small scales is non-zero, the observed isotropy on large scales suggests that is possible to adopt such a statistical approach. One could imagine dividing the universe into a number of sufficiently large regions $\mathcal{R}_1, \mathcal{R}_2, \ldots$, each having volume $\mathcal{V}$, such that the mass distributions in each of the volumes would exhibit identical statistical properties. If the different regions are equipped with identical coordinate systems then the actual density functions in each of the regions $\rho_1(\mathbf{x}), \rho_2(\mathbf{x}), \ldots$ would in general have different values for a given $\mathbf{x}$. The $\rho_i(\mathbf{x})$s could be interpreted as different realisations of a single random variable $\rho(\mathbf{x})$ whose statistical properties can be determined.

Instead of representing the density fluctuations in real space they could be expressed in terms of a Fourier series. Assume that the universe is divided into adjacent regions $\mathcal{R}_1, \mathcal{R}_2, \ldots$ with periodic boundary conditions and that the volume $\mathcal{V}$ of each region is a cube with side $L \gg L_{\max}$ where $L_{\max}$ is the length scale of the largest existing structure. Each region can then be thought of as a fair sample of the universe. The density contrast in a given volume $\mathcal{V}$ can then be written as

$$\delta(\mathbf{x}) = \sum_{\mathbf{k}} \delta_{\mathbf{k}} e^{i\mathbf{k}\cdot\mathbf{x}} \tag{1.15}$$

where the wave vector, because of the periodic boundary conditions, is $\mathbf{k} = (2\pi/L)\mathbf{n}$ where $\mathbf{n}$ is a vector with integer components. The Fourier coefficients are then also stochastic variables defined by

$$\delta_{\mathbf{k}} = \frac{1}{\mathcal{V}} \int_{\mathcal{V}} \delta(\mathbf{x}) e^{-i\mathbf{k}\cdot\mathbf{x}} d\mathbf{x} \tag{1.16}$$

which because of the reality of $\delta(\mathbf{x})$ obey $\delta_{\mathbf{k}}^* = \delta_{-\mathbf{k}}$ where $\delta_{\mathbf{k}}^*$ is the complex conjugate of $\delta_{\mathbf{k}}$.

By definition, the mean value of the perturbation $\delta(\mathbf{x})$ across the ensemble of realisations is identically zero. However, one can construct moments of the density contrast which are non-vanishing, such as the variance σ^2 defined by

$$\sigma^2 \equiv \sum_{\mathbf{k}} \langle |\delta_{\mathbf{k}}|^2 \rangle = \frac{1}{\mathcal{V}} \sum_{\mathbf{k}} \delta_{\mathbf{k}}^2 \ . \tag{1.17}$$

In the limit when $\mathcal{V} \to \infty$ and under the assumption that the density field is statistically homogeneous and isotropic so that there is no dependence on the direction of the wave vector but only on its magnitude $k = |\mathbf{k}|$ the variance becomes

$$\sigma^2 = \frac{1}{2\pi^2} \int_0^\infty P(k) k^2 dk \tag{1.18}$$

where $P(k) \equiv \delta_k^2$ is called the *power spectrum* of the field δ. The power spectrum carries information about the amplitude of the perturbations and is a function of time only. It is usual to assume an initial shape of the power spectrum for different formation scenarios which in most cases is given by a power law of the form

$$P(k) = Ak^n \tag{1.19}$$

where A is a constant and n is called the spectral index. The power spectrum will evolve with time and the mapping from some initial spectrum $P(k, t_i)$ to the spectrum at some later time t is referred to as the *transfer function.* This transfer function depends critically on the nature of the constituent matter in the universe.

The so-called correlation functions will be introduced in Section 1.6 as quantities that measure the degree of spatial dependence that the positions of points in a data set have on each other. In the continuous representation of mass, the analogy of the two-point correlation function is the *autocovariance function* which is defined in terms of the density field by

$$\xi(r) = \langle \delta(\mathbf{x}) \delta(\mathbf{x} + \mathbf{r}) \rangle = \frac{\langle [\rho(\mathbf{x}) - \langle \rho \rangle] [\rho(\mathbf{x} + \mathbf{r}) - \langle \rho \rangle] \rangle}{\langle \rho \rangle^2} \ . \tag{1.20}$$

It is straightforward to prove the so-called *Wiener–Khintchin* theorem which states that the autocovariance and the power spectrum are the Fourier transforms of each other so that

$$\begin{aligned} \xi(\mathbf{r}) &= \frac{1}{(2\pi)^3} \int P(k) e^{-i\mathbf{k}\cdot\mathbf{r}} d\mathbf{k} \ , \\ P(k) &= \int \xi(\mathbf{r}) e^{i\mathbf{k}\cdot\mathbf{r}} d\mathbf{r} \ . \end{aligned} \tag{1.21}$$

1.3.1 Gaussian Perturbations

Suppose a volume $\mathcal{V}$ is discretised into N cells and that the centre of cell i is located at a position vector $\mathbf{x}_i$. In the limit when $N \to \infty$, the probability of $\mathcal{V}$ having a continuous density contrast field $\delta(\mathbf{x})$ can be expressed in terms of the density contrasts of the individual cells $\delta_1, \delta_2, \ldots, \delta_N$ where $\delta_i = \delta(\mathbf{x}_i)$. If the cells were all independent, the joint probability distribution of having density contrasts with value δ_i in cell i for all $i = 1, \ldots, N$ would simply be the product of the probability densities of the individual cells. In the very early universe it is reasonable to assume that the δ_is are uncorrelated or at least only weakly correlated for different locations in space before the gravitational interaction between the cells destroys this mutual independence.

From equation (1.16) it is clear that each of the Fourier modes is a sum of a large number of independent stochastic variables with the same distribution and by virtue of the Central Limit Theorem the probability distribution for $\delta_{\mathbf{k}}$ is consequently a Gaussian. A strict definition of a Gaussian random field requires the amplitudes of the Fourier components $|\delta_{\mathbf{k}}|$ to have a Rayleigh distribution and their phases to be uniformly distributed in the interval $[0, 2\pi]$ but in practice the latter condition alone is considered sufficient. The real space differential probability distribution of $\delta = \delta(\mathbf{x})$ can be shown to be

$$P(\delta) = \frac{1}{(2\pi\sigma^2)^{1/2}} e^{-\frac{\delta^2}{2\sigma^2}} \tag{1.22}$$

and the joint probability distribution for the outcome $\{\delta_1, \delta_2, \ldots, \delta_N\}$ is simply the corresponding N–variate Gaussian. An interesting and useful feature of this type of distribution is that it is fully specified by its variance and hence its power spectrum.

Besides being a convenient distribution to work with there are other reasons for justifying the assumption that the density field is described by a Gaussian distribution at early times. From a theoretical point of view, inflationary models where the density fluctuations are generated by quantum fluctuations in the scalar field generically produce Gaussian random fields. Also, the observational results from COBE are at present consistent with the Gaussian assumption (White *et al.* 1994) although it cannot be regarded as conclusive evidence. Other types of initial conditions that cannot at present be entirely ruled out have also been postulated — such as *textures* and *cosmic explosions* but for the remainder of this text we will conform to the orthodoxy of the

prevailing Gaussian paradigm.

1.4 Gravitational Instability

In Section 1.2 we have seen that observational evidence lends support to the idea that the universe is isotropic and homogeneous on the largest scales and at early times, something which is explicitly assumed in the Standard Big Bang model through the Cosmological Principle. On smaller scales however, structure is observed in abundance — the universe is filled with stars which in turn make up galaxies which themselves form larger structures such as clusters and walls. With the aim of gaining further knowledge of the universe it is necessary to develop an understanding for the mechanisms involved in the formation of structure.

The so-called *Gravitational Instability Paradigm* is the widely accepted framework in which models for structure formation are developed. It assumes that gravitational instability causes initially small density fluctuations to grow and eventually form structures. Sir James Jeans realised that there exists an instability in evolving clouds of gas and used this fact in an attempt to formulate a theory of formation of stars and planets. The Jeans instability adopted to an expanding background and, if necessary, generalised to be relativistically correct lies at the foundation for modern theories of structure formation.

1.4.1 Linear Theory

In the following, it is assumed that the constituent components of the universe can be treated as ideal fluids and that the length scale of the perturbations are much smaller than the Horizon scale so that the Newtonian approximation is valid. Neglecting dissipative terms due to viscosity or thermal conductivity the three equations of motion needed to describe a fluid are the Euler, the continuity and the Poisson equations;

$$\frac{\partial(a\mathbf{v})}{\partial t} + (\mathbf{v}\cdot\nabla_x)\mathbf{v} = -\frac{1}{\rho}\nabla_x p - \nabla_x\phi \tag{1.23}$$

$$\frac{\partial\rho}{\partial t} + 3H\rho + \frac{1}{a}\nabla_x(\rho\mathbf{v}) = 0 \tag{1.24}$$

$$\nabla_x^2\phi = 4\pi G a^2\rho_0\delta \tag{1.25}$$

where $\mathbf{x}$ is the comoving coordinate, $\mathbf{v}$ the peculiar velocity, $\phi(\mathbf{x},t)$ the Newtonian gravitational potential and $\rho(\mathbf{x},t)$ the density. It is further assumed that the quantities in equations (1.23–1.25) can be written as small deviations from a their corresponding homogeneous quantities so that $|\mathbf{v}|, |\frac{\partial \mathbf{v}}{\partial x^a}|, |\delta| = |\delta\rho/\rho_b| \ll 1$ where ρ_b is the smooth background density. The linearised equations are then obtained from the exact equations (1.23– 1.25) by keeping only the first order terms

$$\frac{\partial \mathbf{v}}{\partial t} + \frac{\dot{a}}{a}\mathbf{v} = -\frac{1}{\rho a}\nabla_x p - \frac{1}{a}\nabla_x \phi \tag{1.26}$$

$$\frac{\partial \delta}{\partial t} = -\frac{1}{a}\nabla_x \cdot \mathbf{v} \tag{1.27}$$

$$\nabla_x^2 \phi = 4\pi G a^2 \rho_0 \delta \ . \tag{1.28}$$

By taking the time derivative of the linearised continuity equation, multiplying it by the cosmic scale factor a and subtracting the linearised Euler equation one obtains a second order differential equation for the density contrast as

$$\frac{\partial^2 \delta}{\partial t^2} + 2H\frac{\partial \delta}{\partial t} - 4\pi G\rho_0 \delta = \frac{\nabla^2 p}{\rho_0 a^2} \ . \tag{1.29}$$

Peebles (1980) discusses solutions to equation (1.29) for a variety of special cases and some of them which are of particular interest are presented here.

For a universe dominated by pressure-less matter the spatial and temporal dependences in equation (1.29) can be separated since it is a partial differential equation in time alone. Thus a general solution will have the form

$$\delta(\mathbf{x},t) = A(\mathbf{x})D_+(t) + B(\mathbf{x})D_-(t) \tag{1.30}$$

where $D_+(t)$ and $D_-(t)$ are the growing and decaying modes respectively. The time evolution of these modes are particularly simple for an Einstein-de Sitter universe ($\Omega = 1$) for which $D_+(t) \propto t^{2/3}$ and $D_+(t) \propto t^{-1}$.

Assuming zero initial velocity, the linearised continuity equation can be integrated to give

$$\delta = -\frac{1}{aHf}(\nabla_x \cdot \mathbf{v}) \tag{1.31}$$

where f is a function that depends on the density parameter Ω and is defined as $f \equiv \frac{d\log\delta}{d\log a}$. If only the growing mode is taken into account then $f \simeq H^{-1}\dot{D}_+/D_+$

which, for a zero cosmological constant, has the approximate form of $\Omega_0^{0.6}$ (*e.g.* Lahav *et al.* 1991). Using the fluid equations it can be shown that

$$\mathbf{v} = -\frac{2f(\Omega)}{3\Omega H a}\nabla\phi \tag{1.32}$$

which by inverting the Poisson equation can be written explicitly in δ as

$$\mathbf{v} = aH\frac{f(\Omega)}{4\pi}\int \frac{\delta(\mathbf{x}')(\mathbf{x}-\mathbf{x}')^3}{|\mathbf{x}-\mathbf{x}'|^3}\mathbf{x}' \ . \tag{1.33}$$

This equation provides a relationship between the peculiar velocity field and the density perturbations which is a function only of Ω. As velocities are generated by the gravitational potential of the total distribution of matter and not only of the luminous matter, POTENT uses equation (1.33) and peculiar velocity catalogues for supplying a measurement of the density parameter Ω.

So far we have assumed that the energy density of the universe is furnished by only one component — matter. If radiation is included, the density ρ in the fluid equations has to be replaced by the sum of the matter and radiation energy densities. The Friedmann equations show that the introduction of another component to the fluid will increase the Hubble parameter and therefore decrease the growth of δ. As an example to see qualitatively what effect the radiation component has on the formation of structure we will assume that the universe is flat and that the radiation is unperturbed. The energy density of the radiation is then $\rho_r \propto a^{-4}$ and defining $\tau = \rho_m/\rho_r \propto a(t)$ it can be shown that equation (1.29) has a growing solution $D_+ \propto 1 + 3\tau/2$. From this expression it is clear that as long as the universe is radiation dominated, $\tau \ll 1$, the fluctuations remain frozen and that they can only begin to grow once the universe has become matter dominated.

The pressure term in the partial differential equation for the density contrast has so far been neglected. Rewriting (1.29) in terms of the sound speed $c_s = \left(\frac{\partial p}{\partial \rho}\right)^{1/2}$ gives

$$\frac{\partial^2\delta}{\partial t^2} + 2H\frac{\partial\delta}{\partial t} - \left(\frac{c_s}{a}\right)^2\nabla_x^2\delta - 4\pi G\rho_0\delta = 0 \ . \tag{1.34}$$

If the Fourier expansion of $\delta(\mathbf{x},t) = \sum_k \delta_k e^{i\mathbf{k}\cdot\mathbf{x}}$ is inserted in (1.34) we obtain a partial differential equation for the amplitudes

$$\ddot{\delta}_k + 2H\dot{\delta}_k + \omega_k^2\delta_k = 0 \tag{1.35}$$

and a dispersion relation

$$\left(\frac{kc_s}{a}\right)^2 - 4\pi G\rho = \omega_k^2 \tag{1.36}$$

where k is the comoving wavenumber $k = |\mathbf{k}| = 2\pi a/\lambda$. Equation (1.35) describes an oscillator damped by the expansion of the universe through the $2H\dot{\delta}_k$ term. Depending on the sign of ω_k^2 one obtains different classes of solutions. If the angular frequency is real so that $\omega_k^2 > 0$ the solutions will oscillate as sound waves with decreasing amplitudes and in the case when the ω_k is imaginary the solutions are of the same form as for a pressure-less one component fluid (1.30). The *Jeans wavelength* is defined by the condition $\omega_k = 0$ so that

$$\lambda_J = v_s \left(\frac{\pi}{G\rho}\right)^{1/2} . \tag{1.37}$$

Expressed in terms of length scales thus, perturbations with $\lambda > \lambda_J$ can grow whereas perturbations with $\lambda < \lambda_J$ will oscillate and eventually disappear. It is usual to define an associated *Jeans mass* as the mass which is contained within a sphere of radius $\lambda_J/2$

$$M_J = \frac{\pi}{6}\rho_m \lambda_J^3 . \tag{1.38}$$

There exists several possible perturbation modes in a self-gravitating fluid. Two of these fundamental modes — the *adiabatic* and *isothermal* modes have been given particular attention in a cosmological context.

In the adiabatic case the entropy is almost entirely carried by the radiation so that

$$S = \frac{\rho_r c^2 + p_r}{T} V \propto \frac{\rho_r^{3/4}}{\rho_m} \propto \frac{T^3}{\rho_m} . \tag{1.39}$$

Differentiation gives

$$\frac{\delta S}{S} = \frac{3}{4}\frac{\delta\rho_r}{\rho_r} - \frac{\delta\rho_m}{\rho_m} = 3\frac{\delta T}{T} - \frac{\delta\rho_m}{\rho_m} = 0 \tag{1.40}$$

so that

$$\delta_m \equiv \frac{\delta\rho_m}{\rho_m} = 3\frac{\delta T}{T} = \frac{3}{4}\frac{\delta\rho_r}{\rho_r} \equiv \frac{3}{4}\delta_r . \tag{1.41}$$

With the density and the pressure being $\rho = \rho_m + \rho_r$ and $p \simeq p_r = \rho_r c^2/3$ respectively the sound speed is

$$c_s^{(a)} = \left(\frac{\partial p}{\partial \rho}\right)_S^{1/2} \simeq \frac{c}{\sqrt{3}}\left[1 + \left(\frac{\partial \rho_m}{\partial \rho_r}\right)_S\right]^{-1/2} = \frac{c}{\sqrt{3}}\left[1 + \frac{3}{4}\frac{\rho_m}{\rho_r}\right]^{-1/2} . \tag{1.42}$$

For the isothermal mode it is assumed that there is no inhomogeneity in the radiation component based on the idea that the high thermal conductivity of the cosmological medium levels out the temperature by heat conduction. The sound speed is the same as for a monatomic gas and is given by

$$c_s = \left(\frac{\partial p_m}{\partial \rho_m}\right)_S^{1/2} = \left(\frac{\gamma k_B T}{m_p}\right)^{1/2} \tag{1.43}$$

where $\gamma = 5/3$ for hydrogen.

One can calculate Jeans masses for the two perturbation modes at the time of recombination and thereby estimate the order of magnitude of the mass of the structures that experience uninterrupted growth. For the adiabatic mode this mass is $M_J^{(a)} \simeq 10^{16}(\Omega h^2)^{-2} M_\odot$ corresponding roughly to the observed masses of superclusters of galaxies and for isothermal perturbations the Jeans mass is $M_J^{(i)} \simeq 10^5(\Omega h^2)^{-1/2} M_\odot$ which is on the same order of magnitude as the typical mass of a globular cluster.

Just as sound waves that propagate in air subside because the particles that carry the wave scatter so that their coherent motion is dissipated as heat, cosmic waves of density fluctuations lose their energy at smaller wavelengths due to viscosity and thermal conduction and the effect is to smear out the original fluctuation. Photons and electrons are coupled through Thompson scattering and as the photons dissipate in random directions they carry with them the electrons resulting in exponential dampening of the fluctuations. The length scale of the perturbations below which their amplitudes get dampened due to dissipative processes is called the *Silk length*, λ_s. The corresponding mass scale, the *Silk mass* is defined in a similar way to the Jeans mass as $M_s = \pi \rho_m \lambda_s^3/6$. For isothermal perturbations M_s is too small to be of any cosmological significance but for the adiabatic mode the Silk mass is on the order of $M_s \simeq 10^{12}(\Omega h^2)^{-5/2} M_\odot$ similar to that of a rich cluster of galaxies.

Based on the assumption that either one of the two perturbation modes is correct two different and largely exclusive structure formation scenarios were constructed in the 1970s — the adiabatic scenario advocated by the Soviet school headed by Zel'dovich

and the isothermal model championed amongst others by Peebles. In the adiabatic scenario perturbations smaller than the Silk mass will dissipate away whereas fluctuations in the interval $M_s^{(a)} < M < M_J^{(a)}$ will eventually, after oscillations, grow uninhibitedly and evolve as the perturbations on scales $M > M_J^{(a)}$. These large masses undergo anisotropic collapse to form so-called *pancakes* in which shockwaves are produced that subsequently cause a fragmentation of the large mass into smaller structures. Since large structures form first and then break down into smaller entities it is often referred to as a *top-down* scenario. The main problem with this model is that it requires larger fluctuations in the CMBR than is observed. Structures seen today have $\delta > 1$ which for a flat universe implies that the density perturbation at the time of recombination must have been at least on the order of 10^{-3} which consequently is the required amplitude of the CMBR fluctuations. This problem is exacerbated for $\Omega < 1$ universes.

In the isothermal scenario only fluctuations on the mass scale $M > M_J^{(i)}$ will grow and these lumps of matter that condense out at the time of recombination will behave much like particles that gravitate towards each other to form larger structures. Since structure is formed by accumulating smaller entities to progressively larger structures this scenario is sometimes called the *hierarchical clustering* or the *bottom-up* scenario. The main problem with this model is that is unnatural since it is difficult to conceive of any physical processes that would leave the radiation smooth while perturbing the matter.

1.4.2 Dark Matter

From a theoretical point of view there is ample support for the dark matter hypothesis. As we have seen already, evolution of adiabatic perturbations from sufficiently small initial conditions cannot account for the observed inhomogeneities without violating the constraints from the CMBR. Most Inflationary scenarios produce adiabatic perturbations and in many cases they also predict $\Omega = 1$ universes. Visible matter can in the most optimistic estimates only account for $\Omega \sim 0.05$–0.3 and the amount of baryonic matter limited by constraints from Big Bang nucleosynthesis can only contribute to the density parameter with $0.01 < \Omega_B < 0.09$. The presumption that the universe is closed has therefore led to the postulated existence of non-luminous, dark matter.

The existence of dark matter in the universe is also motivated by a number of obser-

vational facts. The perhaps most compelling piece of evidence is found in the halos of galaxies. According to Newtonian mechanics, the orbital velocity of objects away from a central concentration of mass should drop off as $1/\sqrt{r}$. By observing the 21 cm emission lines from a spiral galaxy it is possible to measure its rotational velocity. The observed rotation curves indicate that the orbital velocities do not decline but in fact remain constant even at distances away from the galactic centres that exceed the visible radii. Thus the mass contained within a radius r must be proportional to that same radius and the absence of luminous matter implies that the necessary mass must be made up of a dark matter component. Similar evidence is found for elliptical galaxies (Carollo *et al.* 1995). The study of gravitational lensing whereby background objects are being lensed by a massive but non-luminous foreground object also adds to the evidence in favour of the existence of dark matter (Tyson *et al.* 1990). The mass of a rich cluster of galaxies such as *e.g.* the Coma cluster relates to the velocity dispersion of the member galaxies by virtue of the virial theorem which can thus be used to get an estimate of the cluster mass. The observed masses of rich clusters are larger than expected from the mass-luminosity ratio of individual galaxies and adds to the necessity for introducing dark matter.

The dark matter models are usually in the form of a fluid containing two non-interacting or weakly interacting components, the first one being the usual baryonic material and the other one being some dissipationless non-baryonic dark matter. Particle physics theories offer a plethora of possible candidates for the dark matter component which are postulated to have been formed in the early stages of the Big Bang. These cosmic relics can be *thermal*, meaning that they remain in thermal equilibrium with the other components of the universe until they decouple, or they can be *non-thermal*. Examples of non-thermal relics are monopoles, axions and cosmic strings. The thermal relics can be subdivided into *hot* or *cold* relics depending on whether they are relativistic or not when they decouple. Massive neutrinos or other weakly interacting massive particles (WIMPs) have been the most favoured candidates particle for the Hot Dark Matter (HDM) scenario and supersymmetric particles (SUSY) such as the neutralino have been suggested for the Cold Dark Matter (CDM) models.

With the dark matter component included, the time of equivalence is reached earlier than when the universe is composed only of baryonic matter. Mass fluctuations can

therefore start evolving well before the time of recombination and will dominate the self-gravity of the combined system. When the baryonic material decouples from the radiation it will thus follow the behaviour of the dark matter. One can define Jeans masses for the dark matter just as in the case of baryons with velocities given as in *e.g.* Coles & Lucchin (1995). Since in general non-baryonic matter does not couple to radiation it is not subjected to Silk dampening. However, dampening caused mainly by *free-streaming* relativistic particles that travel in random directions from high density regions to low density regions will effectively wipe out fluctuations smaller than a certain length scale. The mean distance $\lambda_{\rm fs}$ that a particle travels before it becomes non-relativistic is called the free-streaming length and the corresponding free-streaming mass is defined by $M_{\rm fs} = \frac{\pi}{6} m_X n_X \lambda_{{\rm fs}X}^3$ where m_X is the mass of the dark matter particle and n_X is its number density.

Hot particles become non-relativistic at redshifts $\approx z_{\rm eq}$ and therefore have a large free-streaming distance with corresponding $M_{\rm fs}$ on the order of $10^{14} M_\odot$. HDM scenarios are similar to the adiabatic scenario in that structure is formed top-down with large pancakes being created first that later break down into smaller structures. The problem with this model is that structure forms very late and that it has a difficulty in reproducing the small-scale clustering properties of galaxies. Today HDM has lost almost all support amongst workers in the field.

In the CDM scenario the particles become non-relativistic much before $z_{\rm eq}$ and therefore have a small free-streaming length. The formation of structure resembles that of the isothermal scenario *i.e.* the structure is a result of hierarchical clustering. The CDM scenario is quite successful in modelling the small-scale clustering properties of galaxies and galaxy clusters but predicts fluctuations in the CMBR that are too small. Alternative scenarios have been suggested that try to reconcile the good qualities HDM has on large scales with the success CDM has on small scales. Some of the scenarios involve mixing hot and cold matter in what is sometimes called Mixed Dark Matter or CHDM. Others involve different types of postulated particles that yield Jeans masses in the range of 10^{10} to $10^{12} M_\odot$ and some include a non-zero cosmological constant.

1.4.3 Non-Linear theory

So far structure formation has been discussed in terms of linear theory. When the density contrast reaches values on the order of unity this approximation breaks down and new approaches are needed. Some attempts have been made to find analytic models and others have involved numerical calculations.

Theoretical models

The very simplest non-linear approximations include a spherical collapse model which is used in a simple structure formation scenario in Chapter 4 and will be developed there. However, a more insightful treatment requires more elaborate theories. Only the main ideas of some of the theories are outlined here; for an exhaustive review see Sahni & Coles (1995).

Depending on the degree of non-linear clustering characterised by the *rms* density fluctuation σ, different approximations can be applied. In the so-called quasi-linear regime where the perturbations typically have amplitudes below unity, Zel'dovich (1970) developed an elegant analytic approximation. The *Zel'dovich Approximation* describes a mapping from the Lagrangian space into the Eulerian space at a time t, given by

$$\mathbf{r}(\mathbf{q},t) = a(t)\mathbf{x}(\mathbf{q},t) = a(t)[\mathbf{q} - D(t)\nabla_{\mathbf{q}}\Phi_0(\mathbf{q})] \tag{1.44}$$

where $\mathbf{x}$ is the final (Eulerian) comoving coordinate of a particle initially located at Lagrangian coordinate $\mathbf{q}$, $a(t)$ is the cosmic scale factor, $D(t)$ is a known function that describes the linear growth of perturbations and $\Phi_0(\mathbf{q})$ is the linear potential of the initial velocity field so that $\mathbf{v}_0 \propto \nabla\Phi_0(\mathbf{q})$. The relation between infinitesimal volume elements in Eulerian and Lagrangian space is then equal to the Jacobian of the transformation from $\mathbf{q}$ to $\mathbf{x}$

$$\frac{dV_E}{dV_L} = J\left[\frac{\partial \mathbf{x}}{\partial \mathbf{q}}\right] = \left|\delta_{ij} - D(t)\frac{\partial^2\Phi_0}{\partial q_i \partial q_j}\right| =$$

$$(1 - D(t)\lambda_1(\mathbf{q}))(1 - D(t)\lambda_2(\mathbf{q}))(1 - D(t)\lambda_3(\mathbf{q})) \ , \tag{1.45}$$

where the λs are the eigenvalues of the deformation tensor $\partial^2\Phi/\partial q_i \partial q_j$. Conservation of mass requires that $\rho_0 d^3\mathbf{q} = \rho(\mathbf{x},t)d^3\mathbf{x}$ so that the density distribution is

$$\rho(\mathbf{r},t) = \frac{\rho_0}{a^3}\frac{dV_L}{dV_E} = \frac{\rho_0}{a^3}(1 - D(t)\lambda_1(\mathbf{q}))^{-1}(1 - D(t)\lambda_2(\mathbf{q}))^{-1}(1 - D(t)\lambda_3(\mathbf{q}))^{-1} \quad . \quad (1.46)$$

From this expression we see that the density will become infinite along directions corresponding to the eigenvalues if these are positive. Given a Gaussian potential field one can calculate the probabilities that either one, two or all of the eigenvalues are positive. If only one of the eigenvalues is positive, collapse will occur along one direction and causes the formation of two-dimensional pancakes. It is much less probable that more than one of the eigenvalues are positive but the result of having two or three positive eigenvalues is the creation of one-dimensional filaments and the collapse to a singular point respectively. The Zel'dovich approximation is very accurate in predicting the evolution of the density field until the formation of pancakes and other caustics but breaks down soon after.

In the Zel'dovich approximation, particles can pass right through a pancake without being pulled back by the gravity of the caustic resulting in an artificial broadening and eventually the disappearance of the pancakes. In order to better model gravitational instability in the strong non-linear regime the *adhesion approximation* introduces a viscosity term to mimic the adhesive effects of gravity on small scales and acts to stabilise the caustics.

Numerical Methods

The analytical methods described above can greatly facilitate the understanding of the physical processes of structure formation but one must resort to numerical methods to provide detailed predictions that can be confronted with observations. The simulations are also used to test the validity of analytical approximations assuming that the simulation models which are approximations themselves yield a more accurate representation of the true density field.

The simplest and most straightforward way of performing a simulation is to approximate the fluid by a discrete set of N particles and then calculate the Newtonian force acting on each particle. Assuming that all particles have the same mass m, the force

experienced by a particle located at position $\mathbf{x}_i$ is computed according to

$$\mathbf{F}_i = \sum_{j \neq i} \mathbf{F}_{ij} = \sum_{j \neq i} \frac{Gm^2(\mathbf{x}_j - \mathbf{x}_i)}{(\epsilon^2 + |\mathbf{x}_j - \mathbf{x}_i|^2)^{3/2}} \ , \tag{1.47}$$

where the *softening length* ϵ has been introduced in order to avoid having infinite forces at zero separations. An approximate time evolution of the fluid is then obtained by integrating the equations of motion in small timesteps using the force in (1.47). N-body simulations are normally started at the onset of non-linearity and establishing the initial conditions amounts to generating a realisation of the power spectrum of the scenario to be investigated. In general, the simulation volume is assumed to be cubical with periodic boundary conditions.

The direct summation method described above consumes enormous amounts of CPU time requiring on the order of $N^2/2$ force calculations at each time step. Practical considerations limit the maximum number of particles to about 10^4 which is not sufficient for realistic simulations. Various schemes such as the particle-mesh (PM) technique and extensions of it (P^3M) have been invented to increase computational efficiency. An overview of these methods is given by Klypin (1996).

1.5 Biasing

The observational information of the large-scale structure is given as quantities related to galaxies whereas theory is expressed in terms of the mass density fields. In order to make proper connections between observations and theory one must understand the link between the underlying mass distribution and the positions of galaxies. The most straightforward assumption one can make is that galaxies trace the mass. One way this could be realised is if each galaxy was surrounded by a halo of dark matter with total mass in proportion to the visible mass. However, there is very little evidence in favour of such an argument. Kaiser (1984) suggested that galaxies would form only at the high-density peaks of the mass density field so that the galaxy distribution would be *biased* with respect to the mass distribution. The implication of the peaks biasing model is that the correlation function of the galaxies and matter relate as

$$\xi_{\text{galaxies}}(r) = b^2 \xi_{\text{matter}}(r) \tag{1.48}$$

where b is the *biasing parameter* which is approximately constant, independent of scale and related to the threshold level above which galaxies are assumed to have formed.

Kaiser (1984) was originally concerned with biasing of galaxies relative to clusters of galaxies and observations (*e.g.* Bahcall & West 1992) confirm this type of biasing through the stronger correlation that exists for clusters compared to that of galaxies. Usually the biasing parameter is not defined according to (1.48) but as

$$b^2 = \frac{\sigma_8^2(\text{galaxies})}{\sigma_8^2(\text{mass})} \tag{1.49}$$

where σ_8^2 represents the dimensionless variance in either galaxy counts or mass in spheres of radius $8h^{-1}$ Mpc. It is possible that smaller density peaks that collapse later than the large peaks also should correspond to galaxies and in order to prevent this some mechanisms that inhibit galaxy formation in the lower peaks have to be invoked. The status of the biasing parameter is rather contentious at the moment and one should perhaps see it not as a specific way of relating galaxies to mass but as a way of parametrising the unknown physics that govern galaxy formation.

1.6 Statistical Measures of Structure

Our visual sense is easily deceived and cannot be relied upon for determining whether or not the structure seen in redshift maps is real and to an even lesser extent can it be used for discriminating between contesting structure formation models. It is therefore essential that methods are developed that can describe structure in a quantitative way. Many different approaches have been taken — some of the techniques are successful only in detecting one kind of structure and others treat only one aspect of the galaxy distribution. Thus the quantitative understanding of large scale structures that we have today emerges from a patchwork of results from different methods. Of the great variety of techniques used only the most successful and the most commonly utilised ones are described here.

1.6.1 Correlation Functions

The perhaps most popular of the structure statistics are the correlation functions first suggested by Totsuji & Kihara (1969) and further developed by a number of workers (see Peebles 1980 for a complete account of the theory). The method of using correlation functions is quite general and versatile and can be applied in a number of situations, hence its popularity. Although this method is defined for a discrete distribution of points it also has the advantage of having a corresponding quantity in the continuous

density distribution — the covariance functions — and can consequently be predicted theoretically for a given structure formation scenario.

The correlation functions are useful for determining whether the positions of some objects are dependent on the positions of other objects — as is the case *e.g.* for a clustered distribution of galaxies. The method is general in the sense that it only considers 'points' that are placed according to some statistical distribution. When using observational data to evaluate the correlation function these 'points' can be any kind of objects such as *e.g.* optical galaxies, IRAS galaxies or galaxy clusters.

Definitions

The basic idea of the correlation functions is to compare a given distribution of points with that of a stationary random point process with constant intensity. In a statistically homogeneous spatial distribution of points the probability of finding a point centred in a randomly placed volume element δV is proportional to the size of the element so

$$\delta P = n\delta V \ , \tag{1.50}$$

where the constant of proportionality n is the number density of points. Introducing a second randomly placed volume element separated from the first volume element by a vector $\mathbf{r}_{12}$ the joint probability of finding one object in δV_1 and one object in δV_2 is

$$\delta P = n^2[1 + \xi(r_{12})]\delta V_1 \delta V_2 \tag{1.51}$$

where ξ is the *two-point correlation function* and is a function only of the distance r_{12} and not on the direction of the separation vector. For a random distribution of points evidently $\xi = 0$; if $\xi > 0$ then the points are correlated indicating clustering and if $-1 < \xi < 0$ then the points are anti–correlated indicating dispersion. Generalising (1.51) to include one more point the three- point correlation function is defined in the following way:

$$\delta P = n^3[1 + \xi(r_{12}) + \xi(r_{23}) + \xi(r_{31}) + \zeta(r_{12}, r_{23}, r_{31})]\delta V_1 \delta V_2 \delta V_3 \ . \tag{1.52}$$

The first term comes from the expected contribution from a uniform random distribution. The ξ:s are the two-point correlation functions representing the probability that two points are correlated and the third point is uncorrelated to the other two. ζ

is the contribution to the probability that all three points are correlated and is called the *reduced correlation function.* One can continue to define higher order correlation functions but they become increasingly complicated and difficult to evaluate. It is also possible to define an *angular correlation function* for two-dimensional projected catalogues (see Peebles 1980).

Results

The correlation function is estimated by generating a distribution of objects from a random Poisson point process in a sample volume and subject this distribution to the same selection function as the real data. The estimated ξ is then

$$1+\hat{\xi} = \frac{n_{DD}(r)}{n_{RR}(r)} \tag{1.53}$$

where $n_{DD}(r)$ is the number of pairs with separation r in the actual data catalogue and $n_{RR}(r)$ is the corresponding number of pairs in the random catalogue. There are other ways of estimating ξ that are more robust and less susceptible to boundary effects but the basic idea remains the same. Davis & Peebles (1983) and Shanks *et al.* (1989) found that the two-point correlation function for optical galaxies approximately follows a power law so that

$$\xi(r) = \left(\frac{r_0}{r}\right)^{\gamma} \tag{1.54}$$

where r_0 is the so-called correlation length and γ is a constant. In the interval $0.1h^{-1} \leq r \leq 10h^{-1}$ the estimated values of these two parameters are $r_0 = 5.4 \pm 1h^{-1}$ Mpc and $\gamma = 1.77 \pm 0.04$. A similar analysis was done on Abell clusters and the two-point correlation function was found to have the same power law form as for galaxies. The parameters in this case however have values $r_0 \simeq 12 - 25h^{-1}$ Mpc and $\gamma \simeq 1.8$ in the interval $5h^{-1}$ Mpc $\leq r \leq 75h^{-1}$ Mpc (Bahcall & Soneira 1983). The correlation function for clusters has thus a larger amplitude than for galaxies indicating stronger clustering. Other objects with varying richness also exhibit stronger clustering than galaxies (Bahcall & West 1992).

1.6.2 Detection of Sheets and Filaments

One of the earliest attempts at quantifying the filamentariness was made using a *percolation* technique which yields a measure of the connectedness of a pattern. Suppose

there are N points in a cube with side L. Around each point trace a sphere of diameter $b\ell$ where b is a dimensionless parameter and ℓ is the average separation between points defined as $\ell = LN^{-1/3}$. If the spheres of two points overlap then they are said to be *connected* and chains of connecting points form 'clusters'–following the principle that 'friends of friends are friends'. The terminology is somewhat unfortunate, but of course percolation clusters do not in general correspond to clusters of galaxies.

The number of points that belong to clusters is determined by the parameter b. For small values of b there will be a large number of clusters each containing a small number of points and conversely for large values of b there will be a small number of clusters containing a large number of points. For some value of b a cluster is formed that connects two sides of the cube — the system is then said to have percolated and the value of $b = b_c$ is called the percolation parameter. Depending on the distribution of points different values of b_c will be obtained. For a distribution of points on a cubic lattice obviously $b_c = 1$ and for a Poisson distribution it can be shown that $b_c = 0.86$. A filamentary or sheetlike distribution will percolate more easily than a Poisson distribution so that $b_c < 0.86$ and a distribution where groups of points are isolated percolates with more difficulty so that $b_c > 0.86$. Analyses carried out on galaxy catalogues tend to indicate that $b_c < 0.86$ (Dekel & West 1985) implying that the distribution of galaxies does indeed contain elements of filamentariness and sheetlikeness. More recently Klypin & Shandarin (1993) have suggested some improvements to percolation analysis that tries to confront some of the problems with the original model.

Other methods have been developed that are able to 'recognise' filamentary patterns. One of the more successful of these is the so-called *Minimal Spanning Tree* (MST) technique which uses a graph theoretical method that connects points in a unique way. The method will be described in more detail in Chapters 3 when it is used for investigating the geometrical distribution of voids. Bahvsar & Ling (1988) concluded using the MST technique that filaments do in fact exist. The major inconvenience with the MST is that not many analytical properties are known and can therefore not be used for theoretical predictions.

1.6.3 Voids and Void Probability Function

Since the main type of structure to be studied in this thesis is voids it is interesting to see what statistical methods have been developed for them. The *Void Probability Function* (VPF) makes a connection between the correlation function of a distribution of points and the probability of finding voids of a given size. White (1979) derived the following formula for the probability of finding exactly zero points in a volume V, randomly placed in the sample

$$P_0(V) = \exp\left[\sum_{i=1}^{\infty} \frac{(-n)^i}{i!} \int_{V_i} \cdots \int \zeta_i(r_{ij}) dV_i \ldots dV_i\right] \tag{1.55}$$

where n is the mean number density of galaxies in the sample and ζ_i are the reduced correlation functions of order i. Thus the VPF involves correlation functions of all orders in a symmetric way and therefore yields information that low-order correlation functions do not contain. For a Poisson distribution of points, $\zeta_1 = n$ and all other reduced correlation functions vanish so that the VPF is $P_0 = e^{-nV}$ as expected. A number of studies have been conducted using the VPF; *e.g.* Maurogordato & Lachièze-Rey (1987); (1991), Einasto *et al.* (1991), Vogeley *et al.* (1991); (1994), Little & Weinberg (1994) and most of them seem to support the idea that clustering is hierarchical. Results are not all conclusive but this could be remedied by new more extensive redshift catalogues.

1.6.4 Topology

Another approach to the analysis of large scale structures consists in investigating the topology of the galaxy distribution, *i.e.* to determine its connectivity and examine how filaments, sheets and voids are joined up to form a global pattern. Gott *et al.* (1986); Gott *et al.* (1987) developed a method based on the use of a topological invariant known as the *genus*. Since this method needs a continuous density field the first step is to smooth the discrete galaxy data by applying a filter to it. Let $W(\mathbf{r}_c)$ be the filter function. If the galaxy points have position vectors $\mathbf{r}_i$ then the continuous density at some arbitrary point $\mathbf{r}$ can be written as $\rho(\mathbf{r}) \propto \sum_i W(\mathbf{r} - \mathbf{r}_i)$. In principle it is possible to use any kind of filter but usually there is a preference for a Gaussian function of the form $W(r) = \exp(-r^2/\lambda)$ where λ is the smoothing length. By choosing some threshold level for the density field the volume is divided into over and underdense regions whose contour surfaces can be studied. The genus G of a surface is the number of closed

curves that can be drawn on the surface without cutting it into two separate pieces, or alternatively, the number of holes minus the number of isolated regions. For example one sphere has $G = 0$, two isolated spheres have $G = -2$ and a torus has $G = 1$. The Gauss-Bonnet theorem states that the genus of a two-dimensional surface is given by

$$G = 1 - \frac{4}{\pi}\int_S \kappa dS \tag{1.56}$$

where κ is the intrinsic Gaussian curvature at the location of the surface element dS and the integral is taken over each compact two-dimensional surface. Let ν be the number of standard deviations that the threshold density is away from the mean density. It is usual to divide the genus by the volume of the sample to produce g_s; the genus per unit volume. Hamilton, Gott & Weinberg (1986) derived an analytical expression for the genus per unit volume for a random Gaussian density field as

$$g_s(\nu) = N(1-\nu^2)e^{-\nu^2/2} \ . \tag{1.57}$$

Gott *et al.* (1989) compared observational data smoothed to scales larger that the correlation length r_0 and therefore removed effects of the non-linear evolution of structure. The result indicates that the observed topology is consistent with that of a Gaussian distribution and hence gives support to the model of structure formation where density fluctuations arise from the evolution of Gaussian initial conditions. For smoothing scales smaller than r_0 the topology resembles one where there are isolated high-density regions surrounded by voids.

1.7 Summary

In this Chapter, a brief review of standard Friedmann-Robertson-Walker cosmology and related paradigms has been given. A number of parameters — not all independent but which can each be constrained by various different observations, go into this model. They are the density parameter Ω_0, the Hubble constant H_0, the deceleration parameter q_0, the age of the universe t_0 and sometimes also the cosmological constant Λ. Despite the many observations, there is a fair amount of uncertainty in the measurements of these parameters and much effort in astronomy is directed towards the end of improving our knowledge about their numerical values.

The CMBR provides evidence, by its sheer existence, in favour of the Big Bang model

and along with the observed isotropy of the distribution of galaxies and quasars in different wavelength bands, it also lends support to the Cosmological Principle and thus the FRW models. On smaller scales though, redshift surveys clearly give a visual impression that galaxies are distributed non-uniformly in a cellular network made up of large structures such as clusters, voids and walls. A number of methods have been suggested for quantifying the structure. For example, results from percolation analysis indicate that the sheet-like structures that constitute the 'cell-walls' are real and not simply a visual artefact. Correlation functions which are directly related to the power spectra have been used extensively to investigate the clustering properties of various objects.

The widely accepted view to explain the existence of the observed structures is that they were formed by gravitational instability from small initial density fluctuations. For a number of reasons, Gaussian random fields are the most popular form of initial conditions. They arise naturally from Inflationary theories and they are motivated observationally by Genus analysis which shows that on large enough scales where mass fluctuations are roughly linear, Gaussian characteristics of the density field are registered. Several models have been developed to analytically describe structure formation in the non-linear regime. One such model is the Zel'dovich approximation which predicts the existence of sheets and filaments; another simpler model is the spherical collapse model which will be presented in Chapter 4.

The existence of dark matter has been postulated for a number of reasons. From a theoretical point of view, since structure formation in the dark matter is not inhibited by the radiation pressure in the early universe, larger density fluctuations than possible with just baryonic matter can be produced. Observations of *e.g.* rotation curves in spiral galaxies also support the existence of dark matter. The question of biasing is related to dark matter and exposes the problems of interpreting galaxies as tracers of mass.

This Chapter has discussed the context in which most studies of large-scale structures are done and which therefore represents the main-stream standpoint. However, it should be said that there are a number of alternative and competing cosmologies that are not considered here.

Chapter 2

FVC Void Catalogue

The very largest voids appear as obvious features in any redshift galaxy map and have been picked out visually in earlier literature such as Winkler (1983) and Fairall & Jones (1988). As the number of galaxies in the Southern Redshift Catalogue (Fairall 1994, hereafter SRC) has been steadily increasing and now embodies the redshifts and positions of approximately 16,000 galaxies located in the Southern Hemisphere this has allowed for a more detailed study of the galaxy distribution and has led to the discovery of new voids.

From the SRC, slides of galaxy maps were produced for several distance intervals which enabled Fairall to detect voids by visual inspection in 3 dimensions. The result of this visual search whereby spheres were fitted to the empty regions in the galaxy distribution has been the compilation of the FVC void catalogue (Fairall, in preparation) of which a preliminary version is given in Appendix A. It contains information about the positions of the centroids of the voids and their diameters in redshift units. In FVC, Fairall also marked voids which he considered to belong to well-known wall-like structures.

In most cases Fairall defined the voids as being roughly spherical regions completely devoid of galaxies. However, in the larger voids such as *e.g.* the Eridanus and Microscopium voids he allowed the occasional, isolated galaxy to lie within the boundaries of the void. Also, whenever a 'finger of God' from a major cluster protrudes into an empty region, the entire region has been considered as one single void.

Even if FVC is not an objectively compiled catalogue one could argue that the void identifying process is more 'intelligent' than that of any existing machine algorithm in that it takes into account and removes effects caused by redshift prolongation of clusters. Also, the same arguments used against a void catalogue of this type can be used against the more widely accepted cluster catalogues which also rely on visual identification. Another argument for using FVC is that it gives a direct estimate of the void radii in redshift units.

The aim of this Chapter is to extract some statistics from the catalogue in order to get a better understanding of the quantity and quality of the data. Particular attention will be paid to *void selection effects* which are caused by the influence that sparsely sampled galaxy data has on the detection of voids. A good understanding of these effects is important in subsequent Chapters where FVC is used for the analysis of large-scale structure. Therefore, models for the selection effects will be developed and suggestions will be presented on how to factor out their influence.

2.1 The Crude Catalogue

The term Crude Catalogue simply refers to the unmodified FVC, containing all the voids in the catalogue. Some of the most important features of the catalogue are exposed here for future reference.

2.1.1 The SRC

As the FVC void catalogue was extracted from the SRC it is useful to first have some idea of what selection effects are present in the galaxy catalogue.

Kauffmann (1990) discussed possible selection effects in the SRC in some detail but for our purposes here it is sufficient to consider only the most important ones. The most obvious effect is that the number density of galaxies in the catalogue diminishes with increasing redshift since more distant objects are apparently fainter and consequently more difficult to detect. Secondly, because of the obscuration of galaxies lying behind the Milky Way there is an effect in galactic latitude. The area on the celestial sphere where extinction of light from background objects due to stars in the plane of the Milky Way is important is sometimes called the Zone Of Avoidance (ZOA). The bounding

absolute value of the galactic latitude for the ZOA can be chosen somewhat arbitrarily but most workers use $|b|_{\mathrm{ZOA}}$ in the region of 10° to 20°. Only objects in the Southern Hemisphere are considered so galaxies with declination $> 0°$ are excluded.

The galaxy number density averaged over all angles $\rho(r)$ is shown in figure (2.1) for different values of the bounding galactic latitude of the ZOA. $\rho(r)$ is obtained by excluding points in the ZOA, counting the number of galaxies in 'onion shells' which in this case were of width 250 km s^{-1} and dividing by the volume of the shells. These volumes are thus ones of semi-spherical shells with width $\Delta r = 250$ km s^{-1} with the ZOA cut out of them and are calculated according to

$$V_{\mathrm{shell}}(r) = \frac{2\pi}{3}(1 - \sin|b|_{\mathrm{ZOA}})[(r + \Delta r/2)^3 - (r - \Delta r/2)^3] \ . \qquad (2.1)$$

2.1.2 The Void Catalogue

The FVC catalogue can graphically be represented by plotting the voids in a radius–centroid diagram as in figure (2.2). The data in this figure is equivalent to that contained in the original catalogue except that it does not include any information on the angular distribution of the voids.

An interesting statistic that can be derived from the crude catalogue is the spectrum of voidsizes which is shown in figure (2.3a). The other statistic shown in figure (2.3b) is the fraction of the total volume occupied by voids as a function of distance. The Southern Hemisphere was divided into shells of width 500 km s^{-1} and the volume of voids located partially or entirely in the shell was related to the total volume of the shell. From figure (2.2) there is apparently a trend where smaller voids become scarcer the further away one looks. In order to get a clearer view of how the distance affects the distribution of voids, spectra were produced for four different intervals each of width 2000 km s^{-1} and the result is presented in figure (2.4). It is evident that the number of smaller voids decreases and the proportion of larger voids increases for larger distances. It would be in contradiction with the Cosmological Principle if there was an intrinsic reason for the differing void distributions and must therefore be ascribed to artificial effects that arise from the fact that the number density of points is a function of distance. These effects will be discussed in detail here below.

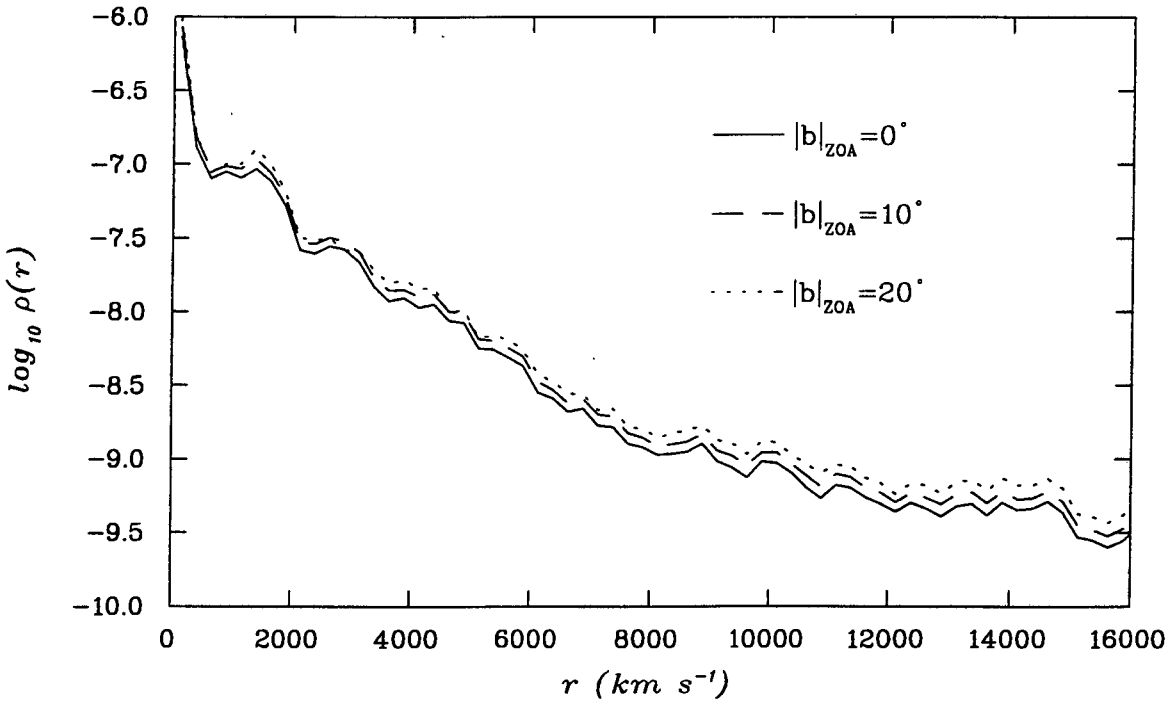

Figure 2.1: Number density of galaxies from the SRC as a function of radial distance for different values of the bounding galactic latitude of the ZOA. ρ is averaged over all angles in the Southern Hemisphere with the ZOA excluded and is given in units of (km s^{-1})$^{-3}$.

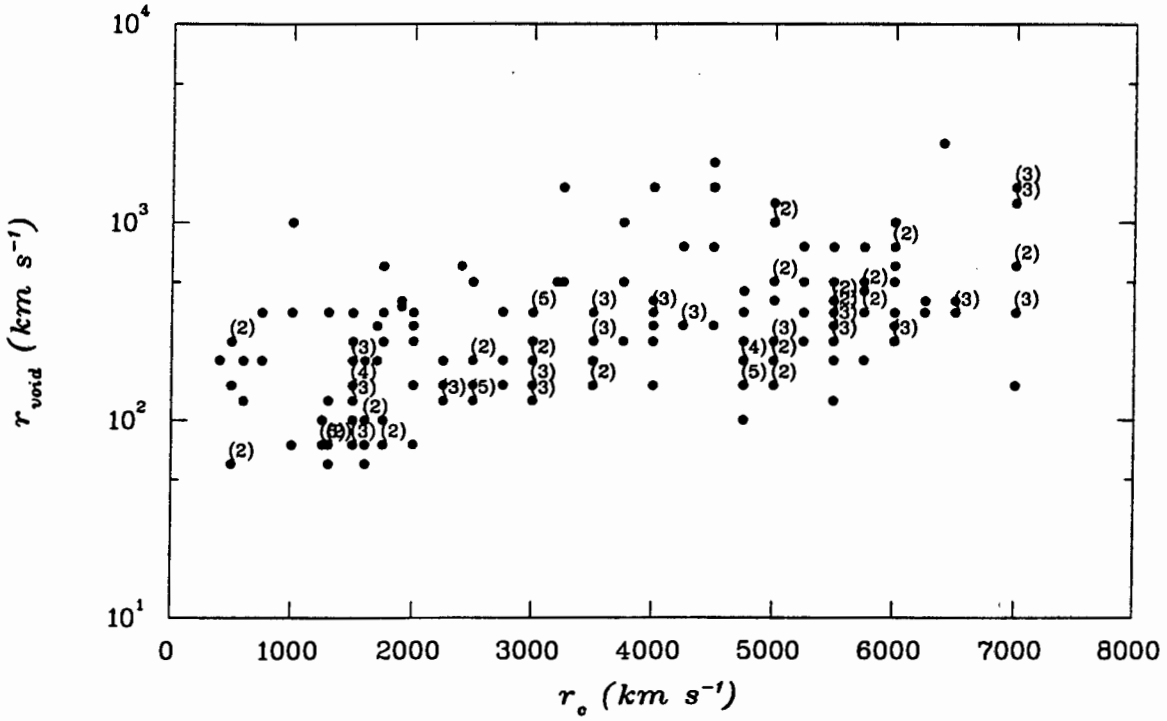

Figure 2.2: Void radii (logarithmic scale) and distance to respective centroids for the voids in the crude FVC catalogue. Numbers in brackets denote the number of voids with a particular radius r_{void} at a particular distance r_c. There is a total of 203 voids.

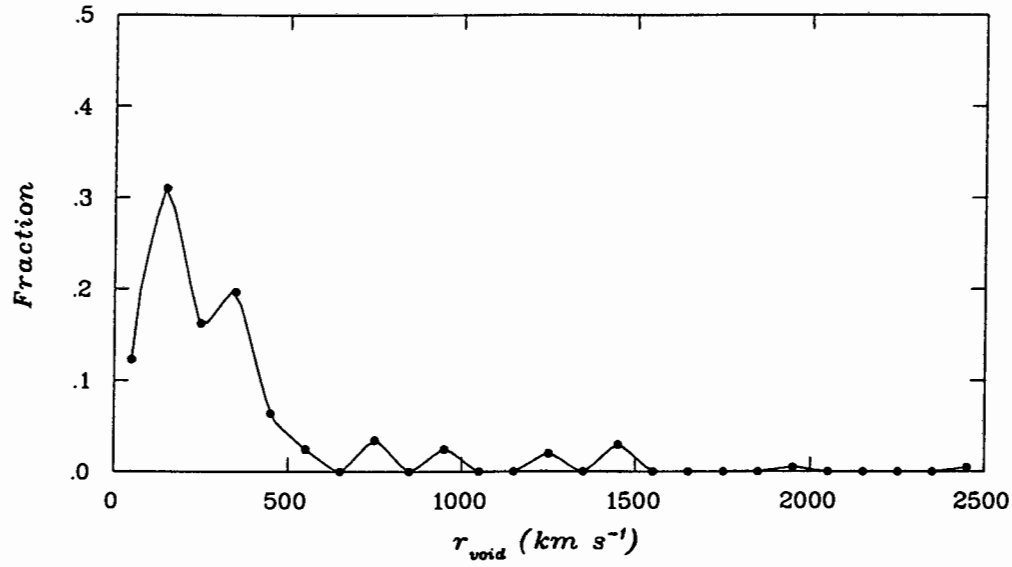

a)

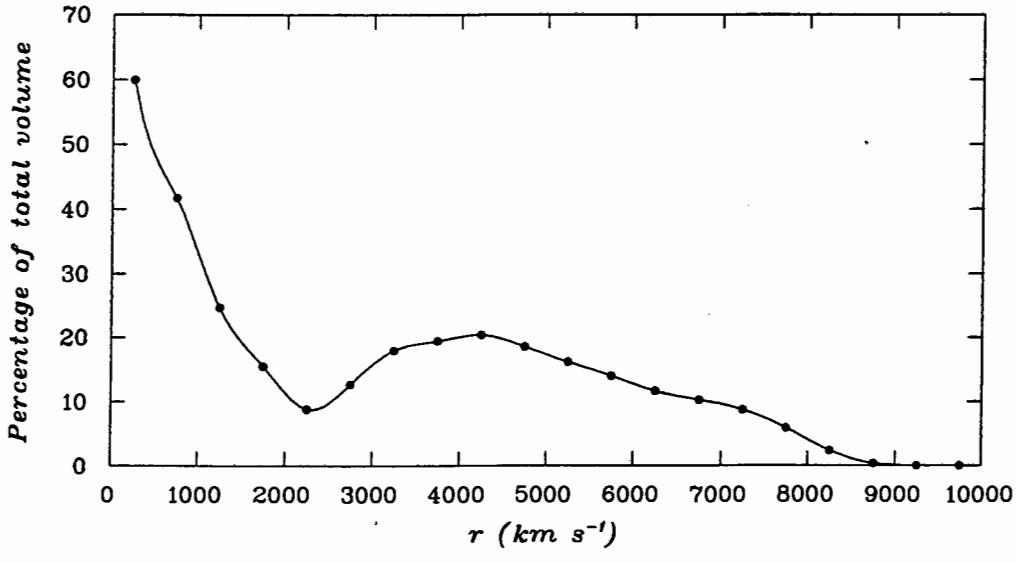

b)

Figure 2.3: a) Voidspectrum of the crude FVC catalogue b) The percentage of total volume occupied by voids as a function of distance. Dots denote the middle points of the binning intervals and curves were interpolated to the data points for reasons of clarity.

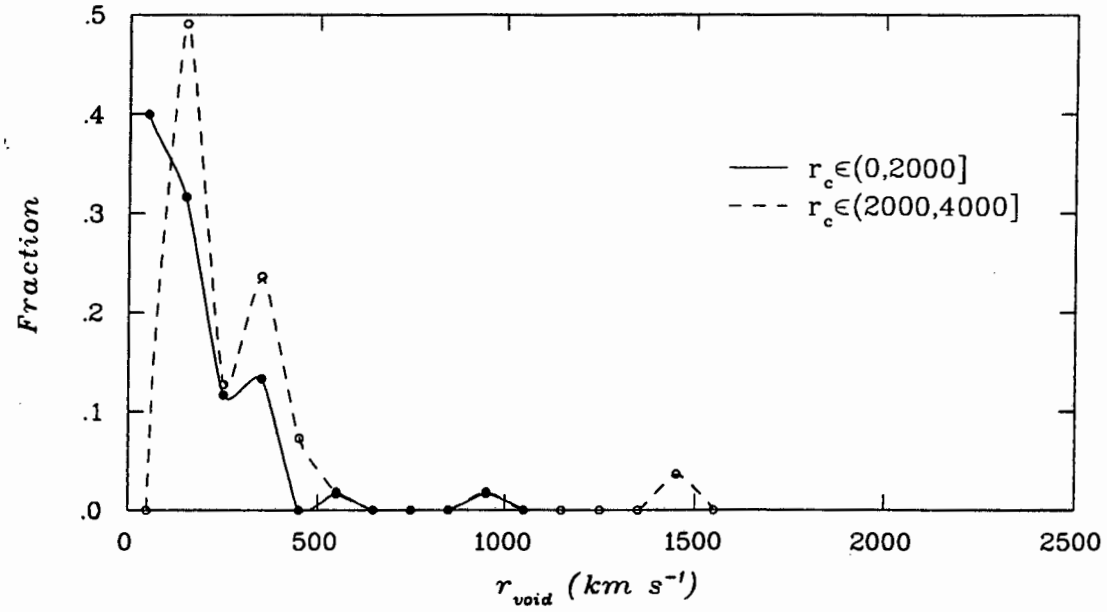

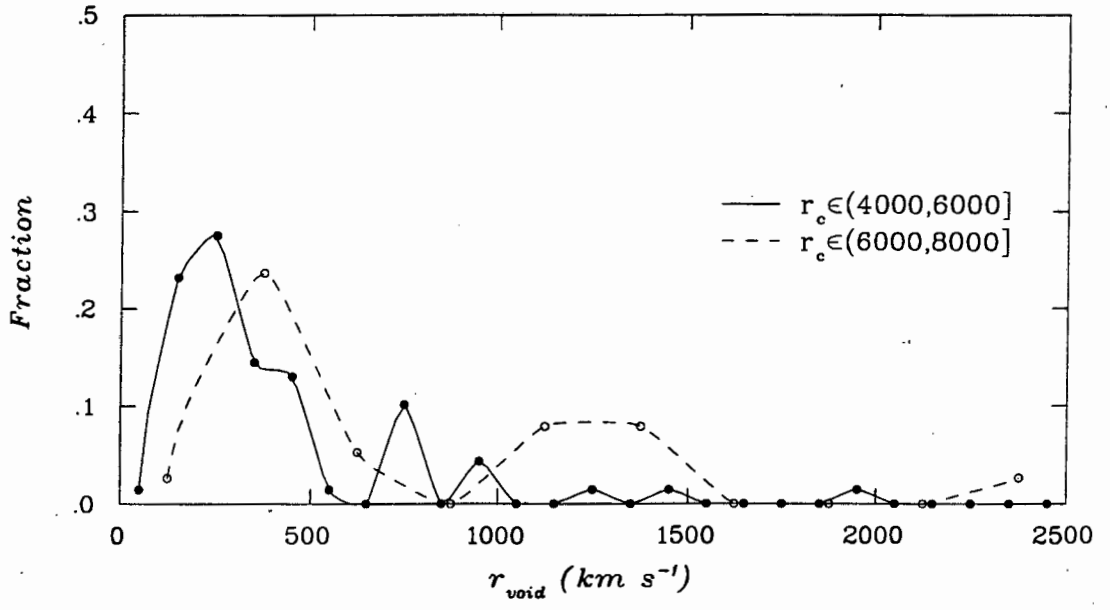

Figure 2.4: Estimated distribution function for void sizes in different distance intervals. Dots denote the mid points of the binning intervals and curves have been interpolated to the data points for reasons of clarity

2.2 Void Selection Effects

Before using the void catalogue it is necessary to investigate to what extent it reflects the true distribution of voids. There is an obvious complication due to the fact that the voids were detected not in real space but in redshift space where the peculiar motions of individual galaxies may distort the shape and size of the voids. Ryden & Melott (1995) compared properties of voids in real and redshift space for two-dimensional simulations of gravitational clustering scenarios with initial power law spectra. They arrived at the conclusion that the sizes of the largest voids increase in going from real to redshift space and they also speculated that the smaller voids in real space are further diminished in redshift space. However it is not clear in which of the two categories the voids in the FVC catalogue fall. As important as it is to investigate the effects of redshift distortion on the voidsizes, such a study would be beyond the scope of this text and therefore the simplistic approach of disregarding these effects is adopted here.

Redshift space distortion is however not the only effect that influences the void catalogue. Normally, the mass distribution in structure formation models is described in terms of a continuous density function whereas the observational data are given as 'pointlike' masses represented by galaxies. In going from the continuous to the discrete description one must, lacking complete knowledge about the galaxy formation process, make some assumption about how the luminous matter traces mass.

The usual interpretation of the presence of galaxies is that they are random realisations of the underlying continuous density field. The most straightforward way of describing this stochastic process is to assume that the probability of finding a galaxy in a small volume around some point $\mathbf{x}$ is proportional to both the continuous mass density $\rho(\mathbf{x})$ and the probabilistic intensity estimated by the mean number of points per unit volume. This is effectively equivalent to assuming the *Poisson clustering model.*

The general viewpoint adopted here is that the structure observed today is a result of a deterministic formation process with initial conditions that are random in some sense. Our universe with its observed distribution of voids and other structures is therefore one particular realisation of an *underlying* distribution in the continuous representation of mass.

Since the information needed to accurately detect the voids is insufficient in the sense that the matter field surrounding the voids is represented by randomly distributed points with a finite probabilistic intensity one would expect the detected distribution of voids to differ somewhat from the underlying distribution. The phenomena that distort the underlying distribution are referred to here as *void selection effects* or sometimes simply as selection effects (not to be confused with the ones associated with the detection of galaxies).

Ideally, one would perform a large number of Monte Carlo simulations with a known underlying distribution of voids and in each case compare with the detected distribution. However, since the identification of voids in FVC is made by visual means, this procedure is impossible to carry out in practice and therefore an analytical description of the selection effects is needed. Arriving at a theoretical model for the selection effects can only be achieved at the cost of making some simplifying assumptions about the underlying structure. We will assume that the underlying voids are perfectly spherical and totally empty and we allow for a local overdensity of galaxies around the boundary of the voids. The volume outside the voids is assumed to be filled with galaxies which are distributed uniformly in a statistical sense.

The selection effects will depend on the background number density of points. The density shown in figure (2.1) is approximately a monotonically decreasing function of distance for a given value of $|b|_{\mathrm{ZOA}}$ so that the selection effects are consequently a function of distance only. There are three different selection effects — each representing a distinct type of error that can be made in the detection process:

1. **Completeness** — real voids are not detected
2. **Authenticity** — non-existent voids are detected
3. **Accuracy** — real voids are detected but with the wrong sizes

These three effects are discussed in more detail in the following sections.

2.2.1 Completeness

In order to detect a void in a galaxy map one cannot simply locate an empty volume of arbitrary size and shape but one must also identify a number of points that are somewhat regularly distributed around the perimeter of the void and therefore demarcate

its extension. If the galaxy data is scarce then there may not be enough points in the vicinity of the void to enable a clear identification of a roughly spherical empty region and the void may therefore escape detection. As the voids in the FVC catalogue were identified by visual inspection, the method of detection is not well defined and any model that attempts to describe this identification procedure must be vaguely enough stated to accommodate for the uncertainty about the nature of the true procedure but strictly enough defined to be useful in practice. The simplified model of the detection process developed here serves as a mental image which is used to arrive at a scaling law valid for all voids.

Take a void of radius r_v and place it entirely in a slightly larger volume with a characteristic size αr_v where $\alpha \gtrsim 1$. Let the space between the larger volume and the void be called 'the neighbourhood' of the void. Imagine that the contour of the void is initially invisible and start placing points randomly in the neighbourhood. The more points that are being added, the more clearly the contour of the void will appear. Let $N_{\min}$ be the minimum number of points required to identify the void. The number density of points around the void is then $\rho \propto N_{\min}/r_v^3$. Note that we do not have to specify exactly what volume we are considering as the volume of the void, the larger volume and consequently the neighbourhood all scale as r_v^3.

Now, take another void of radius r_v' and again place it in a larger volume with characteristic size $\alpha r_v'$. The same number of points in the neighbourhood as before are required to detect the void (zooming in or out does not change the identification procedure) so the minimum local number density for detection therefore scales as

$$\rho_{\min} \propto r_v^{-3} \ . \tag{2.2}$$

So far we have started with a void of a given size and asked ourselves what the minimum required density for detection is. However, what is really more interesting is the converse problem; starting with a region containing a given number of points we want to obtain the minimum size of void that can be detected. Let the average number density of points in this region be ρ. The scaling law (2.2) applies to a local density around the voids and hence allows them to have a ridge of higher density than the average as long as it can be considered to be approximately constant in the neighbourhood.

Bertschinger (1985) investigated different evolutionary scenarios for voids. For com-

pensated voids, the mass from within the boundaries of the void is being pushed out to create a mass surplus around the rim. This causes an overdensity in the neighbourhood of the void which is not necessarily directly proportional to the average background density. In many cases, though, such as when the matter is in the form of a collisional gas and also for uncompensated voids there exists a direct proportionality. Here we will ignore all difficulties involving the local density around the void and simply assume that it is proportional to the background. This assumption is also motivated by the fact that we are investigating the smallest void that can be detected in a given background density and that if the voids have a local overdensity around their perimeter then they will be more easily identified. Therefore by assuming direct proportionality we are in effect considering the worst possible case.

From (2.2), $r_{\min} \propto \rho_{\min}^{-1/3} \propto \rho^{-1/3}$, where $r_{\min}$ is the radius of the smallest void that can be detected in a background density ρ. We can write this proportionality as

$$r_{\min} = \left(\frac{k}{\rho}\right)^{1/3} . \tag{2.3}$$

The constant k is a complicated function which depends on what shape we have chosen for the neighbourhood, what the constant α is, what $N_{\min}$ is and on what the exact relation between the local density and the background is. Instead of determining the parameters that affect k and thereby specifying the detection procedure beyond what is possible considering its subjective nature, the relation (2.3) is assumed to hold for all voids and by comparing the voids in a catalogue one can estimate k. Let $k_i = \rho r_{v,i}^3$ for void i in the catalogue. As $\rho \geq \rho_{\min}$, k_i overestimates the real value of k and we obtain an upper limit for the constant by choosing

$$\hat{k} = \min_{\forall \text{ voids } i}(k_i) . \tag{2.4}$$

Finally, with the estimate for k we can again use formula (2.3) to get a lower limit for the radius of voids that can be detected in a given density ρ.

2.2.2 Authenticity

In the simplified description of the large-scale structure adopted here, the space between the totally empty spherical voids and possibly the regions of local overdensity that surround them is filled with a probabilistically uniform distribution of galaxies. Let $\mathcal{V}$ be a large volume in which there are m real voids, each having a volume V_i. In the

remaining volume $\mathcal{V}_{\rm rem} = \mathcal{V} - \sum_{i=1}^{m} V_i$ it is possible that false voids are detected as a result of statistical fluctuations in the realisation of the underlying uniform distribution of points. It is of course desirable that any void catalogue be ridded of these false voids so that the *authentic* distribution of voids emerges. However, because of the random nature of the occurrence of false voids one can only estimate the probability that a particular voids is real.

In order to calculate the probability of finding a void of a certain volume V in $\mathcal{V}_{\rm rem}$ we cannot use the simple model for the detection procedure outlined in Section 2.2.1 since this would mean having to specify all the parameters in that model. Otto *et al.* (1986, hereafter OPPW) investigated the significance of voids in a spatial distribution of points adopting a somewhat different approach.

Suppose that we have a large volume with points placed randomly in space according to a uniform distribution with constant intensity ρ. The probability of finding a particular region of arbitrary shape and volume V to be completely empty is given by the Poisson formula $P_0(V) = e^{-\rho V}$. However, as argued by OPPW there are infinitely many ways of placing a test volume V and they cannot all be considered independent trials. For example, if one volume V is found to be empty then another volume V displaced by a small distance will also be likely to be empty. If the larger volume $\mathcal{V}_{\rm total}$, in which we place test volumes V, is sufficiently large, then the expected number of voids of a given size scales linearly with $\mathcal{V}_{\rm total}$. OPPW therefore define what they call a *probability per unit total volume* of finding a void with volume V, $\mathbf{P}_0(V)$. For a spherical test volume V this quantity was originally derived in Politzer & Preskill (1986) and is given by

$$\mathbf{P}_0(V) = \frac{3\pi^2}{32}\frac{(\rho V)^3}{V}e^{-\rho V} \quad . \tag{2.5}$$

The name OPPW use for $\mathbf{P}_0(V)$ suggests that the probability of finding a void with volume V in a total volume $\mathcal{V}_{\rm total}$ would simply be $p = \mathbf{P}_0(V)\mathcal{V}_{\rm total}$. However, as the total volume can be chosen to be arbitrarily large, the quantity $\mathbf{P}_0(V)\mathcal{V}_{\rm total}$ can exceed unity so clearly this is not a probability. The argument OPPW used for arriving at expression (2.5) reveals that the quantity p strictly speaking is an expectation value for the number of voids with volume V in a total volume $\mathcal{V}_{\rm total}$. Nevertheless, if the total volume is chosen such that $p < 1$ then it is true that p can be interpreted as the probability of $\mathcal{V}_{\rm total}$ containing one void V.

Suppose the volume $\mathcal{V}_{\rm rem}$ is divided into N equal parts, each with a volume $\mathcal{V}_{\rm total}$ such that $p = \mathbf{P}_0(V)\mathcal{V}_{\rm total} < 1$ and let X represent the random variable that counts the number of voids with volume V in $\mathcal{V}_{\rm rem}$. Thus, the probability of $\mathcal{V}_{\rm total}$ containing a void V is p and regarding each $\mathcal{V}_{\rm total}$ as an independent realisation gives that X is binomially distributed $\mathrm{Bi}(N,p)$. N and $\mathcal{V}_{\rm total}$ depend on how exactly we divide $\mathcal{V}_{\rm rem}$ into subvolumes but if $\mathcal{V}_{\rm rem}$ is very large then N is large enough to enable us to approximate the binomial distribution with a Poisson distribution $\mathrm{Po}(Np)$. The probability of finding x voids with volume V in $\mathcal{V}_{\rm rem}$ is then

$$p_X(x) = e^{-\lambda}\frac{\lambda^x}{x!} \tag{2.6}$$

where $\lambda = Np = N\mathbf{P}_0(V)\mathcal{V}_{\rm total} = \mathcal{V}_{\rm rem}\mathbf{P}_0(V)$. A problem arises when calculating $\mathcal{V}_{\rm rem}$ as we are only supposed to subtract the volumes of the real voids from $\mathcal{V}$ but we cannot know *a priori* which of the voids are in fact real. However, when the volume in which the voids are located is much larger than the volume occupied by the voids we make a small error in equating $\mathcal{V}_{\rm rem}$ with the total volume minus the volume of all voids.

Assume that in $\mathcal{V}_{\rm rem}$ there are $x_{\rm obs}$ voids with volume V. The problem of estimating the probability that these voids are considered to be real when in fact they are false can be formulated as a hypothesis testing. So test

H_0: There are no real voids $\Longleftrightarrow$ X is distributed $p_X(x)$
against
H_1: X is not distributed $p_X(x)$.

The test statistic used to accept or reject H_0 is obviously the observed value $x_{\rm obs}$ and the *significance* of the test for a given value of $x_{\rm obs}$ is

$$\alpha(x_{\rm obs}) = P(\mathrm{reject}H_0|H_0 \text{ is true}) = P(\text{accepting false voids}) \ .$$

Since the hypothesis H_0 entails the total absence of structure in $\mathcal{V}_{\rm rem}$ voids must be more likely under the alternative hypothesis H_1 which thereby implies that the test must be one-sided so that

$$\alpha(x_{\rm obs}) = P(X \geq x_{\rm obs}) = \sum_{i=x_{\rm obs}}^{\infty} p_X(i) = 1 - \sum_{i=0}^{x_{\rm obs}-1} p_X(i) \ .$$

By choosing a maximum allowed value for α we have obtained a method for weeding out voids that are considered to be false at that significance level. Note that we cannot distinguish between the $x_{\rm obs}$ individual voids which must hence be collectively either accepted as real or rejected as false.

2.2.3 Accuracy

Assume that the voids have a density profile such that the density is zero in $r < r_u$ and constant ρ in $r \geq r_u$. There is a non-zero probability that, given that a void has radius r_u in the continuous mass representation, it will be detected as having radius $r_v > r_u$. The conditional probability of this happening is

$$P(r_u \leq \text{Detected radius} \leq r_v | \text{Underlying radius} = r_u) = 1 - \exp(\frac{4\pi}{3}\rho(r_v^3 - r_u^3)) \ . \quad (2.7)$$

We are interested in estimating the error that is made in the determination of the void radii and therefore it would be pertinent to evaluate the probability

$$P(\text{Underlying radius} \leq r_u | \text{Detected radius} = r_v) \ .$$

However, this requires knowledge about the probability distributions of both the detected void radii and the underlying void radii, the latter of which is not available. We can nevertheless ask ourselves what the maximum detected void radius should be for a satisfactorily high probability given that the underlying radius is r_u. Setting this probability to β in equation (2.7) and solving for r_v we obtain

$$r_v = r_u \left(1 - \frac{3}{4\pi\rho r_u^3} \ln(1-\beta)\right)^{1/3} \ . \quad (2.8)$$

The relative error $\delta r = (r_v - r_u)/r_u$ grows with decreasing density and decreasing r_u so that the least accurate radii are the ones of small voids located at large distances. Some numerical examples are given here for $\beta = 0.9$ so that for example there is a 90 % probability that a void with underlying radius 500 km s^{-1} located at a distance of 2000 km s^{-1} will have a detected radius with an error of less than 4 %.

	$r_u = 500$	$r_u = 1000$
$r_c = 2000 \Rightarrow \rho \sim 10^{-7.5}$	$\delta r \leq 4\%$	$\delta r \leq 0.5\%$
$r_c = 4000 \Rightarrow \rho \sim 10^{-8}$	$\delta r \leq 13\%$	$\delta r \leq 2\%$
$r_c = 6000 \Rightarrow \rho \sim 10^{-8.5}$	$\delta r \leq 33\%$	$\delta r \leq 5\%$

The error in the measurement of the redshift also adds to the uncertainty in the void radii with typically a few percent for the largest voids. As mostly we will be using the larger voids as data in subsequent analysis we can, for any practical purposes, ignore the uncertainty in the void radii and regard them as exact.

2.2.4 Remarks

We now have a model for the selection effects and a prescription for how to at least partly correct for them. First, false voids are eliminated at some significance level and then the constant k is estimated by choosing the minimum k_i of all voids. Then, for a chosen value of the smallest void radius r_s we are interested in, a distance of completeness r_{compl} is calculated according to equation (2.3) so that the relation

$$\rho(r_{\text{compl}}) = \frac{\hat{k}}{r_s^3} \tag{2.9}$$

is satisfied. Now, all the voids with radii $r_v \geq r_s$ lying in the distance interval $0 \leq r_c \leq r_{\text{compl}}$ are then included in the selection which it thus complete and authentic.

Ideally, this method would provide a way of determining the underlying distribution of voids from the information available in FVC. The exact nature of the selection effects is however not known and the corrective procedure does not entirely remove even the modelled selection effects. Producing Monte Carlo simulations would be the only way of testing the efficacy of the corrective procedure but this would require an automated void search with the same resolution as the visual search. In the following it will simply be assumed that the corrective procedures applied to FVC yields an approximation to the underlying distribution.

Chapter 3

Geometrical Analysis of the Void Distribution

On scales comparable to the extension of the redshift catalogues there is ample evidence for the existence of large voids that are surrounded by walls and filaments. A more detailed visual inspection of the SRC and in particular of the walls reveals a large number of smaller voids that seem to be contained within the thickness of these planar structures (Fairall, private communication). In order to test this hypothesis, some method must be devised that can objectively quantify the degree to which smaller voids are distributed in sheetlike structures. It also seems that larger voids surround the sheetlike structures and are distributed roughly isotropically An attempt will be made to establish a connection between these voids and the Abell clusters which will later be used in subsequent Chapter to infer a constraint on the density paramter Ω.

Traditional statistical measures of structure such as the lower order correlation functions are not very sensitive to geometrical patterns since the statistical quantity is computed over all space. Other methods that measure the geometry of a distribution more efficiently include the alignment statistics of Kuhn & Uson (1982), the ridge-finding algorithm (Moody *et al.* 1983), the quadrupole statistics of Fry (1985) and Vishniac (1986), the minimal spanning tree technique (Barrow *et al.* 1985), Bahvsar & Ling (1988) and the structure functions of Babul & Starkman (1992). Here a hybrid method that uses a combination of both minimal spanning trees and structure functions will be used much in the way outlined by Pearson & Coles (1995).

3.1 MST

The minimal spanning tree (MST) technique uses concepts that originate in graph theory (Ore 1962). Zahn (1971) developed the MST algorithm further and adopted it to a number of different applications such as the analysis of bubble-chamber particle tracks.

The basic idea of the MST is to connect a set of spatially distributed data points by a *graph*. Following the terminology of Barrow *et al.* (1985, hereafter BBS) the graph consists of *nodes* which correspond to the data points and *edges* which are the straight lines joining two nodes. The number of edges emanating from a node is called its *degree*. A sequence of joining edges is called a *path* and a closed path is referred to as a *circuit*. If there is at least one path between any two nodes then the graph is *connected* and if in addition there are no circuits then the graph is called a *tree*. The tree of a connected graph that contains all the nodes in a data set is called a *spanning tree* and if the length of the tree defined as the linear sum of edgelengths is minimised then it is a *minimal spanning tree* (MST). According to a theorem (see *e.g.* Zahn 1971) the MST is *unique* if no two edgelengths are equal and this is the property that makes the MST useful.

There are two known algorithms for constructing the MST, both of which are presented in Zahn (1971). The one chosen to be used here was originally formulated in a paper by Prim (1957).

Begin with an arbitrary node in the graph G and add the shortest edge from this node. The two nodes with the connecting edge now constitute the first partial tree T_1. Now assume that $k-1$ edges have been joined to the tree. The kth node is added by choosing the shortest edge from any node in the partial tree T_{k-1} to any of the remaining nodes in G that do not belong to T_{k-1}. This procedure continues until all the nodes have been connected.

The MST technique is designed to emphasise the dominant features of a distribution of points by building a skeletal structure to trace it. BBS point out how the method to some extent mimics the human eye's propensity to recognise patterns that result from nearest neighbour effects. There will certainly always be nodes that do not directly

belong to the principal underlying structure and which can be considered to exist as a result of statistical noise. Also, in the MST there may be chance connections between separate structures. There are two operations that can be performed on the MST in order to reduce the noise so that the underlying structure appears more clearly — these are *pruning* and *separating*.

Let a k–branch be a path of k edges that connect a node of degree 1 to a node of degree > 2 where all the intervening nodes are of degree 2. The MST is said to be pruned to a level p when all k–branches with $k \leq p$ are removed. Performing this operation therefore removes the 'foliage' on the MST and therefore enhances the main structure. A separated tree is obtained by removing any edges with length exceeding some given value which is often chosen as a multiple m of the average edgelength $\langle l \rangle$. Any 'accidental' connections due to low point densities are eliminated and enables distinct subclusters to be isolated. The pruned and separated MST will in general consist of several disjoint pieces that can be analysed separately.

Lacking analytical methods of estimating the optimal values for the pruning parameter p and the separation length $m\,\langle l \rangle$ they are normally chosen according to a trial-and-error procedure. The optimal values for the parameters depend on the point distribution and on the structure to be detected — most likely different values should be chosen if the aim is to detect filaments or if it is to detect clusters. Pruning should be used cautiously for structures that extend to 2 or 3 dimensions as any points removed could cause erroneous conclusions to be made about the full spatial distribution of the structure. Great care should be taken in carrying out the separation operation when there is suspicion that structures are intersecting as the aggregated structure could be broken off at the 'wrong' places and therefore create patterns that do not exist.

3.1.1 Statistics on the MST

The MST algorithm picks out the main features of a given point pattern with a high signal-to-noise ratio but it does not in its own right constitute a statistical descriptor. Various quantities have been suggested as measures of structure, such as the frequency distribution of edgelengths (BBS) and the moments of inertia combined with structure functions (Pearson & Coles 1995). The latter method is the one preferred here.

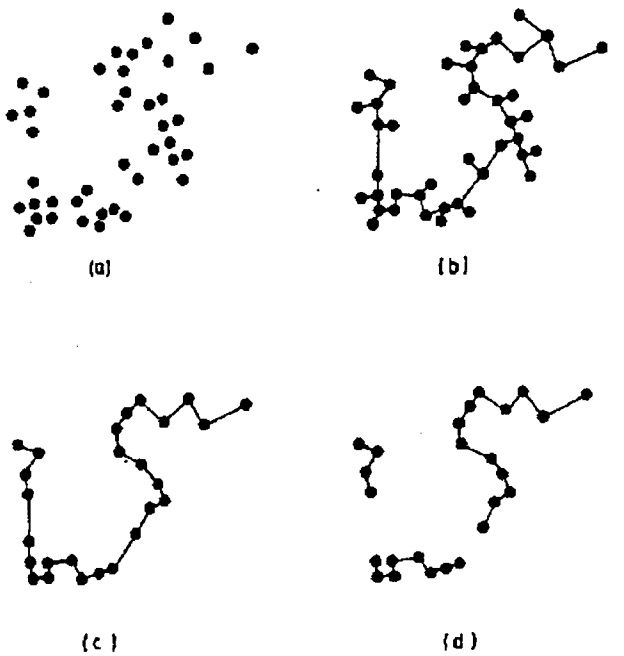

Figure 3.1: The construction and reduction of a MST adapted from Barrow *et al.* (1985). (a) The set of data points. (b) The MST constructed according to the algorithm described in text. (c) Remaining MST after pruning operation at a level 2. (d) Separated MST.

Moments of Inertia

In classical dynamics, the moment of inertia is used as a natural quantity for describing the matter distribution of mechanical bodies. Babul & Starkman (1992) defined and calculated the moments of inertia for point distributions and Pearson & Coles (1995) applied this to points belonging to MST:s.

Assume that in a piece of a pruned and separated tree there is a set of N nodes located at position vectors $\mathbf{r}^{(k)}$ where $k = 1, \ldots, N$. In mechanics the contribution to the moment of inertia of each point is weighed by its mass but since only the distribution of points is important here, every node is weighed by an equal amount so that effectively they are all assigned a unit mass. Define the local moment of inertia of each piece of the MST about its centre of mass as

$$I_{ij} = M_{ij} - M_i M_j \tag{3.1}$$

where M_i and M_{ij} are the first and second moments of the distribution respectively and are defined as

$$\begin{aligned} M_i &\equiv \frac{1}{N} \sum_{k \in \text{ MST}} r_i^{(k)} , \\ M_{ij} &\equiv \frac{1}{N} \sum_{k \in \text{ MST}} r_i^{(k)} r_j^{(k)} . \end{aligned} \tag{3.2}$$

The index k labels the N nodes in the tree and indices i and j take on values $1, 2, 3$ and denote the components of the position vectors. At first sight it may seem that equation (3.1) does not correspond to the standard definition of the moment of inertia but rewriting the equations by replacing the position vectors which are relative to an arbitrary origin with vectors originating from the centre of mass will make the expression take on a more familiar form. Let $\mathbf{G}$ be the position vector of the centre of mass with respect to the origin and let it be defined as $\mathbf{G} \equiv \frac{1}{N} \sum \mathbf{r}^{(k)}$. Let furthermore $\boldsymbol{\rho}^{(k)}$ be the vector from the centre of mass to the kth point in the MST so that $\mathbf{r}^{(k)} = \mathbf{G} + \boldsymbol{\rho}^{(k)}$. Then the first and second order moments can be written as

$$\begin{aligned} M_i &= G_i , \\ M_{ij} &= G_i G_j + \tfrac{1}{N} \textstyle\sum_k \rho_i^{(k)} \rho_j^{(k)} , \end{aligned} \tag{3.3}$$

which gives the moment of inertia as

$$I_{ij} = \frac{1}{N} \sum_k \rho_i^{(k)} \rho_j^{(k)} . \tag{3.4}$$

I_{ij} is a second order symmetric tensor and can be described by a 3×3 matrix. The first submatrix

$$\{I\}_{\text{sub1}} = \begin{pmatrix} I_{11} & I_{12} \\ I_{21} & I_{22} \end{pmatrix} \tag{3.5}$$

has the determinant $\det\{I\}_{\text{sub1}} = I_{11}I_{22} - I_{12}^2$. Cauchy's inequality states that for any two sequences of numbers $x^{(k)}$ and $y^{(k)}$ the following relation holds; $\left(\sum x^{(k)}y^{(k)}\right)^2 \leq \sum(x^{(k)})^2 \sum(y^{(k)})^2$ with equality if and only if $y^{(k)} = Cx^{(k)}$ where C is a constant. This implies that the determinant of the first submatrix $\det\{I\}_{\text{sub1}} \geq 0$. The second submatrix of I_{ij} is simply I_{11} which of course is non-negative since it is a sum of squares. According to a well-known result of linear algebra, a matrix that has non-negative determinants of its submatrices is semi positive definite so that all its eigenvalues are non-negative. Since in addition I_{ij} is symmetric, the eigenvalues, which are sometimes called the principal moments of inertia, are guaranteed to be real. The eigenvalues are independent of the choice of coordinates and characterise the structure uniquely except for its orientation and for the location of the centre of mass. Regarding I_{ij} as a tensor, the set of principal moments of inertia define a triaxial spheroidal tensor surface which is completely determined up to rotations. Hereafter let I_1, I_2, I_3 be the eigenvalues of I_{ij} sorted into decreasing order of magnitude.

Structure Functions

Following Babul & Starkman (1992), two parameters μ and ν are defined in terms of the ratios between the principal moments of inertia by

$$\begin{aligned} \mu &= \left(\frac{I_2}{I_1}\right)^{1/2} , \\ \nu &= \left(\frac{I_3}{I_1}\right)^{1/2} . \end{aligned} \tag{3.6}$$

These parameters then do not depend on the actual size of the structure but only on its shape. Now define three *structure functions* as

$$\begin{aligned} S_1 &\equiv \sin\left[\tfrac{\pi}{2}(1-\nu)^p\right] , \\ S_2 &\equiv \sin\left[\tfrac{\pi}{2}a(\mu,\nu)\right] , \\ S_3 &\equiv \sin\left(\tfrac{\pi}{2}\nu\right) , \end{aligned} \tag{3.7}$$

I_{ij} is a second order symmetric tensor and can be described by a 3×3 matrix. The first submatrix

$$\{I\}_{\text{subl}} = \begin{pmatrix} I_{11} & I_{12} \\ I_{21} & I_{22} \end{pmatrix} \tag{3.5}$$

has the determinant $\det\{I\}_{\text{subl}} = I_{11}I_{22} - I_{12}^2$. Cauchy's inequality states that for any two sequences of numbers $x^{(k)}$ and $y^{(k)}$ the following relation holds; $\left(\sum x^{(k)}y^{(k)}\right)^2 \leq \sum(x^{(k)})^2 \sum(y^{(k)})^2$ with equality if and only if $y^{(k)} = Cx^{(k)}$ where C is a constant. This implies that the determinant of the first submatrix $\det\{I\}_{\text{subl}} \geq 0$. The second submatrix of I_{ij} is simply I_{11} which of course is non-negative since it is a sum of squares. According to a well-known result of linear algebra, a matrix that has non-negative determinants of its submatrices is semi positive definite so that all its eigenvalues are non-negative. Since in addition I_{ij} is symmetric, the eigenvalues, which are sometimes called the principal moments of inertia, are guaranteed to be real. The eigenvalues are independent of the choice of coordinates and characterise the structure uniquely except for its orientation and for the location of the centre of mass. Regarding I_{ij} as a tensor, the set of principal moments of inertia define a triaxial spheroidal tensor surface which is completely determined up to rotations. Hereafter let I_1, I_2, I_3 be the eigenvalues of I_{ij} sorted into decreasing order of magnitude.

Structure Functions

Following Babul & Starkman (1992), two parameters μ and ν are defined in terms of the ratios between the principal moments of inertia by

$$\begin{aligned} \mu &= \left(\frac{I_2}{I_1}\right)^{1/2}, \\ \nu &= \left(\frac{I_3}{I_1}\right)^{1/2}. \end{aligned} \tag{3.6}$$

These parameters then do not depend on the actual size of the structure but only on its shape. Now define three *structure functions* as

$$\begin{aligned} S_1 &\equiv \sin\left[\tfrac{\pi}{2}(1-\nu)^p\right], \\ S_2 &\equiv \sin\left[\tfrac{\pi}{2}a(\mu,\nu)\right], \\ S_3 &\equiv \sin\left(\tfrac{\pi}{2}\nu\right), \end{aligned} \tag{3.7}$$

where the exponent $p = \log(3)/\log(1.5)$ and the function $a(\mu, \nu)$ is defined by

$$\frac{\nu^2}{a^2} - \frac{\mu^2}{a^2(1 - \alpha a^{1/3} + \beta a^{2/3})} = 1 \ . \tag{3.8}$$

The parameters α and β are chosen as

$$\begin{aligned} \alpha &= 1.9 \ , \\ \beta &= -\left(\tfrac{7}{8}\right) 9^{1/3} + \alpha 3^{1/3} \ . \end{aligned} \tag{3.9}$$

This choice for α and β ensures that the family of hyperbolae in the $\mu - \nu$ plane which are parametrised by the function $a(\mu, \nu)$ are non–intersecting (nested) . Figure (3.2) shows the contours of $a(\mu, \nu)$ in the $\mu - \nu$ parameter space where $0 \leq \nu \leq 1$ and $0 \leq \mu \leq \nu$. The line $\mu = \nu$ corresponds to the case when $a \to 0$ and the point $(\mu, \nu) = (0, 1)$ corresponds to the case when $a = 1$. The structure functions S_1, S_2 and S_3 are designed to be measures of *prolateness* (filamentariness), *oblateness* (sheet-likeness) and *uniformity* (sphericity) respectively. For a distribution of points along a straight line, two of the principal moments of inertia vanish so that both μ and ν equal zero giving $(S_1, S_2, S_3) = (1, 0, 0)$. A symmetric 2-dimensional sheetlike distribution will have one principal moment of inertial vanishing and the other two equal yielding $\nu = 1$ and $\mu = 0$ which corresponds to $(S_1, S_2, S_3) = (0, 1, 0)$. For a spherical distribution all the principal moments of inertia are equal so that $\nu = \mu = 1$ which implies that the set of structure functions take on the values $(S_1, S_2, S_3) = (0, 0, 1)$.

In practice no random distribution is perfectly spherical, no filaments are entirely straight and no sheets are without curvature and thickness. Any deviations from the idealised shapes of the distribution will affect the structure functions so that each of the three numbers take on any values ranging from 0 to 1. Given a set of numerical values for the structure functions, the question of determining exactly what kind of structure this represents is of course somewhat arbitrary but figure (3.2) gives an indication of when the transition from one type of structure to another is made.

3.2 Wall and Non-Wall Voids

Walls appear in the galaxy maps as roughly planar regions of galaxy overdensities surrounded by large voids. Fairall investigated four major walls — Centaurus, Fornax,

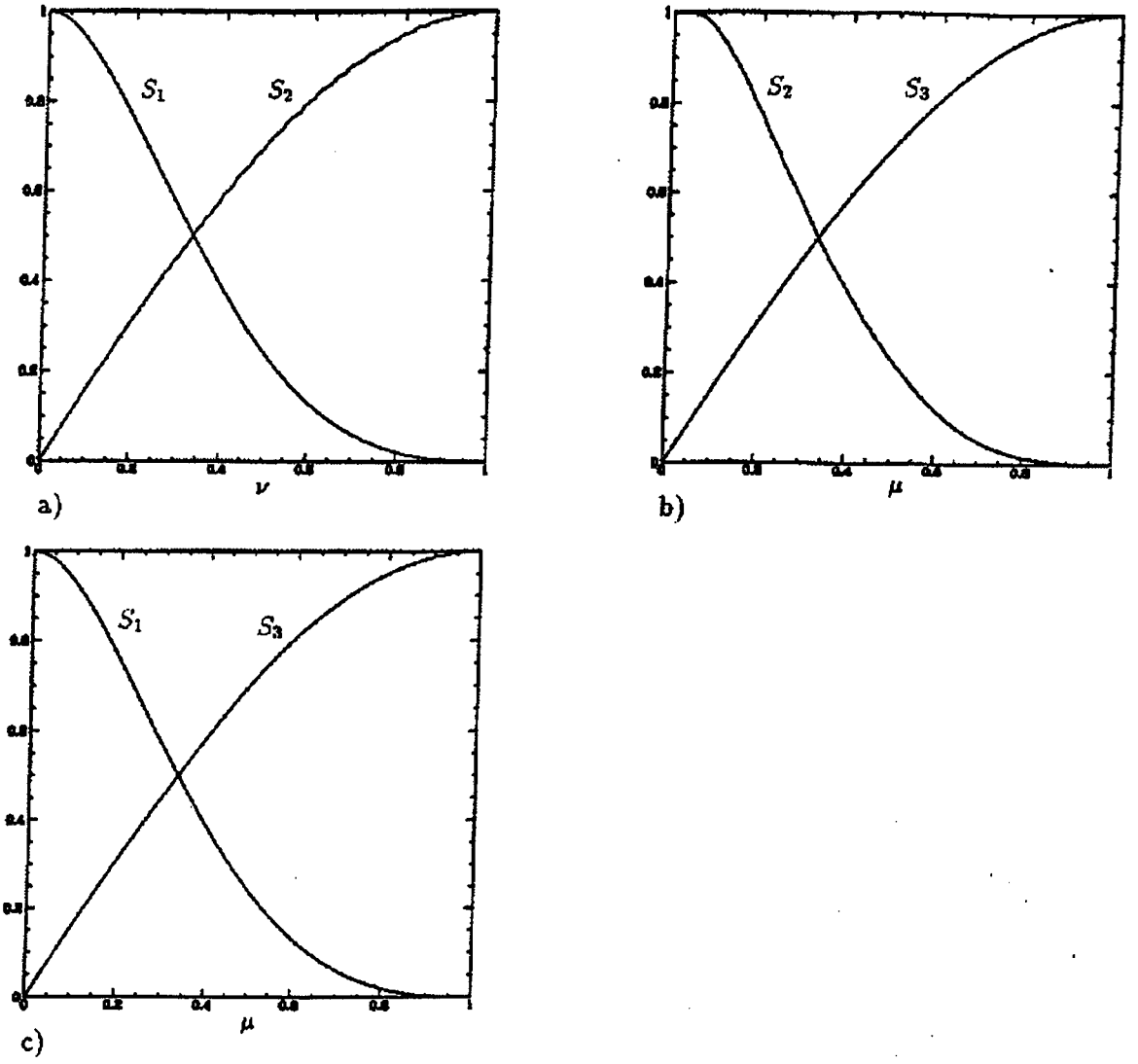

Figure 3.2: $\mu - \nu$ Parameter space adapted from Babul & Starkman (1992). a) $\mu = 0$, transition from a filament to a disc, b) $\nu = 1$, transition from a disk to a sphere, c) $\mu = \nu$, transition from a filament to a sphere. In each diagram, the structure function not shown is identically zero.

Hydra and Sculptor in which he identified embedded voids that were then added to the FVC.

The FVC can therefore be divided into five different subcatalogues — four catalogues for the voids marked by Fairall as pertaining to each of the walls and one for the remaining non-wall voids. First, we will subject the wall catalogues to an MST analysis in order to remove voids that may have erroneously been identified by Fairall as belonging to a particular wall. In addition, the results from this analysis are confirmed by visual inspection carried out on a Silicon Graphics work station where programs written in the computer language iIsh [1] enable an interactive display of the physical distribution of voids in three dimensions.

Having separated the wall voids from the non-wall voids, an analysis can be carried out on these two different constituents of structure independently. The objective of this study is to get an indication of typical void sizes and in the case of the non-wall voids also their spatial distribution.

3.2.1 MST Removal of Non-Wall Voids

As mentioned before there is no *a priori* way of analytically determining the optimal values for the pruning parameter and separation length which instead have to be chosen according to a trial-and-error procedure. Some criteria must be imposed on the structure functions so that when met they define the optimal values for these parameters. Since the aim of this analysis is to remove voids that do not belong to the walls, any desirable operation performed on the MST should result in an increased value of the oblateness structure function S_2 which is hence the quantity to be optimised. Obviously a perfectly planar structure is obtained if all but three points are removed. Therefore, in order to prevent excessive removal of voids from the subcatalogues we must in addition require that after operations on the MST there will be one tree containing most of the voids for which S_2 is maximal and that the number of separated-away voids is small.

Comments about the MST analyses for each wall-void catalogue are found in the captions of figures (3.3)–(3.6) which depict the wall voids in different angles. The positions

[1] Kindly provided by Prof. H. Goosen, formerly of the UCT Computer Science Department

Wall	R.A. (h)	dec(°)	r_c	r_{void}
Centaurus	22.3	-20	5500	350
Fornax	17.7	-50	3500	250
Fornax	19.4	-48	3500	200
Fornax	17.6	-83	3000	150
Hydra	15.0	-22	2750	150
Hydra	10.2	-26	4000	300
Hydra	10.4	-18	4000	350
Hydra	14.7	-34	6000	600
Hydra	15.6	-35	6000	300
Hydra	15.4	-27	5500	400
Sculptor	9.9	-64	3000	150
Sculptor*	2.9	-82	4750	150
Sculptor*	8.0	-80	4750	350

Table 3.1: Removed voids, r_c and r_{void} are in redshift units. Voids labelled with an asterisk were marked in the FVC as uncertain to belong to a wall.

of the voids in the Cartesian coordinate system for which the axes are shown in the figures were calculated according the following simple transformation

$$\begin{aligned} x &= r_c \cos(\alpha)\cos(\delta) , \\ y &= r_c \sin(\alpha)\cos(\delta) , \\ z &= r_c \sin(\delta) , \end{aligned}$$

Π where r_c is the distance to the centre of the void in redshift units, α is the Right Ascension coordinate and δ is the declination. In the figures, the length of the positive part of the axes corresponds to a distance of 1500 km s^{-1} . Table (3.1) contains the voids which have been singled out for removal from the wall subcatalogues and which are added to the non-wall void catalogue. After the MST removal there were a total of 121 wall voids and 82 non-wall voids.

3.2.2 Distribution of Wall Voids

The volumes of the walls are relatively small — at most the walls extend to only a few typical void diameters square with a thickness of a couple of void diameters. This

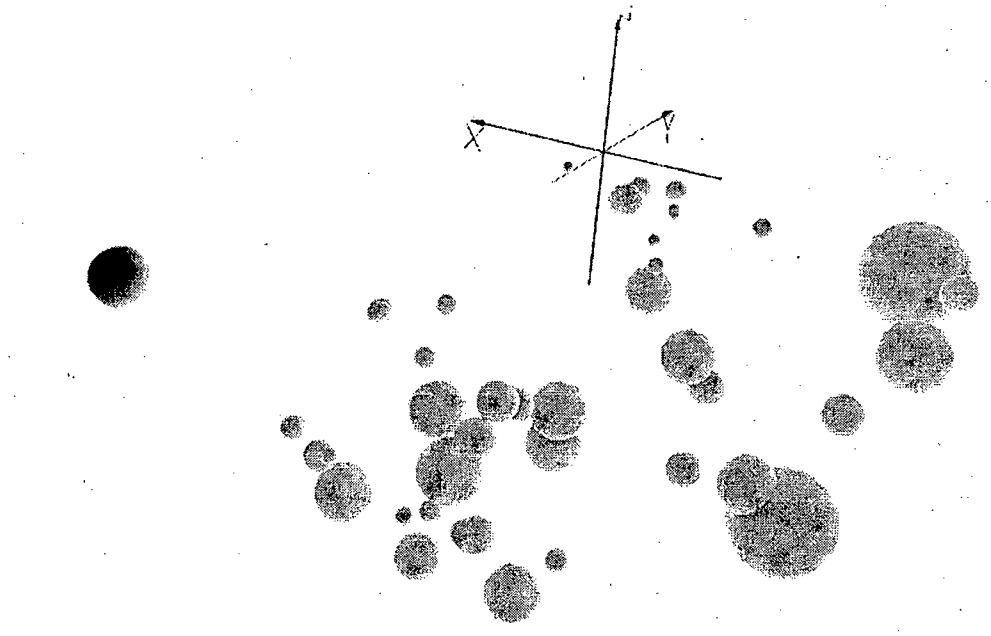

a)

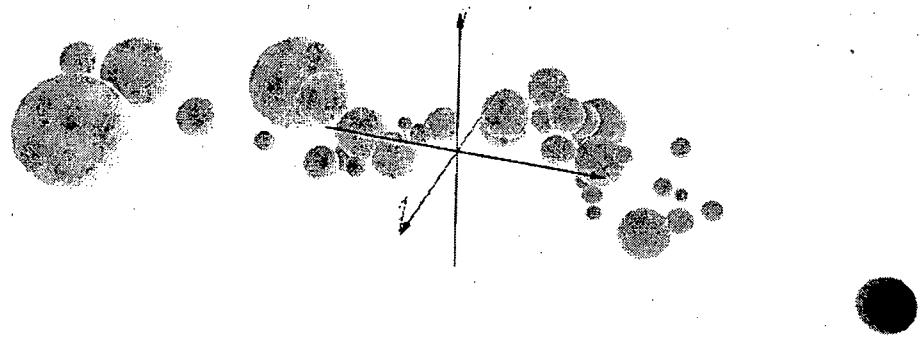

b)

Figure 3.3: Centaurus wall voids a) face on, b) side view. It is clear from visual appearance that there is one void that does not belong to the main structure. Edgelength statistics showed that one of the connections was considerably longer than the average and a separation factor of 2.5 removed that edge. Pruning did not affect the oblateness structure function which at its maximum had the value of approximately 0.52.

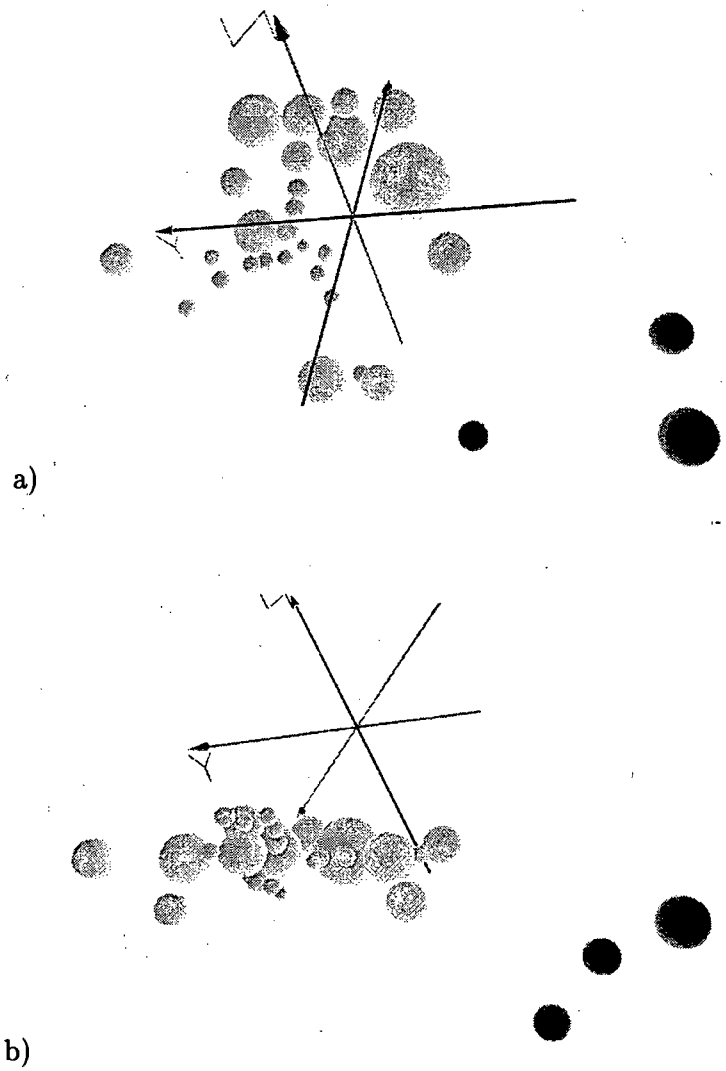

Figure 3.4: Fornax wall voids a) face on, b) side view. A group of 3 voids seems to be disjoint from the wall-like structure. Edgelength statistics clearly showed 2 edges to be much longer than the average edgelength. A separation factor of 3 divides the data set into two trees — one containing the three marked points and the other one containing the rest of the voids. Pruning does not enhance S_2 which takes on its maximum value at just below 0.5. The sphericity function S_3 was also rather high having about the same value.

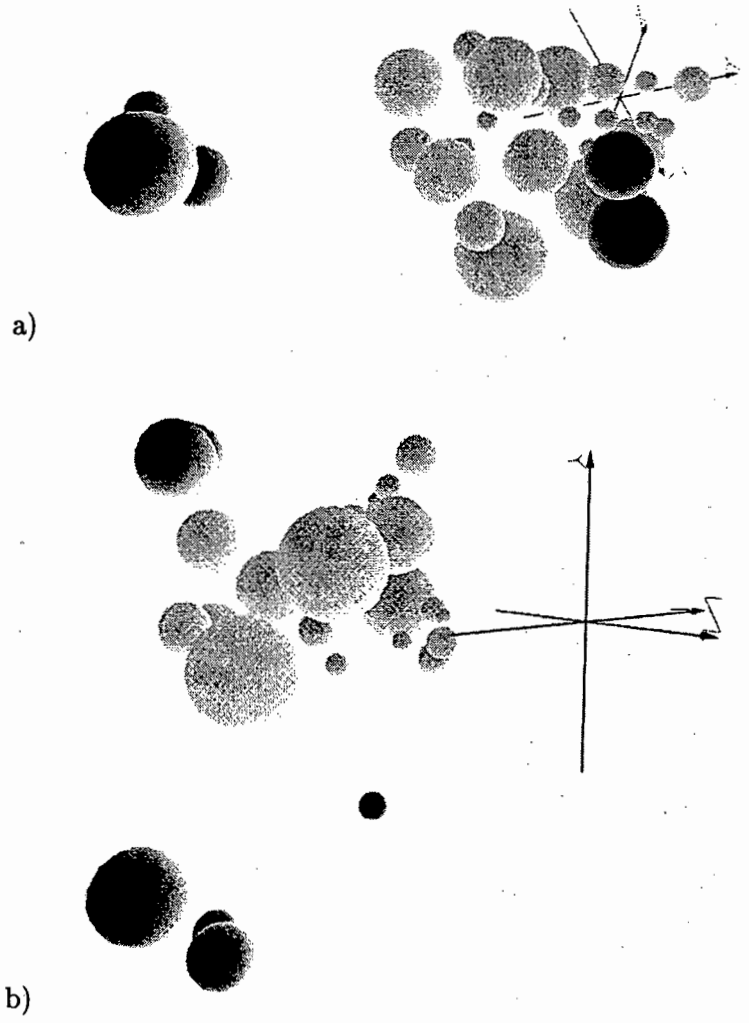

Figure 3.5: Hydra wall voids a) face on b) side view. Edgelength statistics yield that one edge is considerably longer than the average as is also obvious from the figure. However, there are a number of voids that seem to lie off the plane of the main structure. A separation factor of 1.5 removes 6 voids and pruning does not substantially improve the value of S_2. Still after separation the remaining structure is predominantly spherical with S_3 of about 0.75 and S_2 well below that. The reason for this could be that what we see is in fact an aggregate of two intersecting walls.

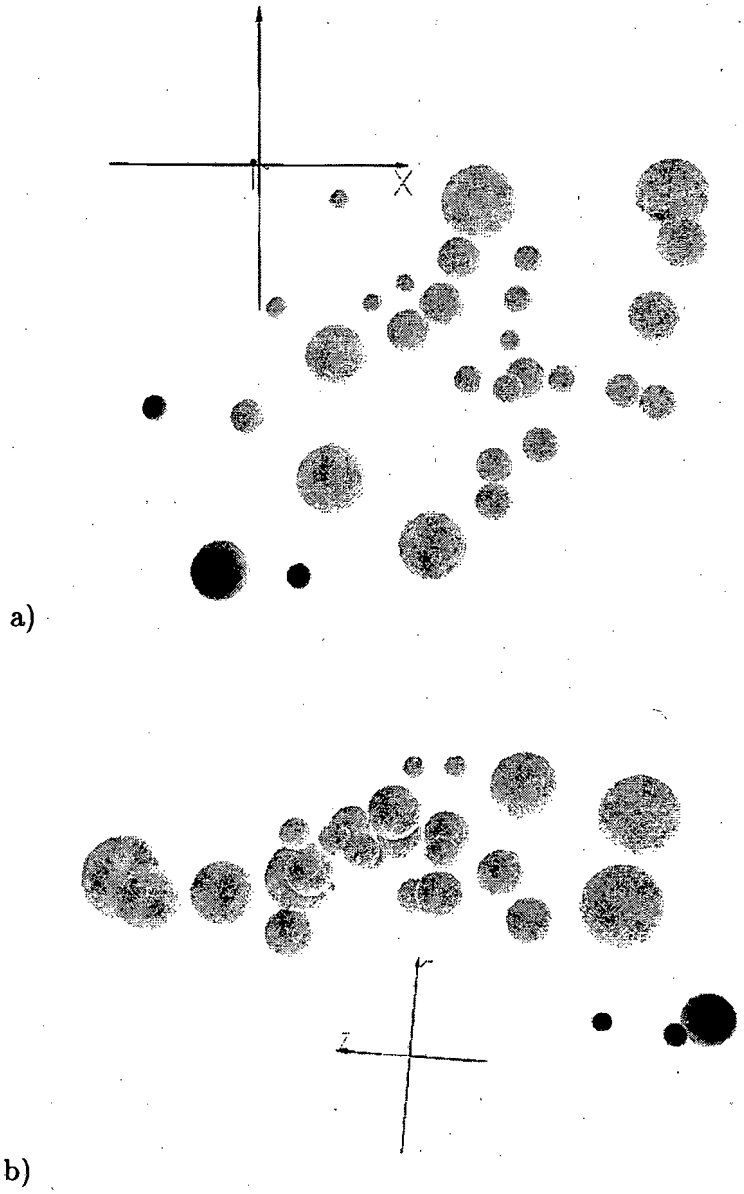

Figure 3.6: Sculptor wall voids a) face on, b) side view. A disjoint group of three voids is easily discerned in the figure and separation with a factor 2 removes it. The optimal value for S_2 is 0.55. Pruning to a level 1 improves the planarity structure function marginally by 0.02 but only at the unacceptable cost of removing another 5 voids.

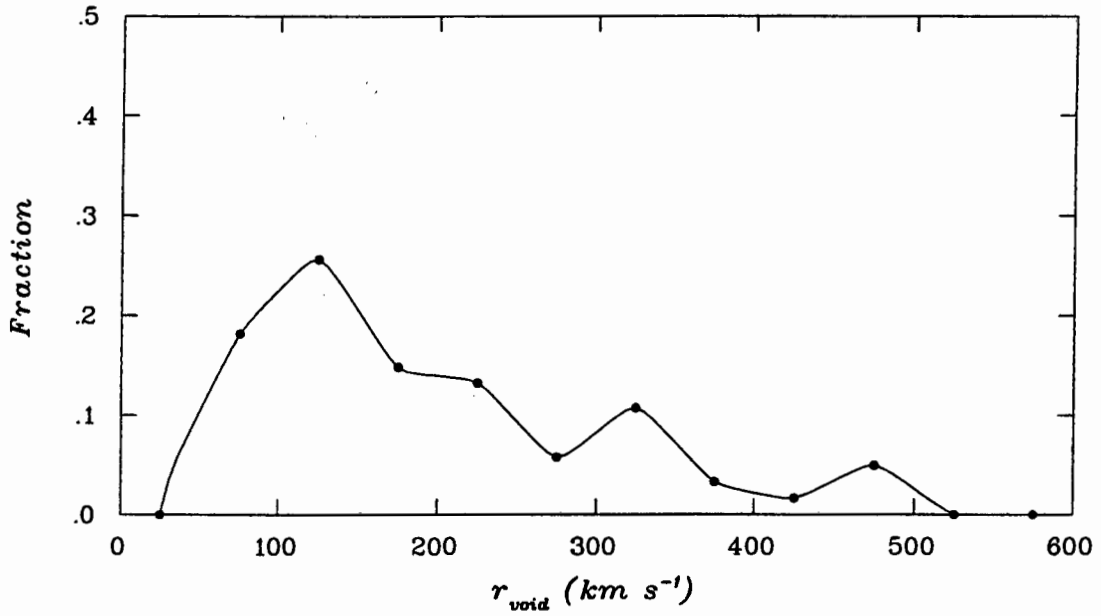

Figure 3.7: Spectrum of the sizes of the wall voids. Dots denote the mid points of the binning intervals and a curve was interpolated to the data points for reasons of clarity.

means that the approximation made to arrive at the method for removing false voids where the volume in which they are located is assumed to be large no longer is valid. The probability of a false void appearing in a given volume decreases with the size of the volume so that voids located within the walls must be more likely to be real than outside the walls. Also, since the walls have a higher number density of galaxies the probability of finding false voids decreases even further.

Instead of applying the corrective procedure suggested in the previous Chapter to the subcatalogue of wall voids it is more sensible to keep all the voids when investigating their spectrum. Due to the small number of voids in each wall they will not be considered separately but will instead be treated as four different realisations of the same underlying distribution of wall voids. The spectrum in figure (3.7) is clearly peaked around a void radius of approximately 100-150 km s^{-1} .

3.2.3 Distribution of Non-Wall Voids

For wall voids, the spatial distribution is of course confined to planar structures. It is however not evidently clear how the non-wall voids are distributed and this will be

Selection	$\alpha_{\max}$	r_s	r_{compl}	N_{voids}
A	0.15	150	7150	28
B	0.01	1000	6500	10

Table 3.2: Selections of non-wall voids for different values of $\alpha_{\max}$ and r_s.

focal point of the investigation here along with an analysis of the voidsize distribution.

Voidsize Spectrum

Since the non-wall voids are located in a volume which corresponds, with the exception of the limited volume occupied by the walls, to the entire Southern Hemisphere with the ZOA excluded, the volume is large enough to make it is possible to apply the correctional procedure outlined in the previous Chapter. The volume $\mathcal{V}_{\text{rem}}$ that is used to calculate λ in equation (2.6) is evaluated by

$$\mathcal{V}_{\text{rem}} = (1 - p_{\text{wall}}(r_c))\frac{2\pi}{3}(1 - \sin|b|_{\text{ZOA}})[(r_c + r_v)^3 - (r_c - r_v)^3] \qquad (3.10)$$

where $p_{\text{wall}}(r_c)$ is the fraction of the total volume occupied by wall voids at a distance r_c and is typically less than 1%. Since voids are such conspicuous features of the galaxy distribution and do not depend on individual galaxies for their detection adopting anything but the lowest value for $|b|_{\text{ZOA}} = 10°$ would unnecessarily decrease the volume to be studied. The number density of galaxies used in formula (2.5) is an average density in a shell around the void and is calculated by

$$\overline{\rho}(r_c, r_v) = \int_{r_c - r_v}^{r_c + r_v} \rho(r) r^2 dr \Big/ \int_{r_c - r_v}^{r_c + r_v} r^2 dr \ . \qquad (3.11)$$

The correctional procedure involves choosing a maximum significance level $\alpha_{\max}$ for the removal of false voids. We must also choose the radius of the smallest void to be considered which then yields a radius of completion according to (2.9). The number of voids in the selection is thus a function of these two parameters whose values should be chosen in such a way that a maximum number of voids are obtained.

Two selections were made for the parameters presented in table (3.2). In order to obtain the spectrum of voidsizes Selection B cannot be used due to its small number of

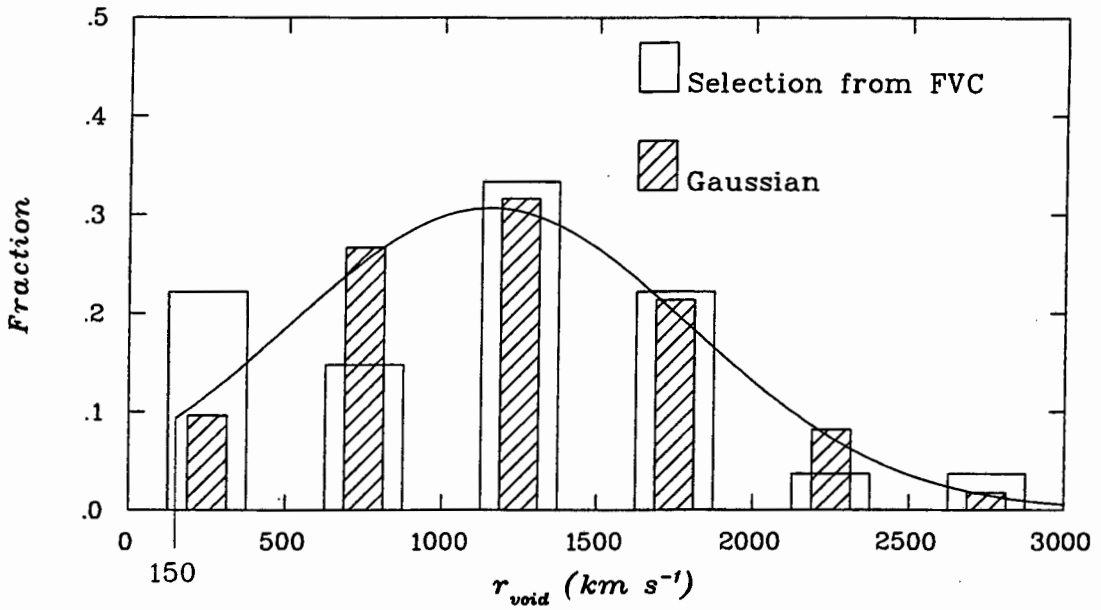

Figure 3.8: Histogram of voidsizes for non-wall voids and comparing Gaussian

data points. For selection A the histogram is plotted in figure (3.8) along with a fitted Gaussian which has been multiplied by the length of the binning interval 500 km s^{-1} for comparison. The mean and standard deviation of the Gaussian were estimated to 1150 km s^{-1} and 650 km s^{-1} respectively. Note that the first binning interval does not stretch from 0 to 500 but is cut off by r_s at 150 km s^{-1} .

A χ^2 test was conducted in order to compare the observed distribution with the hypothesised Gaussian. The calculated value of $\chi^2_6 = 7.1$ does not allow us to accept the hypothesis with any larger significance. However, if the first interval is removed we get $\chi^2_5 = 2.7$ by which we can accept the Gaussian hypothesis at a 75% level. Therefore it seems that at least the peak and the tail of the distribution of voidsizes can be approximately described by the fitted function in figure (3.8).

Spatial Distribution

From looking at three-dimensional images of the spatial distribution of non-wall voids it seems reasonable to suspect that their distribution is roughly isotropic. One could imagine studying the distribution of the coordinates of the void centroids but a simpler

approach would be to make use of the MST technique. The expected structure functions for a uniform distribution of voids are obtained by producing a large number of Monte Carlo simulations. Then by comparing with the observed values of the structure functions for the selections from the FVC one can see if they are in accordance with the simulations.

The simulation algorithm generates the same number of voids as in the selection from the FVC. The coordinates of the centroids are taken from a uniform distribution in a cubic volume with side $r_{\rm compl}$ and points that fall outside the allowed intervals corresponding to constraints on Hemisphere (declination $\geq 0°$), ZOA ($|b| \geq |b|_{\rm ZOA}$) and distance ($r_c \leq r_{\rm compl}$) are discarded and new voids are generated to give the correct number. Because of these additional constraints the centroids of the voids are not entirely randomly distributed since the allowed positions of a given void depends on the other voids and consequently the actual values of the structure functions for the simulations will depend on the spectrum of voidsizes. In all the simulations a Gaussian with mean 1150 and deviation 650 was used. The histograms of S_3 for two series of simulations, one with 28 voids and one with 10 voids are shown in figure (3.10) with the observed values for the two selections indicated. The observed value of S_3 for Selection A is well above the mean of the S_3 distribution for the simulation with 28 voids. This could be explained by the fact that at a significance level of 0.15 there may still be a number of false voids in the selection that will contribute to the sphericity in the spatial distribution. By reducing the maximum allowed significance level to 0.01, the probability of the selection containing false voids is decreased and the observed value is more likely to lie closer to the peak of the distribution of S_3 obtained by simulations. As this is in fact the case the conclusion is that the spatial distribution of non-wall voids is isotropic.

In order to investigate to what extent the void centroids are clustered the obvious method to use is to calculate the two-point correlation function. We use the simple estimator

$$1 + \hat{\xi} = \frac{n_{DD}(r)}{\langle n_{RR}(r) \rangle} \tag{3.12}$$

where $n_{DD}(r)$ is the number of pairs with separation r in the actual data catalogue and $\langle n_{RR}(r) \rangle$ is the corresponding number of pairs in random catalogues averaged over an ensemble of 1000 realisations. The points representing the centroids in the Poisson catalogues were generated without taking into consideration the physical extension of

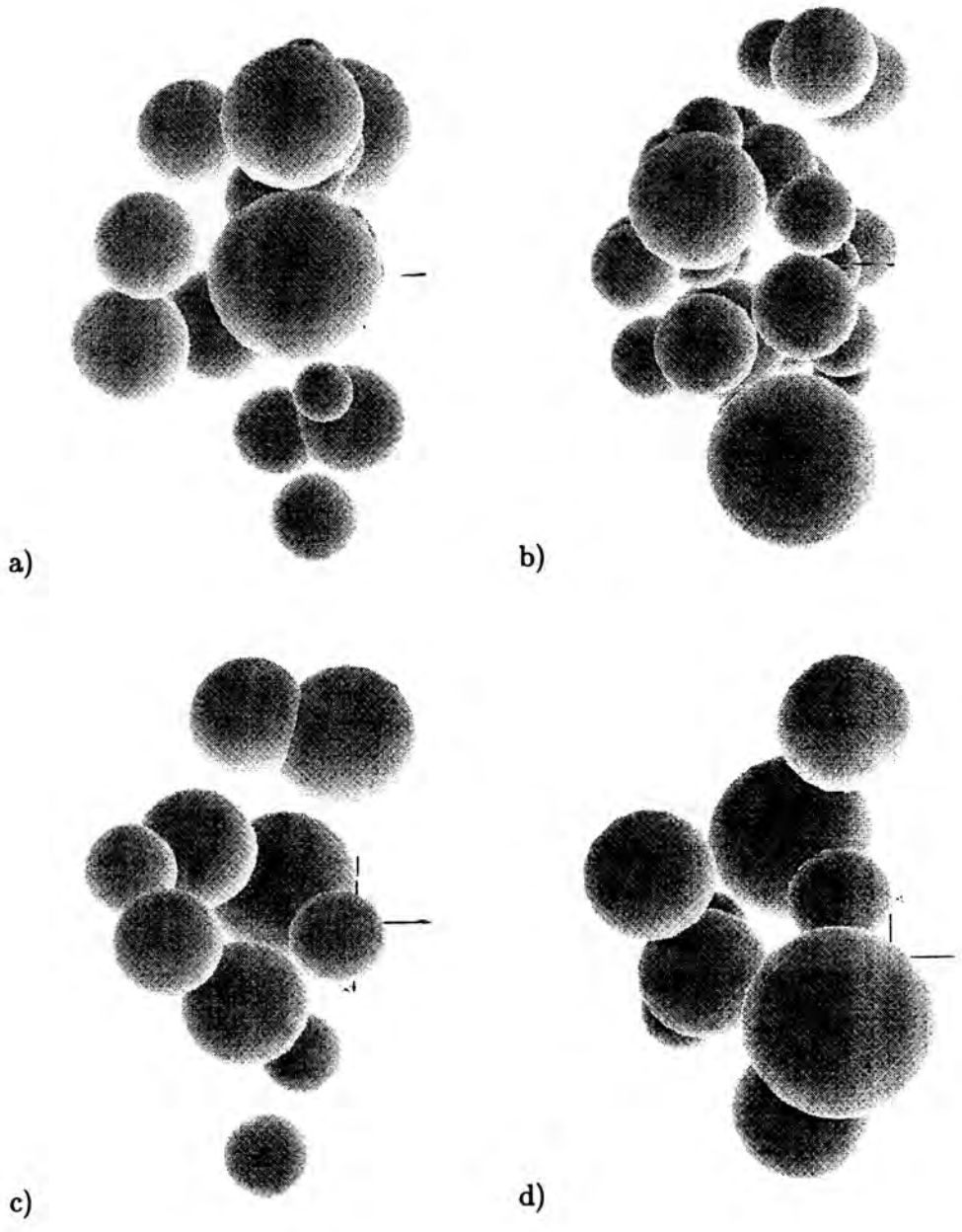

Figure 3.9: a)Non-wall voids, selection A. b) Simulation, 28 voids. c) Non-wall voids, selection B. d) Simulation, 10 voids

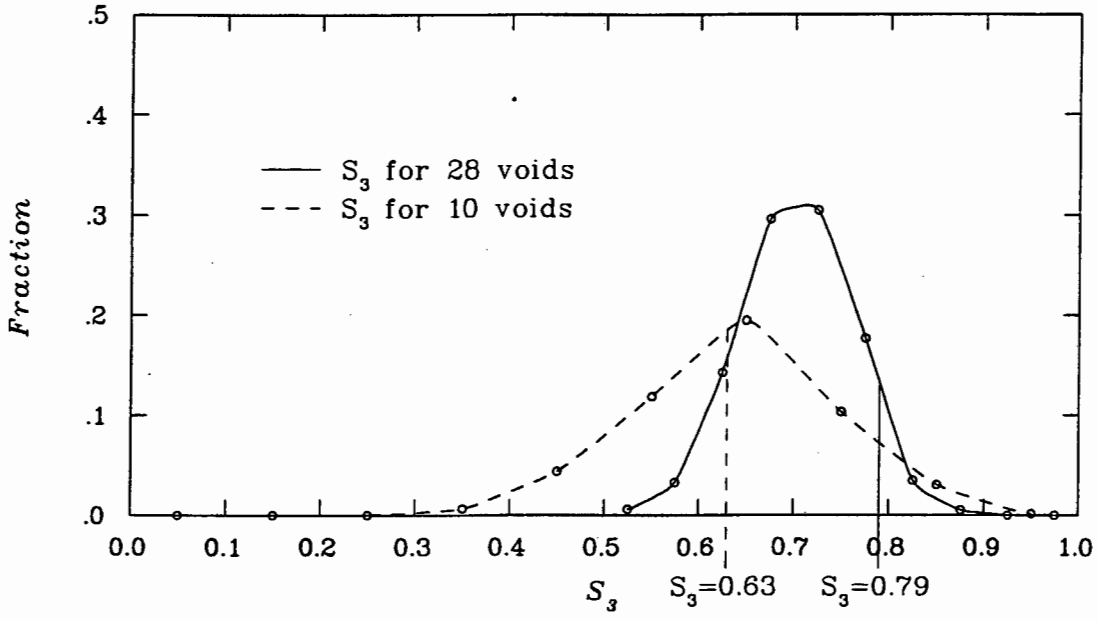

Figure 3.10: Distribution of S_3 for simulations with 28 and 10 voids respectively and observed values of S_3 for selections A and B.

the voids and therefore no restrictions were imposed on how close two points could be to each other. The correlation function shown in figure (3.11) follows the familiar $\xi \propto r^{-1.8}$ power-law in the interval 3000 km s^{-1} $\lesssim r \lesssim$ 7000 km s^{-1} but drops off for $r <$ 3000 km s^{-1} . Selection A is almost certainly 'contaminated' with some false voids that appear in random positions and thereby contribute to decreasing the slope of the correlation function for smaller distances. Unfortunately, Selection B, which may be free of false voids, contains too few voids to be able to offer a reliable comparison. The correlation length r_0 is estimated to about 5200 km s^{-1} corresponding to $52h^{-1}$ Mpc. Compared with the correlation length of Abell clusters (Bahcall & West 1992), the voids are clustered stronger by a factor of 2–4.

3.3 Conclusions

We have now tried to establish the geometrical distribution of voids. By dividing the FVC into two constituent parts — the wall voids and the non-wall voids — these could be studied separately. Because of the uncertainty about how exactly the combination of selection effects and the corrective procedure distorts the underlying spectrum we

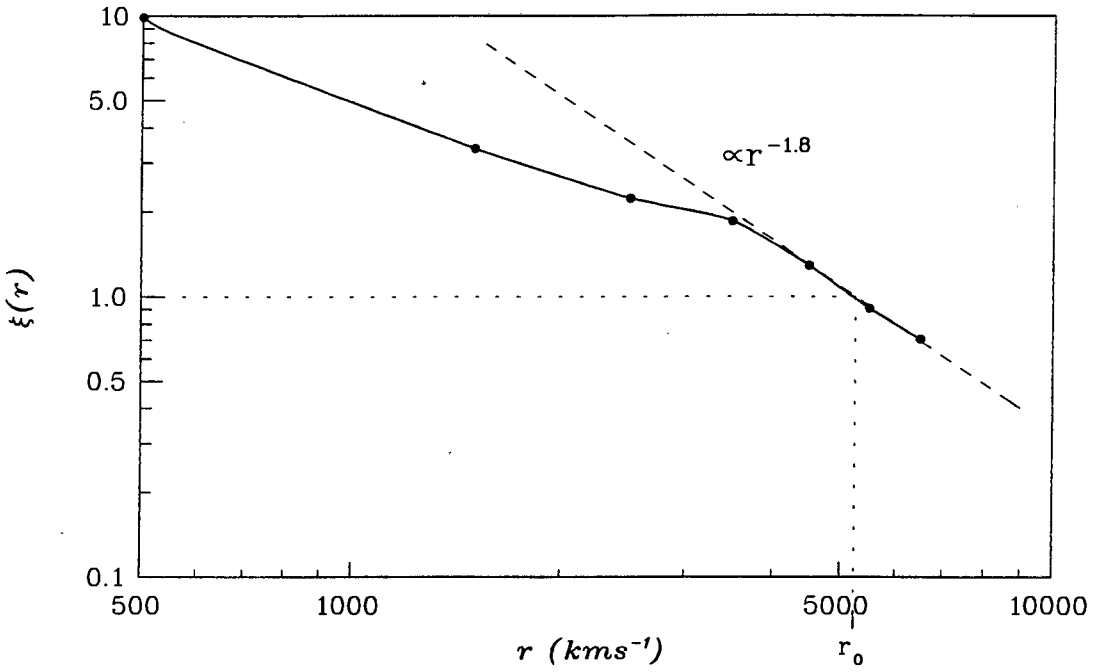

Figure 3.11: Correlation function for voids in Selection A.

cannot say anything conclusive about the true distribution of voidsizes. However, the study of the void spectra give a clear indication that larger voids of typical sizes of 1000 to 1500 km s^{-1} do not belong to the walls and that the walls themselves contain smaller voids having radii of a few 100 km s^{-1} . Furthermore, the larger voids are distributed isotropically throughout the universe and they have a correlation function which corresponds roughly to that of found for Abell clusters.

What emerges is a picture where large voids are distributed isotropically and where the smaller voids are confined to lie in walls in-between the larger voids. A connection between Abell clusters and the largest voids is implied by their correlation functions. Comparing the observed pattern of voids with the pattern predicted by a given model of structure formation is potentially a very powerful test for accepting of rejecting that model and it would therefore be desirable to follow up the kind of analysis that has been presented here using data from simulations.

Chapter 4

A Constraint on Ω.

Some of the outstanding problems in standard cosmology include specifying the initial conditions and finding the parameters in the FRW models. A discussion is presented here concerning the information that can be extracted about these parameters from observable quantities associated with existing structures. A simple structure formation model that makes it possible to relate clusters to voids will then be developed and using observations on these structures, conclusions will be drawn about the value of the density parameter Ω.

In general, any structure that exists today will be a function of three, in principle, distinct factors:

(i) Initial conditions for structure formation,
(ii) Mechanisms of formation,
(iii) Background universe.

Allowing for each of the above factors to be a function of a set of parameters denoted by I,M and B for the initial conditions for structure formation, the mechanisms of formation and the background respectively, one could formally write their influence on a quantity q associated with some structure at a time t as

$$q(t) = q(t, I, M, B) \ . \tag{4.1}$$

As discussed in Chapter 1 the nature of none of the factors (i)–(iii) is not fully known but we have argued in favour of and presented some evidence for the assumptions of Gaussian initial conditions, gravitational instability as the structure formation mechanism

and the homogeneous and isotropic FRW universe as the background. All subsequent analysis will be conducted within the framework of this standard theory

Gaussian initial conditions are completely determined by the power spectrum and if for example the power law $P(k) = Ak^n$ is assumed then the set of parameters I reduces to simply one; the spectral index n. Although it is conceivable that the mechanism for structure formation might be dependent on some parameters this is not the case for the gravitational instability scenario in its simplest version. The dynamics of the background, if FRW, is described by the three equations (1.4) and the assumed equation of state. For a zero cosmological constant, these four equations suffice for finding a general solution but since the equations involve the first and second time derivative of the scale factor, two independent boundary conditions are necessary to fully specify the solutions. Normally, these conditions would consist of a combination of any two of the observables H_0, Ω_0, the age of the universe t_0 or the deceleration parameter q_0.

With the assumptions of Gaussian initial conditions with a power law spectrum, gravitational instability structure formation and FRW background, the quantities related to structures are then $q(t) = q(t, n, B_1, B_2)$ where B_1 and B_2 are any two of the observable boundary conditions. Since the formulation of the initial conditions is inherently stochastic one must use the statistical properties of the quantities q for an analysis. If some appropriate statistic of two independent quantities associated with structure, q_1 and q_2, can be measured thenit is possible to eliminate one of the parameters. For example, the exact form of the initial conditions could be factored out by eliminating n and reciprocal constraints could be put between B_1 and B_2. Conversely, the observed values for B_1 and B_2 can put constraints on the spectral index n.

An analytic investigation using a simple structure formation model is presented here to obtain an indication of the value of the density parameter Ω. Following an idea by Martínez-González & Jones (unpublished) the velocity dispersions of clusters will be compared to the radii of voids by rank so that the cluster with the largest velocity dispersion will be compared with the largest void *et.c.* . The structure formation is described in Section 4.2 by the simplest non-linear gravitational instability model — the *spherical collapse* model. In this model, initial underdensities and overdensities are assumed to evolve unaffected by other structures to form voids and clusters respec-

tively. The initial conditions applied to the model can unfortunately not be described directly in terms of the power spectrum but will instead be given as 'top-hat' density profiles. A heuristic connection will be made between the initial density profiles and Gaussian initial conditions in Section 4.1. The observational data used for the analysis is discussed in Section 4.3 and the results are finally presented in Section 4.4.

4.1 Initial Conditions

Although we cannot use Gaussian initial conditions directly in the spherical collapse model it is desirable that the simplified initial conditions share some common characteristics with the presumed true density field. One requirement that must met for any field is of course that the density contrast averaged over all space vanishes. For a Gaussian random field, in addition, it will further be argued that the density fluctuations, asymptotically, are perfectly symmetric around the zero mean, and this is a feature that we will also require the modelled initial conditions to possess.

As the structure formation model is described in terms of under and overdensities we will in particular be interested in investigating how the local maxima and minima of the Gaussian density field relate to each other. Great attention has been paid to the study of density peaks and has spawned a large number of papers on the subject; see Sahni & Coles (1995) for a review on the literature. In most of the analyses, the initial density peaks have been regarded as possible locations for galaxy formation and although there are some difficulties with this assumption (Katz *et al.* 1993) it seems likely that at least cluster-scale peaks do evolve into clusters (Sahni & Coles 1995).

Bardeen *et al.* (1986, hereafter BBKS), developed a formalism for the description of Gaussian random fields and derived a number of results, some of which will be used here. Their work concerned mainly density peaks but many of their conclusions are valid for minima as well. The first result of relevance here involves a calculation of the number density of extrema of a certain height. Defining a variable $\nu \equiv \delta/\sigma$ they derived a formula in closed form for the number density of peaks with height $\delta = \nu\sigma$. The exact expression is not important here but the relevant fact is that it is symmetric in ν so that $\mathcal{N}_{\text{peaks}}(\nu) = \mathcal{N}_{\text{minima}}(-\nu)$. BBKS further investigated the shape of the density contrast around maxima. They calculated the conditional probability that the

field would take on a value δ at some point $\mathbf{r}$ away from the center of a peak with amplitude $\nu\sigma$. The mean, or equivalently, the most probable, profile around a given peak depends on the height of the peak and the power spectrum only. Hence it is possible to associate a certain spatial extension or a characteristic radius to every peak.

One can regard the function $\delta(x)$ in a limited volume as one particular realisation of an underlying Gaussian probability distribution. In this volume it is not necessarily true that the number of maxima with amplitude $\nu\sigma$ equals the number of minima with the same but negative amplitude. Nor is it necessary that the shapes of the maxima and the minima of same amplitude are exactly mirrored since the shapes themselves are realisations of some probability distribution. However, in the limit when this volume tends to infinity all conceivable realisations will be present and it will be possible to match every maximum with an identical but mirrored minimum. Asymptotically therefore, the Gaussian density field will be perfectly *symmetric* around its zero mean.

Keeping in mind the possible effects of having only a limited volume to work with in practice, it can nevertheless be justified to impose the restriction on the modelled initial conditions that every overdensity with a certain amplitude and spatial extent be matched by an identical but mirrored underdensity. Due to its simple form and consequently its ability to simplify calculations, the top-hat profile is particularly useful. With the density contrast defined in the usual way as $\delta(\mathbf{x},t) = \frac{\rho(\mathbf{x},t)-\rho_b(t)}{\rho_b(t)}$ where $\rho_b(t)$ is the background density, the top-hat profile can formally be written as

$$\delta(r) = \begin{cases} |\delta_i| & r < R_i \\ 0 & \text{otherwise} \end{cases} \tag{4.2}$$

The initial top-hat profile is thus determined by two independent parameters, $|\delta_i|$ and R_i, whereas Gaussian power law initial conditions are fully determined by the spectral index alone which, as argued before, translates into stating that the characteristic size of a peak is determined by its height. Without specifying the exact relation between $|\delta_i|$ and R_i it will simply be assumed that for two perturbations with $|\delta_i|^{(1)} > |\delta_i|^{(2)}$ the radii relate as $R_i^{(1)} > R_i^{(2)}$.

4.2 Spherical Collapse Model

Ignoring tidal effects of neighbouring density perturbations on the evolution of one isolated, homogeneous and spherical density perturbation as justified by Birkoff's theorem in General Relativity or by Gauss' law in Newtonian gravity, Tolman (1934) and Bondi (1947) formulated the spherical collapse model which has since been developed further by others such as *e.g.* Partridge & Peebles (1967).

In the initial density field there will be overdense ($\delta > 0$) and underdense regions ($\delta < 0$). Selfgravity in the overdense regions will counteract the expansion of the universe and will eventually cause them to collapse into gravitationally bound systems which can be observed today as galaxy clusters. The underdense regions on the other hand will expand continuously, pushing matter from the interior of the underdensity to and beyond its rim (see *e.g.* Olson (1979), Hausman (1983) or Bertschinger (1985)). The theory for a generic perturbation is presented first and later applied to the two special cases of an over and an underdensity. The results will be used to arrive at a relation between quantities associated with clusters and voids that can be confronted with observations.

4.2.1 General Perturbation

Suppose the perturbed region is spherically symmetric about some point. The density in the region at some time t_i can then be written as

$$\rho(r,t_i) = \rho_b(t_i) + \delta\rho(r,t_i) = \rho_b(t_i)[1+\delta_i(r)] \tag{4.3}$$

where $\delta_i(r) = \delta(r,t_i)$. Since we are interested in perturbations extending to much smaller domains than the Hubble volume this allows for the dynamics of the region to be studied using the classical formulation. In the Newtonian limit it is convenient to use the proper radial coordinate $r = a(t)x$ where x is the radial comoving coordinate. The gravitational potential is described by

$$\phi_{\rm total}(r,t) = \phi_b(r,t) + \delta\phi(r,t) = -\frac{1}{2}\left(\frac{\ddot{a}}{a}\right)r^2 + \delta\phi(r,t) = \frac{2\pi}{3}G\rho_b r^2 + \delta\phi(r,t) \tag{4.4}$$

where ϕ_b is the equivalent Newtonian potential of the Friedmann metric and $\delta\phi$ is the potential generated due to the density fluctuation $\delta\rho(r,t)$. The equation of motion for

a thin shell of particles located at a distance r is

$$\ddot{\mathbf{r}} = -\nabla\phi_{\rm total} = \frac{4\pi G\rho_b(t)}{3}\mathbf{r} - \nabla(\delta\phi) = -\frac{GM_b}{r^3}\mathbf{r} - \frac{G\delta M(r,t)}{r^3}\mathbf{r} \ , \tag{4.5}$$

recalling that the gravitational force on a particle only depends on the mass $M_b + \delta M$ contained inside the shell for a spherically symmetric density distribution. δM is defined as

$$\delta M(r,t) = 4\pi \int_0^r \delta\rho(q,t)q^2dq = 4\pi\rho_b(t)\int_0^r \delta(q)q^2dq \tag{4.6}$$

and the contribution of mass by the background is given by

$$M_b = \frac{4\pi}{3}\rho_b(t)r^3(t) = \frac{4\pi}{3}\rho_b(t)a^3(t)x^3. \tag{4.7}$$

The adiabatic expansion of the universe yields that ρa^3 is constant and so is consequently M_b. Shell crossing occurs when one shell with initial radius r_1 catches up with a shell initially at a radius $r_2 > r_1$. As long as shell crossing does not occur the subsequent evolution will preserve the ordering of the shells implying that the mass contained within a shell of radius r is constant in time so that $\delta M(r,t) = \delta M(r_i,t_i) =$ constant. Equation (4.5) can be rewritten as

$$\ddot{r} = -\frac{GM}{r^2} \tag{4.8}$$

where

$$M = \rho_b(t_i)\frac{4\pi}{3}r_i^3[1+\overline{\delta}_i] \ , \quad \overline{\delta}_i = \frac{3}{r_i^3}\int_0^{r_i}\delta_i(r)r^2dr \ . \tag{4.9}$$

Here, r_i is the initial radius of the shell with a mass M interior to it and $\overline{\delta}_i$ is the initial average density contrast within r_i. The equation of motion (4.8) can be integrated once to give an energy equation

$$\frac{1}{2}\dot{r}^2 - \frac{GM}{r} = E \tag{4.10}$$

where E is the constant of integration corresponding to the energy per unit mass of a shell. The sign of E determines whether a given shell will expand forever or if it will eventually decouple from the expansion and collapse. If $E > 0$ then it is clear from (4.10) that $\dot{r}^2$ will never become zero thus impellingthe shell to expand forever. If, on the other hand, $E < 0$ then as r increases, $\dot{r}$ will eventually become zero and later negative implying a contraction and subsequent collapse. In the following, the evolution of an overdensity and an underdensity of equal amplitude will be studied separately. For reasons of clarity we shall work with the absolute value of δ and write the densities of the perturbed regions as $\rho_{\rm over} = \rho_b[1+|\overline{\delta}|]$ and $\rho_{\rm under} = \rho_b[1-|\overline{\delta}|]$ respectively.

4.2.2 Overdensity

At an initial time t_i the density contrast δ is small so the overdense region is expanding at approximately the same rate as the background. In other words we assume that the peculiar velocities v_i of the particles in a given shell are negligible at $t = t_i$. Then the general Hubble flow gives the time evolution of the radius of a shell as $\dot{r}_i = H(t_i)r_i \equiv H_i r_i$. The initial kinetic energy per unit mass for a thin shell of radius r is then

$$K_i \equiv \left.\frac{\dot{r}^2}{2}\right|_{t=t_i} = \frac{H_i^2 r_i^2}{2} \ . \tag{4.11}$$

The potential energy $U = -|U|$ at time $t = t_i$ is

$$|U| = \left.\frac{GM}{r}\right|_{t=t_i} = G\frac{4\pi}{3}\rho_b(t_i)r_i^2[1 + |\bar{\delta}_i|\ ] = \frac{1}{2}H_i^2 r_i^2 \Omega_i[1 + |\bar{\delta}_i|\ ] = K_i\Omega_i[1 + |\bar{\delta}_i|\ ] \tag{4.12}$$

where

$$\Omega_i = \frac{\rho_b(t_i)}{\rho_{\rm crit}(t_i)} = \frac{8\pi G}{3}\frac{\rho_b(t_i)}{H_i^2} \tag{4.13}$$

is the initial value of the density parameter Ω of a smooth background. The total energy per unit mass is then

$$E = K_i + U_i = K_i - K_i\Omega_i[1 + |\bar{\delta}_i|\ ] = K_i\Omega_i[\frac{1}{\Omega_i} - (1 + |\bar{\delta}_i|\ )] \tag{4.14}$$

We assume that the overdensity will collapse to a gravitationally bound system so that $E < 0$. This gives the condition for collapse as

$$|\bar{\delta}_i| > \Omega_i^{-1} - 1 \equiv \Delta_i \ . \tag{4.15}$$

Assume further that the density perturbation is only important out to a radius R_i so that $\delta = 0$ for $r > R_i$. In order to calculate the total energy contained in the perturbed region, the contributions of the individual shells must be added to give the following integral

$$E_{\rm total} = \int_0^{R_i} E(r_i)dm(r_i) \tag{4.16}$$

where $E(r)$ is given by (4.14) and $dm(r)$ is the mass of an infinitesimally thick shell of radius r and has the value $dm(r_i) = \rho_b(t_i)(1 + \delta_i(r_i))4\pi r_i^2 dr_i$. Combining (4.14) and (4.16) we get

$$E_{\rm total} = \int_0^{R_i} \frac{1}{2}H_i^2 r_i^2 \Omega_i(\Delta_i - |\bar{\delta}_i|)4\pi r_i^2 \rho_b(t_i)(1 + \delta(r_i))dr_i. \tag{4.17}$$

This integral can be solved analytically if we assume that the initial perturbation has a top-hat profile so that $\delta(r_i) = |\delta_i|$ for $r_i < R_i$ and zero otherwise. With this density contrast the energy equation (4.17) can easily be integrated to give

$$E_{\rm total} = \frac{1}{2}H_i^2\Omega_i(\Delta_i - |\delta_i|)4\pi\rho_b(t_i)(1+|\delta_i|)\frac{R_i^5}{5} = \frac{3}{10}H_i^2\Omega_i(\Delta_i - |\delta_i|)R_i^2 M \qquad (4.18)$$

where M is the mass within a radius R_i according to equation (4.9).

The solution to the equation of motion (4.8) (see *e.g.* Padmanabhan 1993) suggests that the overdense region will initially expand until it reaches a maximum radius and then turns around and eventually collapses to one point. However, long before that happens, the approximation that mass is distributed in non-crossing spherical shells, will break down. The final fate of the collapsed density perturbation will therefore be an equilibrium state having some radius $R_{\rm vir}$ and not a singular point with infinite density. If one assumes that no energy is lost as thermal radiation and that no mass is lost due to effects connected with shock waves one can apply the virial theorem. The total energy of the final virialised system is then equal to the initial energy of the perturbed region.

The kinetic energy, T, of N particles, each assumed to have mass m is simply $T = \frac{1}{2}m\sum_{j=1}^{N} v_j^2$. With the velocity dispersion, σ_v defined as

$$\sigma_v = \langle v^2\rangle^{1/2} = (\frac{1}{N}\sum_{j=1}^{N} v_j^2)^{1/2} \qquad (4.19)$$

the kinetic energy can be written as

$$T = \frac{M}{2}\sigma_v^2 \qquad (4.20)$$

where $M = Nm$ is the total mass of the system. The virial theorem states that $2T + U = 0$, so the total energy is then $E_{\rm total} = T + U = -T$. Using expression (4.18) for the total energy, the velocity dispersion can be written as

$$\sigma_v^2 = -\frac{2E}{M} = H_i^2 R_i^2 \Omega_i \frac{3}{5}(|\delta_i| - \Delta_i) \ . \qquad (4.21)$$

Martínez-González, Sanz & Silk (1990) derived expressions for calculating the temperature anisotropies induced in the CMBR by the gravitational potential associated

with non-linear density fluctuations in an Einstein-de Sitter background. Based on this potential approximation and using a spherical collapse model essentially identical to what has been presented here, Martínez-González & Sanz (1990) evaluated the expected temperature fluctuations in the CMBR caused by an object having the mass of $\sim 10^{16} M_{\odot}$ corresponding to the mass of the Great Attractor which is the name given to a large concetration of mass that exerts a gravitational pull on the local group of galaxies (see *e.g.* Lynden-Bell *et al.* 1988 or Kraan-Korteweg *et al.* 1996). Martínez-González & Sanz (1990) found that the anisotropy would be of order $\Delta T/T \sim 10^{-7}$ which is consistent with the COBE observations. The typical mass of a cluster is on the order of $\sim 10^{15} M_{\odot}$ and as the temperature anistropy increases with the mass of the object causing it (Martínez-González *et al.* 1990) we conclude that the spherical collapse scenario as an approximate model for the formation of present day clusters is consistent with CMBR constraints. It remains to be shown however, that this is the case also for $\Omega \neq 1$ universes.

4.2.3 Underdensity

In contrast to the overdensity which first expands and then undergoes collapse to a system corresponding to a galaxy cluster we will assume that the underdensity continues to expand forever to form a void. In a similar fashion to what was done previously for an overdenstiy we shall write down the energy of a shell, however this time the equations of motion will have to be solved explicitly in order to obtain the time evolution of the shell radii.

The expression for the energy per unit mass of a shell in an underdensity is identical to that of an overdensity with the exception that the contrast, $|\overline{\delta}_i|$, carries the opposite sign in front of it so that

$$E_{\text{under}} = K_i \Omega_i [\Delta_i + |\overline{\delta}_i| \ ] \ . \tag{4.22}$$

If the underdensity is to expand forever we must require that $E_{\text{under}} > 0$. If equations (4.14), (4.15) and (4.22) are combined then

$$E_{\text{under}} = \frac{\Delta_i + |\overline{\delta}_i|}{\Delta_i - |\overline{\delta}_i|} E_{\text{over}} \ . \tag{4.23}$$

E_{over} is negative so the fraction in (4.23) must also be negative in order for E_{under} to be positive. Since the numerator is greater than the denominator and they must have

opposite signs, the only alternative is that

$$\begin{cases} \Delta_i + |\bar{\delta}_i| > 0 \\ \Delta_i - |\bar{\delta}_i| < 0 \end{cases} \tag{4.24}$$

which can be combined in one single inequality

$$|\bar{\delta}_i| > |\Delta_i| = |\Omega_i^{-1} - 1| \tag{4.25}$$

which thus constitutes the condition for spherical collapse to occur. Note that this inequality is trivially satisfied for an Einstein–de Sitter universe. The solution to the integrated equation of motion (4.10) for $E < 0$ is

$$r = A(\cosh\theta - 1), \quad t = B(\sinh\theta - \theta), \quad A^3 = GMB^2 \tag{4.26}$$

where θ is a parameter and A and B are constants. The expression for r is a monotonically increasing function and therefore implies an unbounded growth of the radius of the underdensity. A and B can be expressed in terms of other constants of motion and since the energy of a shell is a conserved quantity it is convenient to find the relation between these three constants. Parametrising (4.10) in θ by substituting $\dot{r}$ for $r'/t' = \frac{dr/d\theta}{dt/d\theta}$, the energy equation becomes

$$E = \frac{1}{2}\left(\frac{r'}{t'}\right)^2 - \frac{GM}{r} = \frac{1}{2}\left(\frac{A\sinh\theta}{B(\cosh\theta - 1)}\right)^2 - \frac{A^3}{B^2 A(\cosh\theta - 1)} \tag{4.27}$$

which after some algebra yields the relation

$$E = \frac{1}{2}\left(\frac{A}{B}\right)^2. \tag{4.28}$$

In the large-θ limit, both hyperbolic functions go as $e^\theta/2$ so that $r \simeq A\frac{e^\theta}{2}$ and $t \simeq B\frac{e^\theta}{2}$ yielding $r = \frac{A}{B}t$. The relation (4.28) between the three constants A,B and E gives that $r = (2E)^{1/2}t$. Recalling (4.22) we can finally write down

$$\frac{r_{\rm void}(t)}{R_i} = H_i\Omega_i^{1/2}(\Delta_i + |\bar{\delta}_i|\,)^{1/2}t\ . \tag{4.29}$$

Implicit in the large-θ approximation is the assumption that shell crossing does not occur so that the equations of motion still apply. It has been shown in several simulations (Olson & Silk 1979, Ikeuchi *et al.* 1983, Hausman *et al.* 1983 and Bertschinger 1985) that shell crossing does occur in general and that therefore the power law $r \propto t$ is not

valid for late times. However, in order to simplify the model we will ignore the effects associated with shell crossing here.

Martínez-González & Sanz (1990) investigated the expected temperature fluctuations one would expect in the CMBR as a result of inhomogeneities of the size of the observed voids. The model formation model they used was somewhat different from the one described here. They used a model due to Bertschinger (1985) for a compensated void having an expansion scaling law $r \propto t^{\gamma}$ with $\gamma \approx 0.8$ and predicted a temperature isotropy of order 10^{-7}. The scaling law $r \propto t$ used here yields a faster growth of voids in the late stages of their evolution so that they would require smaller initial perturbations than if the radius grows as $r \propto t^{0.8}$ and consequently induce smaller anisotropies in the CMBR. However, since voids are not compensated here it means that the universe external to the voids will be affected and an additional term will be added to the total expected anisotropy (Martínez-González *et al.* 1990). We will now proceed after having added a caveat at this point concerning whether the void formation model discussed here is consistent with CMBR constraints.

Before investigating the possible implications that the observed values of the velocity dispersions of clusters and the radii of voids have on the value of the density parameter Ω, the observational data will be reviewed in the ensuing Section.

4.3 Observational Data

In order to confront the theoretical results with observations we need catalogues of both velocity dispersions and voidsizes. The obvious choice of void catalogue is the FVC but for comparison, an analysis based on an objectively compiled catalogue is included. The most extensive objective void catalogue extracted from the SRC is provided by Kauffmann & Fairall (1991, hereafter KF) and is the one used here. A more recent catalogue of voids in the Southern Hemisphere has been compiled by El-Ad, Piran & da Costa (1996) using a computer algorithm for detection but since the galaxy data was not available this catalogue is not used.

The centroids of the clusters and the voids selected for the analysis must be drawn from the same sample volume so as to assure that the study will be statistically correct and

if this volume is large enough it will represent a fair sample of the universe. In terms of spherical coordinates, choosing the sample volume amounts to determining the allowed angles on the celestial sphere and the allowed interval for the radial distance.

We have already restricted ourselves to the Southern Hemisphere, *i.e.* only objects with declination $< 0°$ are included. Furthermore, the ZOA is taken into account by only considering voids and clusters that have galactic latitudes $|b| > |b|_{\mathrm{ZOA}} = 10°$. The relatively low value for the bounding galactic latitude is justified as in Chapter 3 by arguing that neither voids nor clusters depend on individual galaxies for their detection and therefore using a higher value for $|b|_{\mathrm{ZOA}}$ would unnecessarily decrease the sample volume. What still has to be determined are the values of the inner and outer radii that bound the sample volume. Since the cluster catalogues contain a larger number of entries and cover larger volumes of space than the void catalogues, the limiting factor for determining the sample volume will be the latter catalogues.

The comparison between voids and clusters will be made by rank so it is imperative that both catalogues be complete in the chosen sample volume so that no structures are missed and thereby risk skewing the result. The concluding remarks of Chapter 2 provide a prescription for how to obtain the outer radius of the sample volume by guaranteeing that the void catalogue is complete for distances less than the radius of completeness calculated according to equation (2.9).

The radii of completeness will now be determined for the two void catalogues and in the respective sample volumes, clusters from the ACO catalogue will be selected.

4.3.1 FVC Void Catalogue

The procedure for selecting a set of voids for the analysis resembles what was done for non-wall voids in Section 3.2.3. In this case however, we do not want to *a priori* restrict ourselves to non-wall voids only but instead allow for the possibility that also wall voids could be included in the selection. Thus the whole crude FVC catalogue is used as a basis from which a sample is drawn. In practice though, as stringent conditions will be put on the significance of voids and because the emphasis will be placed on choosing the largest voids, we will see that the selection will consist of non-wall voids only.

First we choose a significance level $\alpha_{\max}$ and eliminate voids that have $\alpha > \alpha_{\max}$. It was seen in Section 3.2.3 that some of the voids in the selection with $\alpha_{\max} = 0.15$ were likely to be false so here we apply the stricter criteria of requiring that the significance be $\alpha_{\max} = 0.01$.

The next step is to calculate the estimate for the constant of proportionality in the void scaling law (2.2). The number density for small radial distances is very sensitive to the presence of an occasional nearby void and explains the kink in the curve in figure (2.1) at $r \approx 1000$ km s^{-1} . As the density at these small distances cannot be considered representative the k_i:s calculated for voids in this region will most certainly underestimate the true k. An underestimated k will overestimate the radius of completeness so that consequently the sample volume is chosen in such a way that it might contain undetected voids. Since both the larger voids and the larger clusters are located at distances greater than 2000 km s^{-1} , imposing this value as a lower radial limit for the sample volume does not decrease the number of selected objects and therefore does not affect the final statistical analysis.

The radius of completeness, r_{compl} is the distance out to which the smallest void of the selection, having radius r_s, can be identified. The numerical value for r_{compl} is determined by requiring that it satisfy the relation $r_s = (\hat{k}\,/\overline{\rho}(r_{\text{compl}}, r_s))^{1/3}$ for a given r_s. The voids that will be included in the final selection are thus those that have radii $r_v \geq r_s$ and whose centroids are located at distances in the interval $[r_{\text{low}}, r_{\text{compl}}]$ where r_{low} is the lower radial limit for the sample volume. By trying different values for r_s it can be chosen in such a way that it maximises the number of selected voids. For a significance level $\alpha_{\max} = 0.01$ the optimum of 12 selected voids is found for $r_s = 1250$ km s^{-1} and yields a radius of completeness of 7125 km s^{-1} . The selected voids are listed in table (4.1). By comparison with the results of Section 3.2 where wall voids were separated from non-wall voids it is clear that all the voids in the selection fall into the latter category.

4.3.2 KF91 Void Catalogue

Kauffmann & Fairall (1991) compiled an objective void catalogue (hereafter KF91) by implementing a computer algorithm which divided the redshift data set into a cubical grid where cells containing galaxies would be marked 'on' and those that where empty

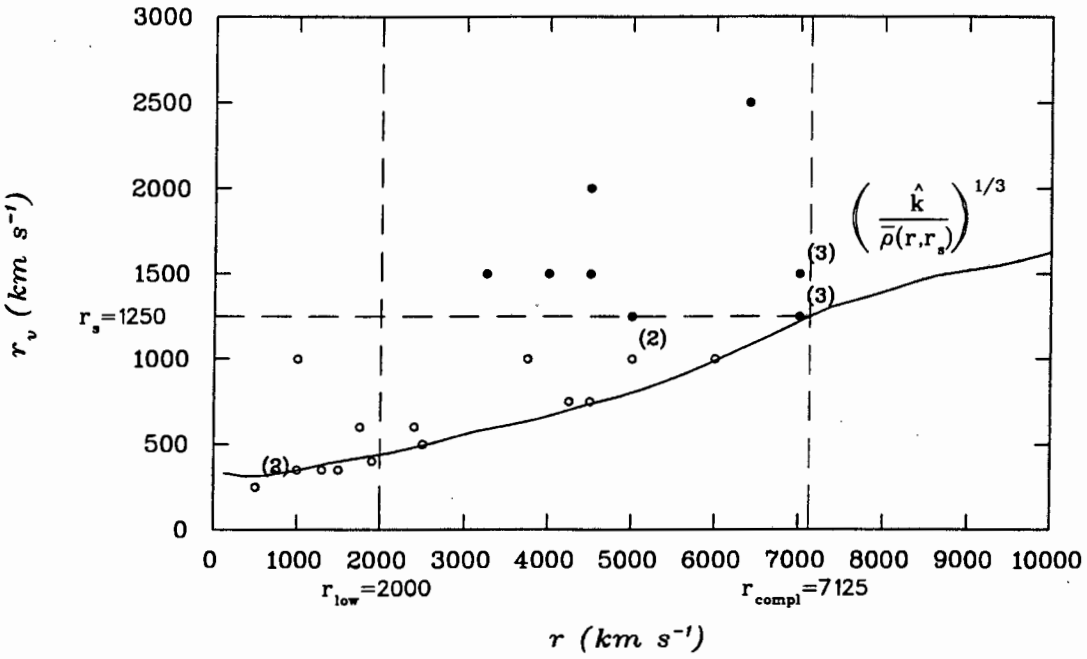

Figure 4.1: FVC catalogue in radius vs. distance diagram. Circles correspond to all voids that are significant to a level $\alpha \leq 0.01$. Filled circles represent the 12 selected voids for $r_s = 1250$. Numbers in brackets denote the number of voids of a particular radius and at a particular distance. The curve $(\hat{k}/\overline{\rho}(r, r_s))^{1/3}$ is plotted for the estimated value of $\hat{k} \approx 4.33$.

Rank	R.A. (h)	dec (°)	r_{center} (km s^{-1})	r_{void} (km s^{-1})
1	12.5	-12	6400	2500
2	6.3	-18	4500	2000
3	4.4	-10	7000	1500
4	7.8	-51	7000	1500
5	14.5	-76	7000	1500
6	8.2	-53	4500	1500
7	11.7	-5	4000	1500
8	1.5	-47	3250	1500
9	4.1	-32	7000	1250
10	5.8	-42	7000	1250
11	12.3	-11	7000	1250
12	11.9	-28	5000	1250

Table 4.1: Selected voids from the FVC catalogue ranked according to radius.

would be marked 'off'. The algorithm would then search for cubical aggregates of grid cells marked 'off' and refer to these as the base voids. Since the average separation between galaxies in the densest regions of the catalogue was about 400–500 km s^{-1} , the gridding length was taken to be 200 km s^{-1} and the smallest aggregate to be considered a void would consist of four cells. To get a better estimate of the true size of the void, layers of rectangular groupings of 'off' cells were added to the sides of the base void as long as the space occupied by the cells was empty. KF's study lists a number of voids with the position of the centres of the base voids, the number of cells in the side of the base void and the total number of cells. From this, crude estimates of the maximum and the minimum radii of the voids can be deduced if we, by assumption, restrict the shapes of the voids to be spherical.

Let Δ_g be the side of one grid cell, *i.e.* $\Delta_g = 200$ km s^{-1} . Let further the number of cells in the side of the base void be n_b and the radius of the void be r_v. Then as a base void with side $n_b\Delta_g$ must be inscribed in sphere with radius r_v which in turn must be

inscribed in a cube with side $(n_b + 1)\Delta_g$ then

$$r_\ell \equiv \frac{n_b \Delta_g}{\sqrt{2}} < r_v \leq \frac{(n_b + 1)\Delta_g}{\sqrt{2}} \equiv r_u \tag{4.30}$$

Another estimate of the void size is obtained by using the total number of 'off' cells, $N_{\rm cell}$. The volume of the cells is $N_{\rm cell}\Delta_g^3$ which is to match the volume of a sphere with radius $r_{\rm vol}$ so that

$$r_{\rm vol} = \left(\frac{3N_{\rm cell}}{4\pi}\right)^{1/3} \Delta_g \tag{4.31}$$

Under the assumption that the void is spherical, $r_{\rm vol}$ would be a conservative estimate of the radius but in reality the voids depart from the idealised shape and can sometimes cause $r_{\rm vol}$ to be larger than r_u. This could happen *e.g.* for an elliptical void orientated at an angle to the gridding. To be on the safe side, the smallest and largest possible radii are chosen to be $r_{\rm min} = \min(r_\ell, r_{\rm vol})$ and $r_{\rm max} = \max(r_u, r_{\rm vol})$ respectively.

As is the case for FVC , void selection effects are present also in KF91 and care must be taken to attempt to remove their influence. Having the possibility of comparing with randomly generated galaxy catalogues, KF devised a method for determining whether the voids in the catalogue are 'real' based on Monte Carlo simulations rather than the analytical approach that was necessary for FVC. KF judged a void significant if the probability of finding a void of the same size in a random distribution with the same average number density of galaxies, is small. They produced a large number of mock galaxy catalogues with a random distribution of points but corrected for different galaxy selection effects present in the real catalogue. The result of running their void searching algorithm on these simulated galaxy catalogues then give an estimate of the probabilities necessary to assess the significance of the voids from the real catalogue.

The voids listed by KF all have a probability of appearing in a random catalogue which is less than 1% and can therefore be considered 'real'. It is still necessary to calculate the radius of completeness in order to determine the sample volume. Although the method of detection in KF91 is completely different from that of FVC we can still assume that the scaling law (2.2) applies since the method of detection only affects the constant k. As for the FVC, the lower bounding radius of the sample volume is chosen to be $r_{\rm low} = 2000$ km s^{-1} . In estimating the constant k, we must use the minimal value $r_{\rm min}$ for the radius of each void. The procedure for calculating $r_{\rm compl}$ is then

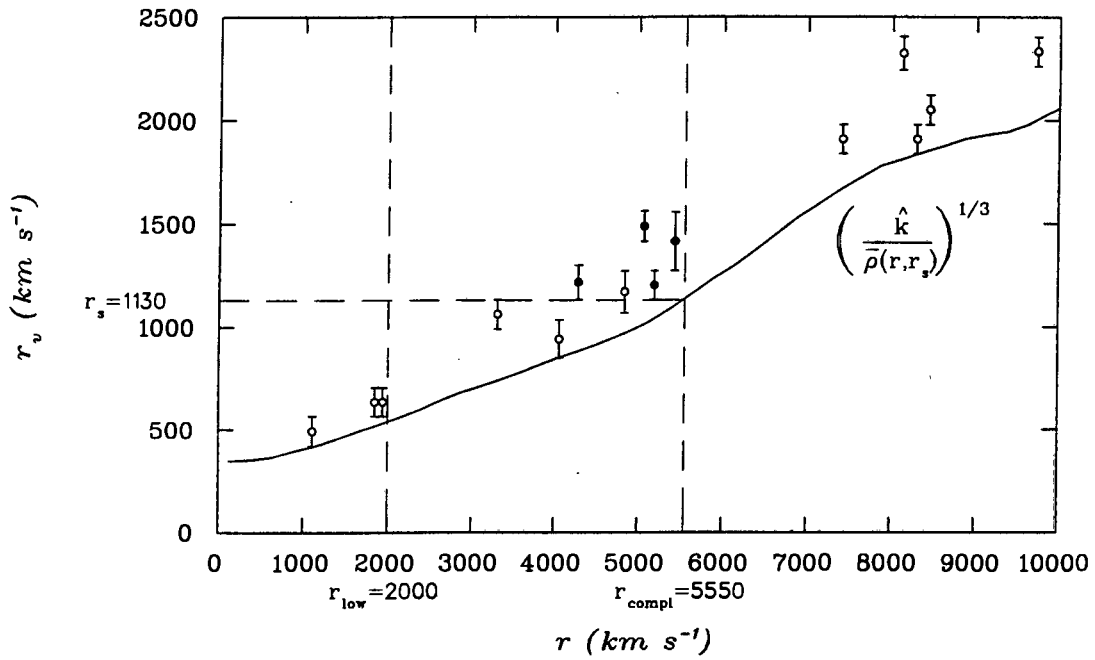

Figure 4.2: KF91 catalogue in radius vs. distance diagram. Circles with error bars correspond to all voids that are significant to 1%. Filled circles represent the 4 selected voids for $r_s = 1130$ km s^{-1} .

identical to the one used for the FVC catalogue. The maximum number of voids that can be selected is unfortunately only 4 and is obtained for $r_s = 1130$ km s^{-1} and gives $r_{\rm compl} = 5500$ km s^{-1} .

4.3.3 ACO Cluster Catalogue

Abell, Corwin & Olowin (1989, hereafter ACO) produced a catalogue of 5250 rich (A-) and supplementary (S-) clusters, 334 of which have known velocity dispersions. Andernach *et al.* (1995, hereafter ATS) regularly updates a catalogue compiled from a number of sources where some of the redshifts have been cross-identified and some of the velocity dispersions have been recalculated. Figure (4.3) shows the distribution of the velocity dispersions of the ACO clusters.

The velocity dispersions catalogued by ATS are the line-of-sight dispersions calculated according to the prescription of Danese *et al.* (1980) whereas in the spherical collapse model, the full 3-dimensional velocity dispersion was used. The definition (4.19) of

Rank	n_b	N_{cell}	r_{min}	r_{max}	$cz(kms^{-1})$
-	16	6105	2262	2404	9735
-	16	5909	2243	2404	8122
-	13	4065	1979	2121	8449
-	13	3887	1838	1979	8296
-	14	3359	1838	1979	7413
1	10	2000	1414	1563	5064
2	9	1973	1272	1556	5429
3	8	1150	1131	1299	4280
4	8	1061	1131	1272	5188
-	7	637	1067	1272	4836
-	6	600	989	1131	3311
-	8	576	848	1032	4055
-	4	108	565	707	1939
-	4	96	565	707	1844
-	3	39	420	565	1109

Table 4.2: All voids from the KF91 catalogue, with the selected voids marked by their rank

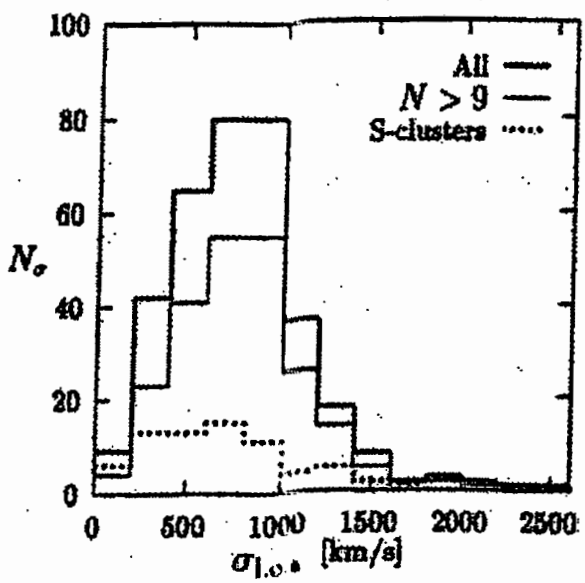

Figure 4.3: The distribution of cluster line-of-sight velocity dispersions, adapted from Andernach, Tago & Stengler-Larrea, (1995). Thick line represents all clusters, thin line corresponds to clusters having more than 9 redshifts available, and dotted line plots the $\sigma_{\rm l.o.s}$ distribution for S-clusters.

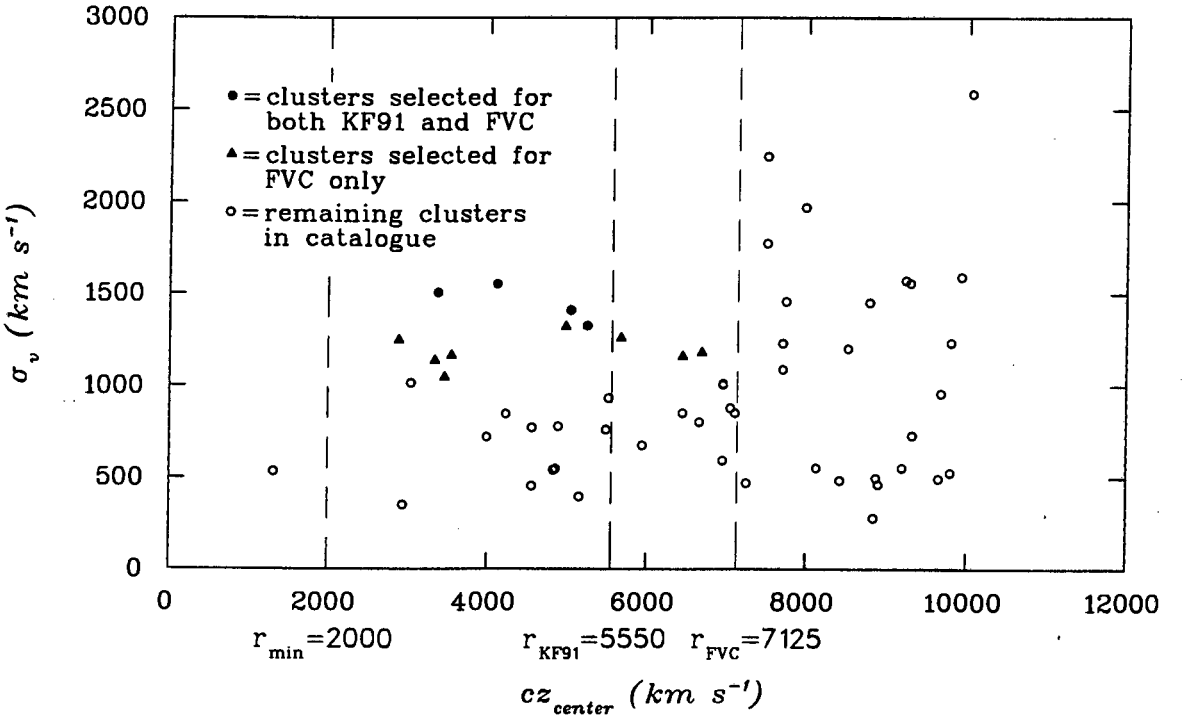

Figure 4.4: All ACO clusters with declination < 0 and $|b| > 10°$ out to a distance of approximately 10,000 km s^{-1} .

the velocity dispersion yields that $\sigma_v^2 = \langle v^2 \rangle = \langle v_x^2 + v_y^2 + v_z^2 \rangle$ where v_x, v_y and v_z are the components of the velocity in some arbitrary coordinate system. Choose one of the coordinates, say x, to correspond to the line-of-sight, then $\sigma_v^2 = 3\langle v_x^2 \rangle$ since the equipartition of energy in a virialised system distributes the energy isotropically and consequently compels all the velocity components to be equal. In conclusion, the 3-dimensional dispersion relates to the line-of-sight dispersion as

$$\sigma_v = \sqrt{3}\sigma_{\text{l.o.s}} \ . \tag{4.32}$$

Figure (4.4) shows the velocity dispersions of clusters plotted against their radial distance and table (4.3) gives more details on the selected clusters.

4.4 Results

From spherical collapse of initial top-hat perturbations we have now derived expressions for two observable quantities; the velocity dispersion of clusters (4.21) and the radii

Rank FVC	Rank KF91	Abell	R.A (h)	dec (°)	N	$cz(kms^{-1})$	$\sigma_v(kms^{-1})$
1	1	A3537	13.0	-32.2	23	4107	1554
2	2	S 707	12.7	-42.7	173	3358	1507
3	3	S 655	11.1	-46.7	6	5036	1412
4	4	S 866	20.3	-49.9	16	5246	1328
5	-	S 840	20.0	-56.1	26	4976	1323
6	-	A3656	20.0	-38.7	12	5666	1259
7	-	S 636	10.5	-35.1	56	2878	1252
8	-	S 301	2.8	-31.4	34	6685	1181
9	-	A3565	13.6	-33.7	31	3537	1167
10	-	A3698	20.6	-25.5	6	6445	1162
11	-	S 714	12.8	-26.2	30	3328	1138
12	-	A1060	10.6	-27.3	122	3447	1046

Table 4.3: AST galaxy clusters selected for FVC and KF91 with their ranks in respective catalogue, Abell number, coordinates, number of galaxies used in velocity dispersion calculation, distance to centroid and 3-dimensional velocity dispersion.

of voids (4.29), as functions of the four unknown parameters $R_i, |\delta_i|, H_i$ and Ω_i. In order to compare the voids and the clusters we will assume that the cluster of rank m originates from an overdensity whose corresponding underdensity with the same radius and amplitude gives rise to the void of rank m. Implicit in this assumptions is also the notion that overdensities and underdensities evolve separately and in isolation from other density perturbations in the universe. Since the number of unknowns exceed the number of equations we cannot hope to solve for all the parameters but by noting that in redshift units, r_{void} has the same units as σ_v, the ratio $\Phi = \sigma_v / (H_0 r_{\text{void}})$ must be dimensionless and therefore a function of only $|\delta_i|$ and Ω_i so

$$\Phi(|\delta_i|, \Omega_i) = \frac{\sigma_v}{r_{\text{void}}} = \left(\frac{3}{5}\right)^{1/2} \left(\frac{|\delta_i| - \Delta_i}{|\delta_i| + \Delta_i}\right)^{1/2} t^{-1} \ . \tag{4.33}$$

The function Φ becomes particularly simple for an Einstein-de Sitter universe for which Ω is constant in time and hence gives $\Delta = 0$. Also, for an Einstein-de Sitter universe $t_0 = 2/(3H_0)$ so that

$$\Phi = \left(\frac{3}{5}\right)^{1/2} \frac{1}{H_0 t_0} = \left(\frac{27}{20}\right)^{1/2} \approx 1.16 \ . \tag{4.34}$$

The observed values for Φ are plotted in diagram (4.5b) were the expected value for a flat universe is also marked. The data points from the KF91 catalogue seem to be consistent with the $\Omega = 1$ hypothesis but the FVC data points clearly indicate that the observed Φ is lower than the predicted value 1.16. The difference between the observed values for the two catalogues could be attributed to the fact that the largest voids in FVC do contain a few isolated galaxies within their boundaries and therefore show up as several distinct and smaller voids in KF91. For this reason we let the result from FVC supersede the result from KF91 and we will investigate alternatives to the $\Omega = 1$ hypothesis.

First consider an $\Omega > 1$ universe. Let the initial density contrast be $\Omega_i = 1 + \epsilon$ where $0 < \epsilon < 1$. After Taylor series expansion $\Delta_i = \frac{1}{1+\epsilon} \simeq -\epsilon$ which combined with the collapse condition (4.25) yields $0 < \epsilon < |\delta_i| \ll 1$. Then

$$\left(\frac{|\delta_i| - \Delta}{|\delta_i| + \Delta}\right)^{1/2} \simeq \left(\frac{1 + \epsilon/|\delta_i|}{1 - \epsilon/|\delta_i|}\right)^{1/2} \simeq 1 + \frac{\epsilon}{|\delta_i|} > 1 \ . \tag{4.35}$$

It can be shown that the age of the universe for a closed universe is given by

$$t_0 = \frac{1}{2H_0} \frac{\Omega_0}{(1 - \Omega_0)^{3/2}} \left[\cos^{-1}\left(\frac{2}{\Omega_0} - 1\right) - \frac{2}{\Omega_0}(1 - \Omega_0)^{1/2}\right] \ , \tag{4.36}$$

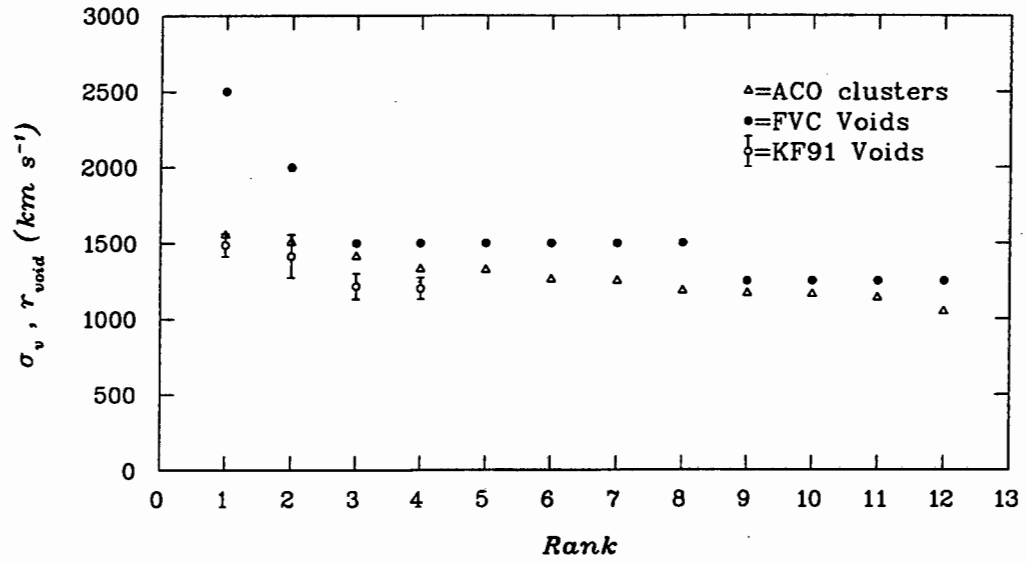

a)

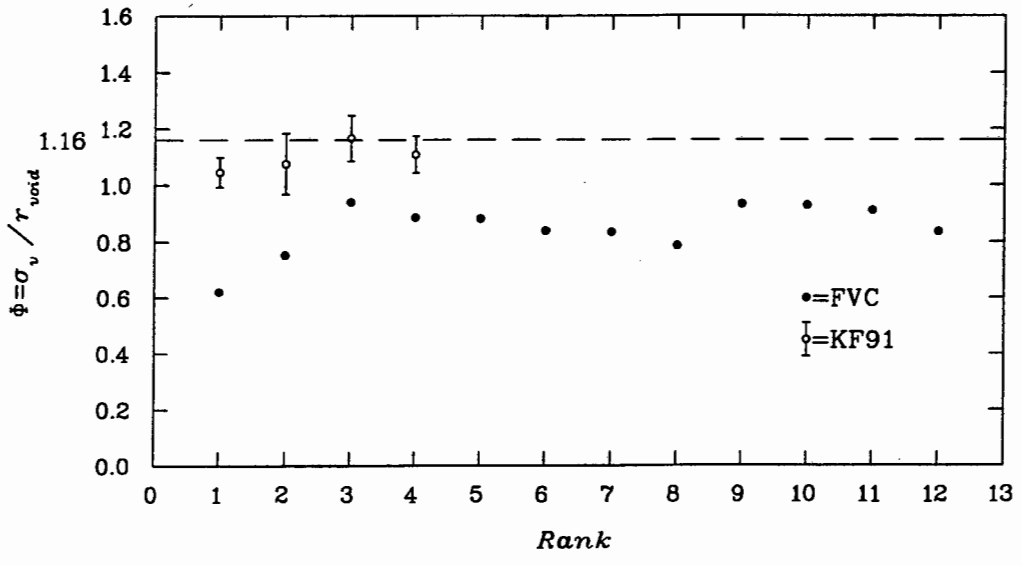

b)

Figure 4.5: a) Ranked clusters and voids, b) Φ as a function of rank with expected value 1.16 for an Einstein-de Sitter universe.

which is a monotonically decreasing function of Ω_0 with its asymptotic maximum at $2/(3H_0)$ so that $t_0^{-1} > 3H_0/2$. This, together with the factor (4.35) which is larger than 1 yields that the expected value for Φ in the case of a closed universe is larger than 1.16.

In a similar way as was done for a closed universe we can investigate an $\Omega < 1$ universe. Let $\Omega_i = 1 - \epsilon$ where as before $0 < \epsilon < 1$ so that $\Delta_i \simeq \epsilon$. The factor

$$\left(\frac{|\delta_i| - \Delta_i}{|\delta_i| + \Delta_i}\right)^{1/2} \simeq 1 - \frac{\epsilon}{|\delta_i|} \ , \tag{4.37}$$

and can therefore take on any value between 0 and 1. The age of the universe for an open Friedmann model is

$$t_0 = \frac{1}{2H_0} \frac{\Omega_0}{(1-\Omega_0)^{3/2}} \left[\frac{2}{\Omega_0}(1-\Omega)^{1/2} - \cosh^{-1}\left(\frac{2}{\Omega_0} - 1\right)\right] > \frac{2}{3H_0} \ . \tag{4.38}$$

The exact value of Φ, from which Ω in principle could be deduced, depends on the amplitude of the initial perturbation which is not known. Hence only the qualitative result that $\Omega < 1$ can be obtained.

4.5 Discussion

In this Chapter we have argued for the virtue of comparing quantities associated with two independent structures in order to limit the degrees of freedom in structure formation scenarios. Already, using the naive spherical collapse model, it has allowed us to infer the constraint on the density parameter that $\Omega < 1$.

Within the general framework presented at the beginning of this Chapter many improvements can be made to provide more accurate results than is possible with the simple model used here. The first suggestion regards the initial conditions. If an analytical model for the structure formation is to be used then the proper connection must be made between the power spectrum and the statistical properties of the amplitudes and shapes of the initial perturbations. An alternative and perhaps more straightforward procedure is of course to do simulations where the initial conditions are generated randomly.

Many methods exist for describing the formation of structure that are much more sophisticated than the spherical collapse model and hence would allow for more accurate theoretical predictions of the quantities related to structure. A requirement on any formation model is that the structures must be created from fluctuations that are within the bounds provided by the observed anisotropy of the CMBR. The type of analysis carried out by Martínez-González *et al.* (1990) should therefore be extended to cases where the background is not Einstein-de Sitter. Finally, the number of available redshifts will increase dramatically within the next few years and will enable the detection of more voids and clusters and therefore improve on the statistical quality of the results. Hopefully, with some of the improvements suggested here, the method of analysis presented in this Chapter can provide a useful tool for putting constraints on the parametersin the standard model.

Chapter 5

Summary

Chapter 1 served to provide the general framework of standard cosmology within which the subsequent work was done. Arguments — theoretical and observational were presented in favour of mainly three assumptions; the Friedmann-Robertson-Walker background, Gaussian initial conditions and structure formation by means of gravitational instability.

The principal tool for investigating the large-scale structure in this thesis has been the visually compiled FVC void catalogue. Chapter 2 was entirely devoted to establishing the quantity and quality of the data contained in the catalogue — a necessary procedure before using the catalogue for analysis. Even as redshift distortions were ignored, effects due to the interpretation of galaxies as random point processes realised from a matter density field skew the observed distribution of voids with respect to the true underlying distribution. Assuming that galaxies trace matter, three selection effects were identified which are manifested as three distinct errors that can be made in the detection of voids. The selection effects were modelled and the measures suggested for how to factor out their influence, when taken together amount to a prescription for a corrective procedure that can be applied to the FVC. The modelling of selection effects was purely analytical since the visual identification of voids does not allow for comparison with voids detected in large numbers of randomly generated galaxy catalogues. In order for the analysis of selection effects to be complete, Monte Carlo simulations must be done where realisations of galaxy catalogues with known underlying void distributions can be compared with void distributions detected by a computer implemented algorithm. Nevertheless, not having available such an automated method of detection

for the moment, the corrective procedure suggested here presents a useful way of ridding the FVC, at least partly, of the selection effects.

Any successful structure formation scenario must be able to reproduce the observed spatial and size distribution of voids and the study thereof would thus constitute a potentially powerful tool for discriminating between contesting theories. Based on the observation that smaller voids apparently lie imbedded in planar structures and using the information given in the FVC about voids identified by Fairall as pertaining to a particular wall, the FVC was divided into five subcatalogues, one for each of the four walls and one for the remaining non-wall voids. An MST analysis was performed on the individual wall catalogues in order to remove voids that were erroneously marked by Fairall as wall voids. The corrective procedure is not applicable to the wall voids since the volume they inhabit is too small for the procedure to be valid. Instead, using all the available wall voids and regarding the four subcatalogues as different realisations of the same distribution, a spectrum of voidsizes was obtained which showed that the typical radius of a wall void is around 150 km s^{-1} .

The non-wall voids were studied separately, and corrected for selection effects it was found that the distribution of voidsizes, at least for the larger voids, is approximately fitted by a Gaussian with mean 1150 km s^{-1} and standard deviation of 650 km s^{-1} . An MST analysis showed that the spatial distribution of non-wall voids is isotropic and in the range $r \in [3000, 7000]$, the calculated two-point correlation function approximately follows a $\xi \propto r^{-1.8}$ power law. The correlation length of 5200 km s^{-1} is a factor 2–4 higher than the one found for Abell clusters. This order of magnitude agreement of the correlation lengths of the largest voids and the Abell clusters seems to imply that there exists a link between the two structures. Bardeen *et al.* (1986) found that peaks in a Gaussian random field above a certain threshold have approximately the same correlation function as the one observed for galaxies. It would be interesting to do an analysis using the same formalism for larger peaks that would correspond to Abell clusters and the largest voids to see if the observed correlation functions are obtained. Possibly then, it could be firmly established that the seeds of clusters and voids are density peaks in an initial Gaussian random field.

In the simple non-linear spherical collapse model, initial overdensities and underdensi-

ties are assumed to evolve independently of other structures to form clusters and voids respectively. It would be desirable to have a formal connection between the Gaussian initial conditions and the initial top-hat profiles for the collapse model but here only a rather heuristic discussion is presented in Chapter 4. The Gaussian-like constraint that the initial density field be exactly symmetrical around the zero mean so that every overdensity is matched by precisely one underdensity is imposed on the top-hat initial conditions. This enables us to associate a given void with one particular cluster in a unique way.

The possible benefits of investigating the relation between independent quantities associated with structure, whereby constraints can be put on parameter that go into the standard model, were first discussed in general terms. An example was then provided by the spherical collapse model which was used to derive a relation between the velocity dispersions of clusters and the radii of voids that can be confronted with observations. During structure formation in the collapse model, the ranking is preserved so that the largest initial density perturbations give rise to the largest cluster and the largest void *et.c.* . The ratios of the ranked velocity dispersions and void radii are a function of the background density and the amplitude of the initial perturbations. Since the amplitudes and the density parameter relate to each other through the collapse condition $|\delta_i| > |\Omega_i^{-1} - 1|$, we obtain an upper limit for Ω. The conclusion of this analysis yields that the density parameter $\Omega < 1$ implying that the universe is open.

Acknowledgements

My greatest gratitude should be extended to my sponsors Wallenbergs Stipendiefond, Rotary International and Centrala Studiestöds Nämnden who made my stay in Cape Town possible through their generous financial support.

External to the Department of Astronomy I am indebted to Prof. H. Goosen and Ashton Mason of the UCT Computer Science Department for assistance with the visualisation, to Dr. Chris Koen at the SAAO for help with the probabilistic calculations and to Dr. Peter Dunsby of the Applied Mathematics Department for useful comments on a near-final draft. For inspiration and ideas without which this thesis would not have seen the light of day I extend my deepest appreciation to Dr. Peter Coles. I also acknowledge contributions of great importance to my work due to Dr. Bernard Jones.

At the Department of Astronomy, *mis gracias á* Dr. Peter Martínez for his patience in helping to track down FORTRAN bugs and thanks also to my supervisor Prof. A.P. Fairall for providing me with the hardware needed for my work, both in terms of his void catalogue and in terms of computer facilities. Special thanks must be directed to Prof. M.W. Feast for encouragement and for stimulating discussions on literally everything between heaven and earth. The students at the department all deserve appreciation for a variety of things; Thebe Medupe for his ear-to- ear smile, for cooking delicious pap and for sharing with me some of his favourite music, Lerothodi Leeuw for constant updates on the South African soccer scene, François Vuille for putting up my with French and, in times of hardship, for reminding me that happiness is only a glass of Chardonnay away and last but not least my office mate Patrick Woudt for showing me what a real galaxy looks like, for teaching me a few words of decent Dutch and on numerous occasions for sinking the eight-ball in the wrong pocket after having cleared the pool table way ahead of me.

References

Abell G.O., 1958, *Astrophys. Journ. Suppl. Series* , **3**, 211

Abell G.O., 1965, *Ann. Rev. Astron. Astrophys.*, **3**, 1

Abell G.O., Corwin, H.G.Jr & Olowin, R., 1989, *Astrophys. Journ. Suppl. Series* , **70**, 1

Albrecht A., Steinhardt P., 1982, *Phys. Rev. Letters*, **48**, 1220

Andernach, H., Tago, E., Stengler-Larrea, E., 1995, 'A compilation of measured redshifts of ACO clusters', Proc. *The World of Galaxies II, Astrophys. Lett. & Comm.* , **31**, 27

Babul A., Starkman G.D., 1992, *Astrophys. J.* , **401**, 28

Bahvsar S.P., Ling E.N., 1988, *Astrophys. Journ. Letters* , **331**, L63

Bahcall N., Soneira R.M., 1983, *Astrophys. J.* , **270**, 20

Bahcall N.A., West M.J., 1992, *Astrophys. J.* , **392**, 419

Bardeen J.M., Bond J.R., Kaiser N., Szalay A.S., 1986, *Astrophys. J.* , **304**, 15, (BBKS)

Barrow J.D., Bahvsar S.P., Sonoda D.H., 1985, *Mon. Not. R. Astr. Soc.* , **216**, 17, (BBS)

Barrow J.D., Bhavsar S.P., 1987, *Quart. J. Roy. Astr.*, **28**, 109

Bertschinger E., 1985, *Astrophys. Journ. Suppl. Series* , **58**, 1

Bondi, H., 1947, *Mon. Not. R. Astr. Soc.* , **107**, 410

Broadhurst, T.J., Ellis, R.S., Koo, D.C., Szalay, A.S., 1990, *Nature*, **343**, 726

Carollo C.M., de Zeeuw P.T., van der Marvel R.P., Danziger I.J., Quian E.E., 1995, *Astrophys. J.* , **441**, 25

Chincarini G., 1978, *Nature*, **272**, 515

Chincarini G., 1983, in *IAU Symp. 104*, Chincarini G., Abell G.O. eds., Reidel, Dordrecht, p.159

Coles P., Lucchin F., 1995, *Cosmology: The Origin and Evolution of Cosmic Structure*, Wiley & Sons, Chichester U.K.

Coles P., Pilonis M., 1991, *Mon. Not. R. Astr. Soc.* , **250**, 75

da Costa L.N., Pellegrini P.S., Sargent W.L.W., Tonry J., Davis M., Meiksin A., Lantham D.W., Menzies J.W., Coulson I.A., 1988, *Astrophys. J.* , **327**, 544

da Costa L.N., Pellegrini P.S., Davis M., Meiksin A., Sargent W.L.W., Tonry J., 1991, *Astrophys. Journ. Suppl. Series* , **75**, 935

Danese L., De Zotti G., di Tullio G., 1980, *Astron. Astroph.* , **82**, 322

Davis M., Peebles P.J.E., 1983, *Astrophys. J.* , **267**, 465

de Lapparent V., Geller M.J., Huchra J.P., 1986, *Astrophys. Journ. Letters* , **302**, L1

de Vaucouleurs G., 1953, *Astr. Journ.*, **58**, 29

Dekel A., 1994, Dynamics of Cosmic Flows, *Ann. Rev. Astr. Astrophys.*, **32**, 371

El-Ad H., Piran T., da Costa L.N., 1996, *Astrophys. Journ. Letters* , **462**, L13

Efsthatiou G., Kaiser N., Saunders W., Lawrence A., Rowan-Robinson M., Ellis R.S., Frenk C.S., 1990, *Mon. Not. R. Astr. Soc.* , **247**, 10P

Einasto J., Einasto J., Gramann M., Saar E., 1991, *Mon. Not. R. Astr. Soc.* , **248**, 593

Einasto J., Jôeveer M., Saar E., 1980, *Mon. Not. R. Astr. Soc.* , **193**, 353

Einasto J., Klypin A.A., Shandarin S.F., 1983, in *IAU Symp. 104*, Chincarini G., Abell G.O. eds., Reidel, Dordrecht, p.265

Fairall A.P. and undergraduate students, 1985, *Publ. Dept. Astr. Univ. Cape Town*, **no 8**

Fairall A.P., 1989, in *Morphological Cosmology Proc. XIth Cracow Cosmological School*, Flin P., Duerbeck H.W., Springer, Berlin, p.145

Fairall, A.P., Jones, A., 1988, *Publ. Dept. Astr. Univ. Cape Town*, **no 10**

Fairall A.P., Maurellis A., Jones A., Kauffmann G.K., Matravers D.R., Ellis G.F.R., 1990, in *Large Scale Structures and Peculiar Motions in the Universe*, Latham D.W., da Costa L.N. eds., Astron. Soc. of the Pacific, Provo

Fairall, A.P., 1994, *Publ. Dept. Astr. Univ. Cape Town*, **no 12**

Fisher K.B., Strauss M.A., Huchra J.P., Davis M., Yahil A., Schlegel D., 1995, *Astrophys. Journ. Suppl. Series* , **100**, 69

Fry J.N., 1985, *Astrophys. J.* , **289**, 10

Geller M.J., Huchra J.P., 1989, *Science*, **246**, 897

Gott J.R., Melott A.L., Dickinson N., 1986, *Astrophys. J.* , **306**, 341

Gott J.R., Weinberg D.H., Melott A.L., 1987, *Astrophys. J.* , **319**, 1

Gott J.R., Miller J., Thuan T.X., Schneider S.E., Weinberg D., Gammie C., Polk K., Vogeley M., Jaffrey S., Bahvsar S.P., Melott A.L., Giovanelli R., Haynes M.P., Tully R.B., Hamilton A.S., 1989, *Astrophys. J.* , **340**, 625

Gregory P.C., Condon J.J., 1991, *Astrophys. Journ. Suppl. Series* , **75**, 1011

Gregory S.A., Thompson L.A., 1978, *Astrophys. J.* , **217**, 385

Gregory S.A., Thompson L.A., Tiftt W.A., 1981, *Astrophys. J.* , **243**, 411

Gunn J.E., Gott J.R., 1972, *Astrophys. J.* , **176**, 1

Gunn J.E., Weinberg D.H., 1995, in *Wide-Field Spectroscopy and the Distant Universe*, Maddox S.J., & Aragón-Salamanca A. eds., World Scientific (Singapore)

Guth A.H., 1981, *Physical Review D*, **23**, 347

Hamilton A.J.S., Gott J.R., Weinberg D., 1986, *Astrophys. J.* , **309**, 1

Hausman, M.A, Olson, D.W., Roth, B.D, 1983,*Astrophys. J.* , **270** , 351

Huchra J.P., Davis M., Latham D.W., Tonry L.J., 1983, *Astrophys. J. Suppl. Series*, **53**, 89

Hubble E., 1929, A Relation between Distance and Radial Velocity among Extragalactic Nebulae, *Proc. Nat. Acad. Sci.*, **15**, 169

Ikeuchi S., Tomisaka K., Ostriker J.P., 1983, *Astrophys. J.* , **265**, 583

Jahoda K. Lahav O., Mushotzky R.F., Boldt E., 1992, *Astrophys. Journ. Letters* , **378**, L37

Jôeveer M., Einasto U., 1978, in *IAU symposium 79 "The Large Scale Structure of the Universe"*, Longair, Einasto eds., Dordrecht, Reidel.

Jôeveer M., Einasto U., Tago E., 1978, *Mon. Not. R. Astr. Soc.* , **185**, 357

Kaiser N., 1984, *Astrophys. Journ. Letters* , **284**, L9

Katz N., Quinn T., Gelb J.M., 1993, *Mon. Not. R. Astr. Soc.* , **265**, 689

Kauffmann G., 1990, MSc Thesis, *Dept. Astr. Univ. Cape Town*

Kauffmann G., Melott A.L., 1992, *Astrophys. J.* , **393**, 415

Kauffmann G., Fairall A.P., 1991 *Mon. Not. R. Astr. Soc.* **248**, 313

Kirshner R.P., Oemler A., Schechter P.L., Schectman S.A., 1981, *Astrophys. Journ. Letters*, **248**, L57

Kirshner R.P., Oemler A., Schechter P.L., Schectman S.A., 1987, *Astrophys. J.* , **314**, 493

Klypin A.A., Shandarin S.F., 1993, *Astrophys. J.* , **413**, 48

Klypin A.A, 1996, preprint, astro-ph/9605183

Kraan-Korteweg R.C., Woudt P.A., Cayette V., Fairall A.P., Balkowski C., Henning P.A., 1996, *Nature*, **379**, 6565

Kuhn J.R., Uson J.M., 1982, *Astrophys. J.* , **263**, L47

Lahav O., 1987, *Mon. Not. R. Astr. Soc.* , **225**, 213

Lahav O., Lilje P.B., Primack J.R., Rees M.J., 1991, *Mon. Not. R. Astr. Soc.* , **251**, 128

Lin H., Kirshner R.P., Shectman S., Landy S.D., Oemler A., Tucker D.L., Schecter P.L., 1996, *Astrophys. J.* , **464**, 60

Linde A., 1990, *Particle Physics and Inflationary Cosmology*, Harwood Academic Publishers, London

Lindner U., Einasto J., Einasto M., Freudling W., Fricke K., Tago E., 1995, *Astron. Astroph.* , **301**, 329

Little B., Weinberg D.H., 1994, *Mon. Not. R. Astr. Soc.* , **267**, 605

Lynden-Bell D., Faber S.M., Burstein D., Davies R.C., Dressler A., Terlevich R.J., Wegner G., 1988, *Astrophys. J.* , **326**, 19

Maddox, S.J., Efstathiou, G., Sutherland, W.J., Loveday, J., 1990, *Mon. Not. R. Astr. Soc.* , **242**, 43P

Martínez-González E., Sanz J.L., 1990, *Mon. Not. R. Astr. Soc.* , **247**, 473

Martínez-González E., Sanz J.L., Silk J., 1990, *Astrophys. Journ. Letters* , **355**, L5

Maurogordato S., & Lachièze-Rey M., 1987, *Astrophys. J.* , **320**, 13

Maurogordato S., & Lachièze-Rey M., 1991, *Astrophys. J.* , **369**, 30

McCarthy P.J., Persson S.E., West S.C., 1992, **386**, 52

Milne E.A., 1935, *Relativity, Gravitation and World Structure*, Oxford, Clarendon Press

Moody J.E., Turner E., Gott J.R., 1983, *Astrophys. J.* ,**273**, 16

Mould, J.R., Staveley-Smith L. Shommer R.A., Bothun G.D., Hall P.J., Han M.S., Huchra J.P., Roth J., Walsh W., Wright A.E., 1991, *Astrophys. J.* , **383**, 467

Olson, D.W, & Silk, J., 1979, *Astrophys. J.* , **233** , 395

Oort J.H., 1983, *Ann. Rev. Astron. Astrophys.*, **21**, 273

Ore O., 1962, *Am. Math. Soc. Colloq. Publ.*, **38**

Otto S., Politzer H.D., Preskill J., Wise M.B., 1986, *Astrophys. J.* , **304**, 62

Padmanabhan, T., 1993, *Structure formation in the Universe*, Cambridge University Press, Cambridge

Partidge R.B., Peebles P.J.E, 1967, *Astrophys. J.* **148**, 377

Pearson R.C., Coles P., 1995, *Mon. Not. R. Astr. Soc.* , **272**, 231

Peebles P.J.E., 1980, *The Large-scale Structure of the Universe*, Princeton University Press, Princeton

Peebles P.J.E., 1988, *Astrophys. J.* , **332**, 17

Peebles P.J.E, 1994, *Physical Cosmology*, Princeton Universiy Press, Princeton

Pellegrini P.S., da Costa L.N., de Carvalho R.R., 1989, *Astrophys. J.* , **339**, 595

Penzias A.A., Wilson R.W., 1965, *Astrophys. J.* , **142**, 419

Politzer H.D., Preskill J., 1986, *Phys. Rev. Lett.*, **56**, 99

Postman M., Lauer T.R., 1995, *Astrophys. J.* , **440**, 28

Prim R.C., 1957, *BellSys. Tech.J.*, 'Shortest connection networks and some generalizations', p. 1389

Ryden B.S., 1995, *Astrophys. J.* , **452**, 25

Ryden B.S., Melott A.L., 1995, preprint, astro-ph/9510108

Sachs R.K., Wolfe A.M., 1967, *Astrophys. J.* , **147**, 73

Sahni V., Coles P., 1995, *Phys. Rep.* , **262**, 1

Sandage A., 1987, in *Observational Cosmology, IAU Symp. 124*, Hewitt A., Burbidge, G, Fang L.Z. eds., Reidel, Dordrecht, p.13

Shane C.D, Wirtanen, C.A., 1967, *Publ. Lick Obs.*, **22**, part I

Shanks T., 1990, in *Observational Tests of Cosmological inflation*, ed. Shanks T., 205, Dordrecht, Kluwer

Shanks T., Hale-Sutton D., Fong R., Metcalfe N., 1989, *Mon. Not. R. Astr. Soc.* , **237**, 589

Shapley H., Ames A., 1932, A Survey of the External Galaxies brighter than the 13th Magniture., *Annals of the Harvard College Observatory*, **88**, 41

Shaver P.A., 1991, *Austr. J. Phys.*, **44**, 759

Smoot G.F., Bennett C.L., Kogut A., Wright E.L. Aymin J., Boggess N.W., Cheng E.S., de Amici G., Gulkis S., Hauser M.G., Hinsaw G., Jackson P.D., Janssen M., Kaita E., Kalsall T., Keegstra P., Lineweaver C., Loewnstein K., Lubin P., Mather J., Meyer S.S., Moseley .H., Murdock T., Rokke L., Silverberg R.F., Tenorio L., Weiss R., Wilkinson D.T., 1992, *Astrophys. J.* , **396**, L1

Strauss M.A., Davis M., Yahil A., Huchra J.P., 1992, *Astrophys. J.* , **385**, 421

Strauss M.A., Willick J.A., 1995, *Phys. Rep.* , **261**, 271-431

Taylor K., 1995, in *Wide-Field Spectroscopy and the Distant Universe*, p.15, Maddox S.J., & Aragón-Salamanca A. eds., World Scientific (Singapore)

Tolman, R.C, 1934, *Proc. Nat. Acad. Sci*, **20**, 169

Totsuji M., Kihara T., 1969, *Pub. Astr. Soc. Jap.*, **21**, 221

Tully R.B., 1986, *Astrophys. J.* , **303**, 25

Tully R.B., 1987, *Astrophys. J.* , **323**, 1

Tyson J.A., Valdes F., Wenk R.A., 1990, *Astrophys. Journ. Letters* , **349**, L1

Vishniac E.T., 1986, in Kolb E.W., Turner M.S., Lindley D., Olive K., Seckel D., eds, *Inner Space/ Outer Space*, University of Chicago Press, Chicago, p 190

Vogeley M.S., Geller M.J., Huchra J.P., 1991, *Astrophys. J.* , **382**, 44

Vogeley M.S., Geller M.J., Park C., Huchra J.P., 1994, *Aston. Journal*, **108**, 745

White M., Scott D., Silk J., 1994, Anisotropies in the Cosmic Microwave Background, *Ann. Rev. Astron. Astrophys*, **32**, 319

White S.D.M., 1979, *Mon. Not. R. Astr. Soc.* , **186**, 145

Winkler H, 1983, *Mon. Not. Astr. Soc. Southern Africa*, **42**, 74

Zahn C.T., 1971, *IEEE Trans. Comput.*, **C20**, 68

Zel'dovich Ya.B., 1970, *Astron. Astroph.* , **5**, 84

Zwicky F., Herzog E., Wild P., Karpowicz M., Kowal C.T., 1961–1968, *Catalogue of Galaxies and Clusters of Galaxies*, 6 vols, California Institute of Technology, Pasadena

Appendix A

The FVC Catalogue

A preliminary version of the FVC (1995) is listed here. The first column lists the numbers given to the voids by Fairall. The following two columns give the coordinates of the centroids, the fourth column lists the distance to centroids in redshift units, and the fifth presents the diameters also in redshift units. The penultimate column marks voids that belong to walls and the last column contains remarks.

Question marks appearing next to a value indicate uncertainty in the determination of the value. In using the catalogue uncertainties have been disregarded and the listed values have been used.

N°	R.A. (h)	Dec. (°)	cz_{center} (km s^{-1})	Diameter (km s^{-1})	Wall	Remarks
1	18.6	-30	1000	2000		SAGITTARIUS void
2	16.0	-82	?1000	700		Extends to 2200 km s^{-1}
3	0.5	-58	400	400		
4	0.4	-33	?500	120	Centaurus	Possible small void
5	2.3	-20	500	500		Extends N of Cel. Equator
6	7.5	-53	500	500		Check gal in middle
7	5.1	-18	500	300		
8	6.2	-17	?500	120		Possible void

N°	R.A. (h)	Dec. (°)	cz_{center} (km s^{-1})	Diameter (km s^{-1})	Wall	Remarks
9	8.5	-13	750	> 700		Extends N of Cel. Equator
10	6.3	-28	?1000	150		
11	12.0	-56	?600	400	Centaurus	
12	12.4	-30	?600	250	Centaurus	
13	11.0	-17	750	400		
14	21.0	-17	?2400	1200		Extends N of Cel. Equator
15	21.1	-38	1900	750		
16	21.5	-75	1500	700		
17	22.7	-56	1700	400	Fornax	
18	22.8	-13	1700	600		
19	0.0	-10	1500	400	Fornax	
20	23.7	-33	1300	700	Fornax	
21	1.5	-47	3250	3000		ERIDANUS void
22	1.3	-16	1500	500	Fornax	
23	1.0	-3	1500	250	Fornax	Possible void
24	1.9	-3	1500	400	Fornax	
25	2.4	-15	1500	300	Fornax	
26	2.7	-25	1600	200	Fornax	
27	3.0	-30	1600	200	Fornax	
28	3.4	-41	1600	120	Fornax	
29	4.0	-40	1600	150	Fornax	
30	3.3	-48	1250	150	Fornax	
31	4.1	-52	1250	150	Fornax	
32	4.7	-62	1250	150	Fornax	
33	3.8	-32	1250	200	Fornax	
34	4.2	-27	1500	400	Fornax	
35	5.0	-33	1250	150	Fornax	
36	5.4	-29	1250	150	Fornax	
37	5.8	-26	1500	150	Fornax	
38	6.4	-24	1750	150	Fornax	
39	8.2	-63	1600	400	Fornax	
40	9.4	-73	1500	150	Fornax	Possible void

N°	R.A. (h)	Dec. (°)	cz_{center} (km s^{-1})	Diameter (km s^{-1})	Wall	Remarks
41	11.0	-73	1500	300	Fornax	
42	4.2	-8	1750	?1200		Extends N of Cel. Equator
43	5.1	-24	1750	150	Fornax	
44	6.0	-12	1750	700		
45	8.5	-10	1750	500		
46	10.2	-17	2000	700	Hydra	
47	11.0	-12	2500	?1000	Hydra	
48	11.6	-6	1500	150	Hydra	Possible void
49	11.5	-17	1500	250	Hydra	
50	10.7	-29	1500	250		
51	12.2	-6	1500	300	Hydra	
52	12.7	-18	1500	300	Hydra	
53	12.3	-27	1750	200	Hydra	
54	11.4	-47	1900	800	Hydra	
55	13.5	-44	1500	200	Centaurus	
56	13.7	-35	1300	150	Centaurus	
57	13.3	-18	1300	120	Centaurus	
58	13.4	-15	1300	150	Centaurus	
59	13.5	-4	1300	250	Centaurus	
60	14.2	-13	3000	?		
61	14.6	-38	2000	600	Centaurus	
62	15.1	-7	2000	300		
63	14.6	-6	2000	150		
63b	17.7	-50	3500	500	Fornax	
64	19.4	-48	3500	400	Fornax	
65	20.7	-44	2500	250	Centaurus	
66	21.9	-40	3000	250	Centaurus	
67	22.8	-43	3000	250	Centaurus	
68	17.1	-69	3000	700	Centaurus	
69	17.6	-83	3000	300	Fornax	

N°	R.A. (h)	Dec. (°)	cz_{center} (km s^{-1})	Diameter (km s^{-1})	Wall	Remarks
70	19.0	-69	3000	400	Centaurus	
71	20.1	-69	3000	500	Centaurus	
72	21.4	-53	?3000	250	Centaurus	
73	3.4	-19	2250	300	Fornax	
74	2.7	-6	2000	500	Fornax	
74b	5.5	-14	2500	300	Fornax	
75	8.6	-25	2250	400	Hydra	
76	9.3	-33	2250	250	Hydra	
77	9.5	-20	2250	250	Hydra	
78	9.7	-24	2250	250	Hydra	
79	10.3	-30	2500	250	Hydra	
80	10.9	-34	2500	250	Hydra	
81	10.0	-38	2500	400	Hydra	
82	11.3	-43	2750	400	Hydra	
83	12.3	-53	3000	400	Hydra	
84	12.8	-38	2500	250	Hydra	
85	12.7	-33	3000	300	Hydra	
86	12.6	-18	2750	700		
87	12.8	-7	2500	250	Centaurus	
88	14.1	-40	3000	700	Centaurus	
89	14.3	-25	2500	400		
90	15.0	-22	2750	300	Hydra	
91	13.5	-3	2500	?		
92	17.3	-32	?	?		
93	0.0	-40	?	?		
94	17.0	-65	3500	700	Centaurus	
95	20.0	-67	3500	500	Centaurus	
96	20.2	-57	3500	700	Centaurus	
97	22.3	-57	3200	1000	Grus	
98	23.7	-53	3000	700	Grus	
99	0.2	-43	3000	700	Grus	

N°	R.A. (h)	Dec. (°)	cz_{center} (km s^{-1})	Diameter (km s^{-1})	Wall	Remarks
100	1.3	-16	3750	2000		
100b	0.5	-5	3500	300		
101	2.5	-8	3750	1000	Sculptor	
102	4.7	-8	4000	300	Sculptor	
103	5.5	-34	3500	300	Sculptor	
104	9.9	-64	3000	300	Sculptor	
105	10.9	-42	4000	700	Hydra	
106	12.2	-45	4000	700	Hydra	
107	11.4	-28	3000	700	Hydra	
108	12.4	-31	3500	700	Hydra	
109	11.9	-23	3750	500	Hydra	
110	12.3	-12	3250	1000	Hydra	
111	13.0	-35	3500	500	Hyd-Cen	
112	17.7	-49	5000	2000		
113	16.5	-66	5000	300	Centaurus	
114	17.6	-71	5250	700	Centaurus	
115	18.4	-61	5000	400	Centaurus	
116	18.9	-56	5000	300	Centaurus	
117	20.0	-65	4000	800	Centaurus	
118	20.8	-49	4750	200	Centaurus	
119	21.2	-44	4750	300	Centaurus	
120	0.9	-4	4500	600		
121	2.9	-82	4750	300	Sculptor?	
122	8.0	-80	4750	700	Sculptor?	
123	1.9	-38	4750	400	Sculptor	
124	2.6	-38	4750	400	Sculptor	
125	2.2	-30	4750	300	Sculptor	
126	2.3	-23	4750	?400	Sculptor	
127	2.3	-16	4750	?400	Sculptor	
128	3.0	-18	4250	600	Sculptor	
129	3.1	-27	4250	600	Sculptor	

N°	R.A. (h)	Dec. (°)	cz_{center} (km s^{-1})	Diameter (km s^{-1})	Wall	Remarks
130	3.5	-33	4250	600	Sculptor	
131	4.7	-36	4750	900	Sculptor	
132	4.3	-26	4750	300	Sculptor	
133	3.9	-22	4750	300	Sculptor	
134	6.0	-48	4750	500	Sculptor	
135	2.6	-3	5000	?		
136	4.1	-13	4500	1500		
137	6.3	-18	4500	4000		
138	8.2	-53	4500	3000		
139	13.5	-74	5000	2000		
140	9.2	-11	4250	1500		
141	10.2	-26	4000	600	Hydra	
142	10.4	-18	4000	700	Hydra	
143	11.7	-5	4000	?3000		
144	11.9	-28	?5000	2500		
145	13.8	-43	5000	800	Centaurus	
146	14.8	-41	5000	500	Centaurus	
147	14.4	-33	4000	500	Centaurus	
148	18.2	-61	5000	500	Centaurus	
149	19.0	-59	5500	600	Centaurus	
150	18.9	-51	5500	250	Centaurus	
151	19.7	-47	5500	800	Centaurus	
152	20.5	-46	5000	400	Centaurus	
153	19.6	-34	5750	400		
154	20.7	-30	6000	500		
155	20.3	-8	6000	700		
156	20.7	-2	6250	?700		
157	22.3	-20	5500	700	Centaurus	
158	5.6	-10	6000	1500		
159	0.2	-3	5500	?1500		

N°	R.A. (h)	Dec. (°)	cz_{center} (km s^{-1})	Diameter (km s^{-1})	Wall	Remarks
160	1.2	-4	5750	?1000	Sculptor	
161	1.0	-10	5750	700	Sculptor	
162	1.1	-20	5750	700	Sculptor	
163	0.8	-30	6000	500	Sculptor	
164	1.3	-30	6000	500	Sculptor	
165	1.8	-32	5500	400	Sculptor	
166	2.3	-33	5500	600	Sculptor	
167	1.6	-42	5500	?500	Sculptor	
168	1.7	-52	5500	?500	Sculptor	
169	2.1	-47	5500	?500	Sculptor	
170	2.4	-60	5750	900	Sculptor	
171	4.6	-54	5500	1000	Sculptor	
172	9.1	-69	5000	1000		
173	11.1	-74	5500	700		
174	10.9	-8	5000	?1000		
175	12.1	-8	5250	500	Centaurus	
176	12.5	-17	5250	1000	Centaurus	
177	12.7	-4	5250	?1500	Centaurus	
178	13.3	-25	5500	600	Centaurus	
179	13.6	-42	5750	1500	Centaurus	
180	12.9	-53	5000	500		
181	14.7	-34	6000	1200	Hydra	
182	15.6	-35	6000	600	Hydra	
183	15.4	-27	5500	800	Hydra	
184	18.3	-46	5750	900		
185	18.0	-58	6500	800		
186	19.1	-59	6250	800		
187	19.7	-48	6500	700		
188	20.3	-48	7000	700		
189	20.9	-44	7000	700		

N°	R.A. (h)	Dec. (°)	cz_{center} (km s^{-1})	Diameter (km s^{-1})	Wall	Remarks
190	19.8	-36	6500	700		
191	20.2	-33	7000	700		
192	21.5	-12	6400	5000		
193	0.3	-18	6000	2000		
194	1.9	-15	?			
195	2.7	-45	6000	1500		
196	4.1	-32	7000	2500		
197	4.4	-10	7000	?3000		
198	5.8	-42	7000	2500		
199	7.8	-51	7000	3000		
200	14.5	-76	7000	3000		
201	10.8	-50	6500	700		
202	12.6	-49	7000	1200		
203	12.3	-11	7000	2500		
204	12.8	-28	6000	1000		
205	12.6	-39	7000	1200		
206	14.0	-28	7000	300		